Defatted Soy Flour Substitution in Phenol Formaldehyde and Methylene Diphenyl Diisocyanate Wood Adhesives and their Curing Kinetic Behavior

by

William Glover Hand, III

A dissertation submitted to the Graduate Faculty of
Auburn University
in partial fulfillment of the
requirements for the Degree of
Doctor of Philosophy

Auburn, Alabama
May 5, 2018

Keywords: soy flour, bio-adhesive, wood adhesive, phenol formaldehyde, methylene diphenyl diisocyanate, oriented strand board

Approved by
W. Robert Ashurst, Chair, Uthlaut Associate Professor, Chemical Engineering, Auburn University
Virginia A. Davis, Alumni Professor, Auburn University
Brian K. Via, Director of the Forest Products Development Center and Regions Bank Professor, School of Forestry and Wildlife Sciences, Auburn University
Marko J. Hakovirta, Department Head and Professor, Department of Forest Biomaterials, North Carolina State University
Sujit Banerjee, Professor Emeritus, School of Chemical & Biomolecular Engineering, Georgia Institute of Technology

Abstract

Composite wood products are manufactured utilizing reconstituted cellulosic material formed with thermosetting adhesives, primarily adhesives made from non-renewable materials. Natural wood adhesives, or bio-adhesives, had been used until the mid-20th century. Eventually bio-adhesives were replaced with synthetic adhesives because of superior qualities such as water resistance, durability, and eventually cost. Recent published work has shown the incorporation of bio-adhesives in composite wood products that required chemical modification and functionalization of the bio-adhesives. Defatted soy flour (SF) has shown the highest potential as a bio-adhesive due to its protein content and low cost. This work encompassed an investigation of the partial substitution of synthetic resins with SF for use in composite wood products. Other soy products investigated in this work included soy protein isolate (SPI) and denatured, defatted soy flour (soy-D). The synthetic adhesives studied were phenol formaldehyde (liquid and powder) and polymeric methylene diphenyl diisocyanate (pMDI) and are both used in the production of oriented strand board.

The overall objective of this work was to advance the understanding of interactions between soy flour and synthetic wood adhesives in the use of composite wood products. An evaluation of the degree to which SF could be substituted into either phenol formaldehyde (PF) or pMDI in the formation of strand board was studied in the first phase of this work. The amount

of SF substitution possible without compromising performance of the formed board was determined.

The mechanism of adhesion enhanced through SF interaction with the PF or pMDI was studied in the second phase of this work. Curing kinetic data of neat PF, neat pMDI, and soy products substituted into PF or pMDI were analyzed. There were two possible primary mechanisms of adhesion influenced by the substitution of SF: SF influenced the cohesiveness in the bulk by chemically crosslinking with the PF or pMDI, or the SF affected the adhesiveness to the wood substrate by altering the wood/resin interface.

This work was driven by the hypothesis that SF hydrolyzed during the pressing process to chemically crosslink with the synthetic resin in the bulk adhesive. This work differed from prior published works by focusing on the incorporation of SF during the board forming process. Other published works focused on SF modification or pretreatment which added cost. Some works incorporated the modified SF in the synthetic resin synthesis which decreased the pot life of the overall adhesive. The incorporation of SF during the board forming process required minimal equipment upgrades and used existing materials (PF and pMDI). Cost was the chief motivation for this work as SF was about half the cost of PF and less than half the cost of pMDI. Non-renewable resource elimination through substitution with a bio-adhesive was a secondary motivator. The board produced from the SF substituted adhesive also required equal or improved mechanical property data of the board produced with the synthetic adhesive. Mechanical properties measured were flexural strength and modulus, internal bond, thickness swell, and water absorption.

Higher viscosity due to SF substitution in liquid PF inhibited penetration of the wood substrate and likely decreased resin spread. Less adhesive penetration benefited board strength with lesser amounts of SF substitution due to a decrease of overpenetration of the adhesive into the wood substrate. Larger amounts of SF substitution resulted in adhesive failure due to under-penetration. A decrease in the resin spread likely affected the wood/resin contact area which resulted in adhesive failure in higher density boards. SF substitution of 10-14% in liquid PF was possible without compromising performance. Resin spread was not an issue with SF substituted powder PF. SF substitution of 21-30% in powder PF was possible without compromising performance.

There were two possible interactions affecting the SF substituted pMDI boards: urea formation due to SF substitution in pMDI positively affected wet properties of the formed board, or higher viscosity due to SF substitution in pMDI decreased overpenetration of pMDI into the substrate and contributed to the bulk. SF substitution of up to 30% in pMDI was possible without compromising performance.

Thermogravimetric analysis (TGA) of the PF/soy product mixtures showed no new chemical structures formed in the degradation profile compared with TGA data of neat PF. Activation energies for curing reactions of PF/soy product mixtures showed no considerable difference to the curing reaction activation energies of neat PF. Fourier transform-infrared (FT-IR) spectral analysis of neat PF and PF/soy product samples subjected to differing heat treatments showed no significant difference of concentrations of methylene and ether bridge formation signifying no change in curing reaction with soy product interaction with PF. All

curing kinetic analyses of PF and PF/soy product samples refuted the original hypothesis of the primary interaction being affected with soy product substitution in PF was a chemical crosslinking one. The higher viscosity of the soy flour substituted PF affected the resin spread and penetration during the blending and pressing process of strand board formation, therefore the primary mechanism of adhesion affected by the substitution of soy products in PF was adhesion affecting the wood/resin interface.

TGA of the pMDI/soy product mixtures showed a new degradation profile of soft segments not observed in the neat pMDI TGA data indicating new chemical structures formed as a result of soy products interacting with pMDI. The formation of carbodiimide was identified through TGA for neat pMDI and pMDI/soy product mixtures. FT-IR spectral and activation energy analyses confirmed the formation of carbodiimide as two separate reaction pathways: polymerization reaction for neat pMDI and part of the urethane degradation reaction in the pMDI/soy product mixtures. Urethane and urea formation in the pMDI/soy product mixture was discovered as the primary polymerization reaction through FT-IR spectral analysis. All curing kinetic analyses of pMDI and pMDI/soy product samples supported the original hypothesis of the primary interaction being affected with soy product substitution in pMDI was a chemical crosslinking one.

Acknowledgments

First and foremost, the person who has stood with me from the beginning and has been my biggest support before, during, and after the process of performing this work deserves the most acknowledgement – my partner, my wife, my best friend – Nancy Helen Tilton Hand, J.D. Thank you for keeping me healthy, keeping me fed, and managing every aspect of our lives for that matter. Most of all, thank you for the training with the Hands On Plan. It was situations like this process where the Hands On Plan works best.

I would like to thank Dr. Kerry Tilton. Your encouragement sparked this journey into an advanced degree far before it ever started. Thank you for seeing in me what no one else did. I know that you were smiling up there while you watched as I completed this work. Karen Molan, thank you for coaching me through this process. Your help in keeping me on task kept me aligned with completing this work. Thank you to Dr. Joshua Tilton for your support and advice through this work.

I would like to express my gratitude to my committee. Dr. W. Robert Ashurst, thank you for the guidance throughout this process, especially the latter half. Dr. Brian Via, thank you for your guidance from the beginning of this work. Your industrial and academic advice helped tremendously in this work and will go on to help me in my career. Dr. Sujit Banerjee, thank you for the advice and help that you provided through all this work. I was able to better visualize phenomena on multiple levels because of your guidance. Thank you for opening my eyes to

observing in a fundamental and practical way. Thank you for the phone conversations. Your encouragement and advice made it possible to complete this work. Dr. Marko Hakovirta, thank you for starting me on this work. Thank you for always bridging the gap between lab and industrial scale. Dr. Virginia Davis, thank you for the advice towards making this a more academic work. Your editing helped tremendously, and I appreciated the talks that we had in your office. Dr. Soledad Peresin, thank you for your advice whenever I presented this research. I always respected your suggestions for other techniques to further characterize and learn more about interfacial interactions. Thank you for agreeing to lend your support as an outside reader. Thank you for the incredibly helpful edits for this work.

I would also like to thank my friends, both new and old, for their support during this process. The relationships that I have formed during my time in the graduate program supported me in countless ways and made the journey a lot more pleasant. I would like to thank the OG group in Chemical Engineering for their support. The social gatherings between work kept me sane. I would like to also acknowledge the Via/Peresin group. I enjoyed their feedback on my work and the social gatherings. Thank you to the Davis group for their help in developing my work into a better academic work.

Table of Contents

List of Tables

List of Figures

List of Abbreviations

PF	Phenol Formaldehyde
MDI	Methylene Diphenyl Diisocyanate
pMDI	Polymeric Methylene Diphenyl Diisocyanate
SF	Soy Flour
SPI	Soy Protein Isolate
OSB	Oriented Strand Board
MOR	Modulus of Rupture
MOE	Modulus of Elasticity
IB	Internal Bond
TS	Thickness Swell
WA	Water Absorption
TGA	Thermogravimetric Analysis
DTGA	Derivative Thermogravimetric Analysis
DSC	Differential Scanning Calorimetry
FT-IR	Fourier Transform-Infrared

Chapter 1: Introduction

The overall objective of this work was to advance the understanding of interactions between soy products and synthetic adhesives in the use of wood composites. Specifically, the objective evaluated whether, and how much, soy product could be substituted into composite wood adhesives. The objective also determined the mechanism of adhesion (cohesive bulk or wood/resin adhesion) in each phenol formaldehyde (PF) and polymeric methylene diphenyl diisocyanate (pMDI) that was enhanced through soy product interaction. The soy products studied in this work were defatted soy flour (SF), soy protein isolate (SPI), and denatured, defatted soy flour (soy-D). The synthetic wood adhesives studied were PF and pMDI.

The objective of this work was carried out in two phases: a screening stage (applied objective), and an adhesion properties stage (fundamental objective). The applied objective was to discover if SF was a viable adhesive substitute for synthetic wood adhesives and to what degree SF could be partially substituted into the synthetic adhesive without compromising performance. Performance was measured through mechanical testing analysis of strand boards formed with these adhesives. The fundamental objective was to examine the interaction between soy products and the synthetic wood adhesive, PF or pMDI, and how it affected the overall adhesive characteristics. Curing kinetics were characterized in each adhesive employing thermogravimetric analysis (TGA), differential scanning calorimetry (DSC) analysis, and Fourier

transform-infrared (FT-IR) spectral analysis to examine how soy products affected the overall adhesive.

Motivation

The primary motivation of this work was cost reduction. Typical commercial PF prices used in the manufacture of oriented strand board (OSB) ranged in price from $0.60-$0.83/lb [1], and polymeric MDI prices ranged from $0.80-$1.25/lb [2]. In comparison, soybean meal sold as a commodity at $0.193/lb [3] when this work was documented. There were processing costs involved with grinding the soybean meal into flour that typically double the price to about $0.35-$0.40/lb. Defatted soy flour (SF) costs were generally half of the cost of PF and about a third of the cost of pMDI. There was a potential cost reduction with SF substitution in synthetic resins. For example, a 20% SF substitution in PF would result in a savings of about 10% for the overall wood adhesive.

The secondary motivation for this work was the partial elimination of non-renewable resources used to synthesize PF and pMDI through substitution of the bio-adhesive, SF. Formaldehyde, a known carcinogen [4], is used to synthesize both PF and pMDI. Formaldehyde off-gassing during the manufacturing of composite wood using PF could be a potential danger to those exposed in an industrial setting. Formaldehyde off-gassing in the finished product was also of concern if the PF resin was not fully cured. Slower curing rates and short press times attribute to the incomplete cure of the resin [5]. There were also concerns with isocyanates, the primary reactive group contained in pMDI, which have been shown to have negative health effects involving asthma and other maladies [6]. PF synthesis required phenol, and pMDI synthesis required aniline. Phenol and aniline are both petroleum-based categorizing them as non-renewable resources. The price of PF and pMDI adhesives were also partly based on the

petroleum market. According to some estimates, the world currently consumes petroleum at about 100,000 times the rate at which the earth can produce it [7]. Cost and the declining supply of petroleum products has generated research in replacing these petroleum products with more environmentally friendly alternatives [8]. Partial substitution of SF into PF and pMDI would decrease the amount of synthetic resin in the composite wood therefore decreasing these non-renewable resources.

Cost reduction and non-renewable resource reduction were benefits associated with substituting SF into the synthetic adhesives, but these SF substituted resins had to achieve as good or better mechanical properties in the finished product with a given amount of substitution of SF. The strength of the composite board formed with these SF substituted adhesives was important because the product must meet structural guidelines through testing standards like the American Plywood Association (APA) PS 2 standard [9]. Mechanical data of the formed boards were measured using flexural strength and modulus, internal bond, thickness swell, and water absorption using the ASTM D1037-12 standard [10].

Background

Most industrial wood products manufactured for construction purposes are reconstituted cellulosic materials held together by synthetic thermosetting adhesives, usually formaldehyde-based adhesives. Natural wood adhesives had been used until the mid-20th century. These natural wood adhesives were obtained from sources such as hooves, hides, milk, and soybeans. Defatted soy flour has shown more promise due to cost effectiveness. However, soy-based composite wood was not as water resistant without modifying or pretreating the soy flour. Because of this weakness, wood products used in interior construction were the primary focus when using soy flour as adhesives. Urea-formaldehyde replaced soy flour-based adhesives in interior wood

products, and phenolics replaced the soy product-based adhesives in outdoor wood products due to superior moisture resistance and durability. Synthetic resin cost eventually lowered because of an expanding petrochemical industry which allowed for the shift to composite wood products as the primary construction material over traditional solid wood [11].

Oriented strand board (OSB) was the primary industry product intended for the adhesive research in this work. OSB is a wood engineered product. It consists of strands of wood that are formed together with an adhesive. Pressure, time, and temperature are the primary controlling parameters in the formation of OSB. The surface layers of the formed board are oriented in the longitudinal direction to increase bending strength. The core layer is oriented in the perpendicular direction of the surface layers to help in directionality of the wood properties. It should be noted that the strand boards formed in this work were randomly oriented and not oriented as in OSB.

Phenol Formaldehyde

Phenol formaldehyde (PF) has dominated the wood composite manufacturing world as an adhesive for structural based applications. It was most commonly used in the production of oriented strand board (OSB), plywood, and other engineering wood products in the composite wood industry [12]. The base structure of PF is made up of a phenol and formaldehyde group (Figure 1). Formaldehyde forms methylol groups on free ortho and/or para sites of the phenol group. The polymerization of PF involved these methylol groups on the methylated phenol reacting with other phenol groups.

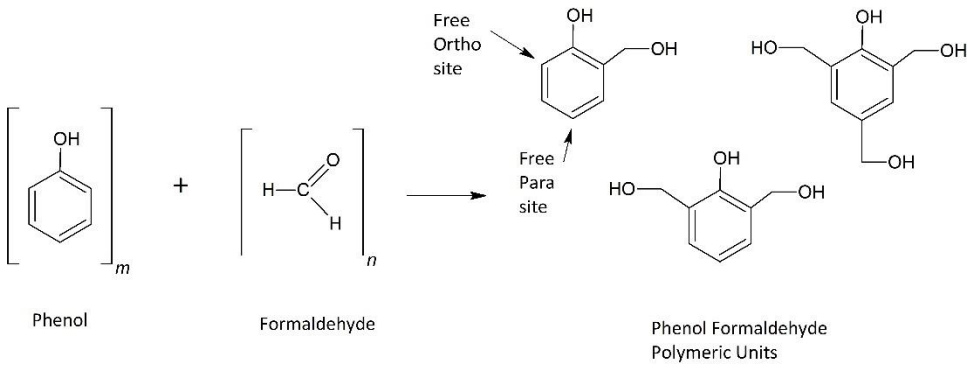

Figure 1: Chemical structure of Phenol Formaldehyde and its counterparts

The methylol groups from the methylated phenols either cross-link with free ortho or para sites on other phenols to form methylene bridges (Figure 2) or crosslink with other methylol groups on methylated phenols to form ether bridges (Figure 3). Ether bridges can also degrade forming a methylene bridge and releasing free formaldehyde (Figure 4).

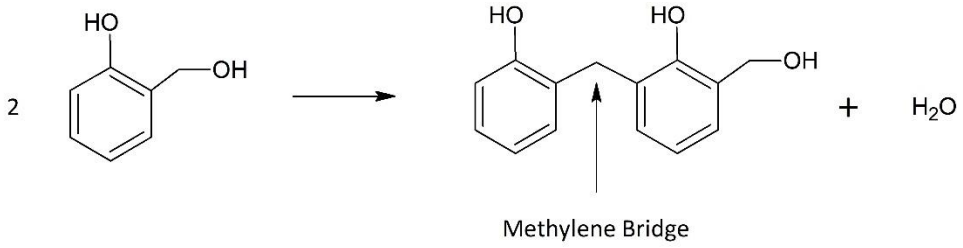

Figure 2: Phenol formaldehyde forming a methylene bridge between methylol group and free - ortho site

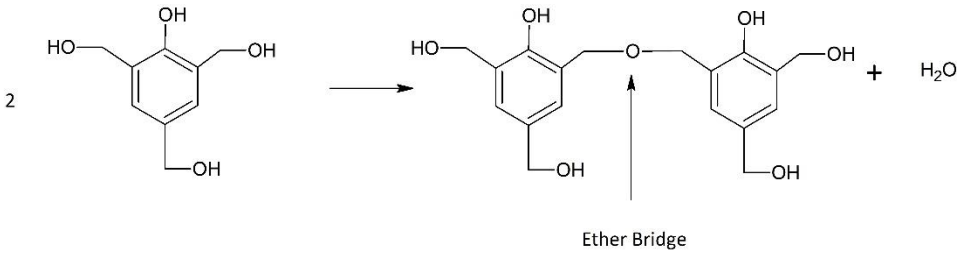

Figure 3: Phenol formaldehyde forming ether bridge between two methylol groups

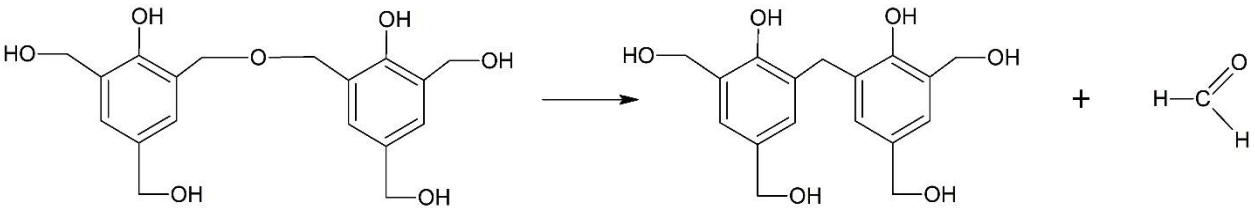

Figure 4: Ether bridge degradation to methylene bridge with formaldehyde off-gassing

Methylene Diphenyl Diisocyanate

Methylene diphenyl diisocyanate (MDI) has been used in its polymeric form (pMDI) as an effective wood binder. It reacts very aggressively with hydroxyl groups which was of great benefit to the wood adhesive industry as there are so many hydroxyl groups in which to react within cellulose. There are also reactivity with amines which were present in soy protein [13]. Use of pMDI started in the late 1960s in particleboard manufacture [14]. As the composite wood industry grew, the demand for MDI and pMDI grew and has shown prominence in the OSB market [15]. Its effectiveness increases since it reacts well with water. The pressing environment contains elevated moisture levels due to the water content of the wood substrate which increases the effect of the pMDI adhesive cure [15], [16]. This reaction with water forms polyurea which was a major gap-filling component in the pMDI/wood bond [15], [17].

Synthesis of MDI begins with an HCl catalyzed condensation of formaldehyde and aniline forming a methylene bridge. One mole of formaldehyde and two moles of aniline form the three possible isomers (4,4'-, 2,4'-, and 2,2'-) of methylenedianiline. The diamine isomers then react to form methylene bridged polyphenylene polyamines [15], [18], [19]. These structures reflect the isocyanate structures to be formed (Figure 5 and Figure 6). Phosgenation is then applied to the neutralized and dried polyamine mixture which occurs in a high boiling aromatic solvent. The amino groups were then converted to isocyanate groups [15], [18], [20]. Monomers (Figure

5) make up about 50% of polymeric MDI with the primary isomer formed being the 4,4'-MDI isomer which constitutes about 95% of the monomers formed. The other half of the pMDI mixture consists of the oligomeric polyisocyanate (Figure 6). This more complex polyisocyanate structure typically has a degree of polymerization of one to three but can be as high as twelve [15].

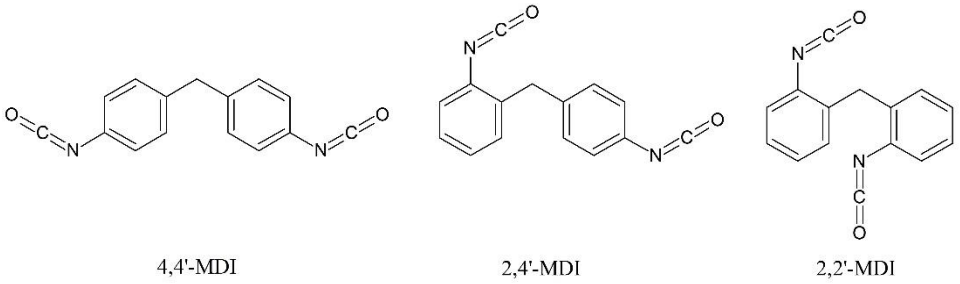

Figure 5: Three possible MDI isomers

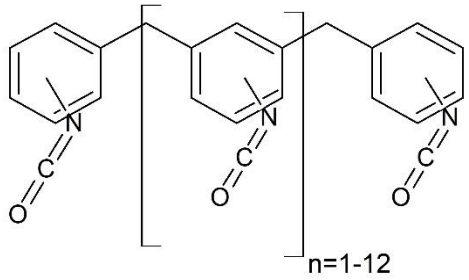

Figure 6: Typical polyisocyanate structure found in polymeric MDI

The isocyanate group from MDI can react in multiple reaction pathways to aid in the polymerization of the adhesive. Table 1 illustrates most of the reaction pathways available for the isocyanates and their relative reaction rates at ambient temperatures.

Table 1: Relative reaction rates of isocyanates with varying reaction partners [21]

Active **H** compound	Structure	Relative uncatalyzed reaction rate at 25 °C
Primary aliphatic amine	R-N**H**$_2$	100,000
Primary secondary amine	R$_2$N-**H**	20,000-50,000
Primary aromatic amine	Ar-N**H**$_2$	200-300
Primary hydroxyl	R-CH$_2$-O**H**	100
Water	**H**$_2$O	100
Carboxylic acid	R-COO**H**	40
Secondary hydroxyl	R$_2$CHO**H**	30
Urea	R-N**H**-CO-N**H**-R	15
Tertiary alcohol	R$_3$CO**H**	0.5
Urethane	R-N**H**-COOR	0.3
Amide	R-CO-N**H**$_2$	0.1

The primary reaction pathway thought to occur in wood composites was with hydroxyl groups to form urethane linkage (Figure 7). This was based on the large amount of hydroxyl groups available in the wood substrate. This was only an assumption as there was no experimental evidence supporting this theory [13].

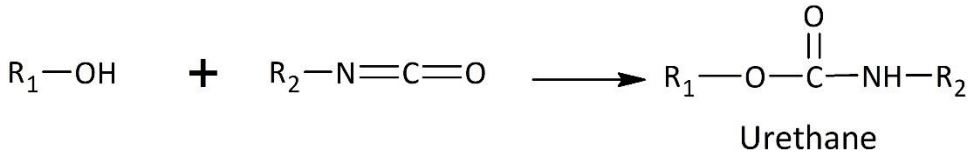

Figure 7: Reaction between a hydroxyl and isocyanate to form urethane linkage

The secondary amine in the urethane in turn can continue to react with other isocyanate groups from other MDI molecules to form allophanate bridges (Figure 8). This continues the crosslinking and hardening of the adhesive [13].

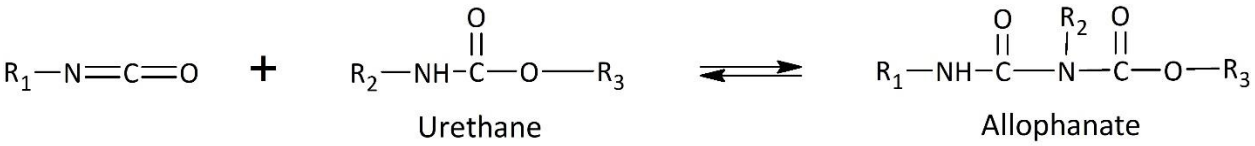

Figure 8: The reaction of an isocyanate and urethane to form an allophanate bridge

There is also water present in the wood substrate that can readily react with isocyanates (Figure 9). The reaction between water and isocyanate forms carbamic acid which quickly degrades into an amine with carbon dioxide gas being released.

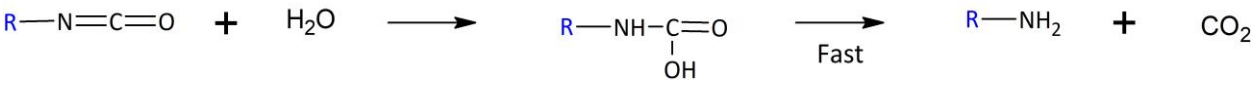

Figure 9: The reaction of isocyanate and water forming a primary amine

Amines react readily with an isocyanate group – especially in the case of a primary amine. This reaction occurs at a higher reaction rate than the water and hydroxyl reactions with isocyanate (Table 1). the isocyanate group can react with amines from either a substance that contains them (e.g. soy protein) or the water reaction to form substituted urea.

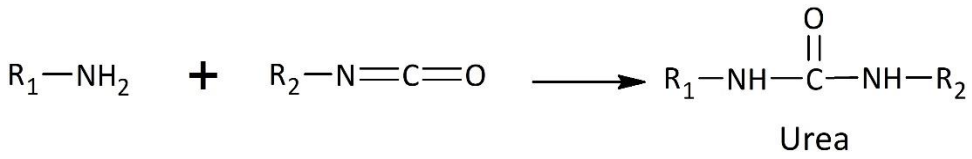

Figure 10: The reaction of the primary amine formed from isocyanate and water with another isocyanate to form urea

As in urethane, this substituted urea can then react with other isocyanate groups to form biuret bridges (Figure 11). These biuret bridges also strengthen crosslinking and help harden the cured adhesive [13].

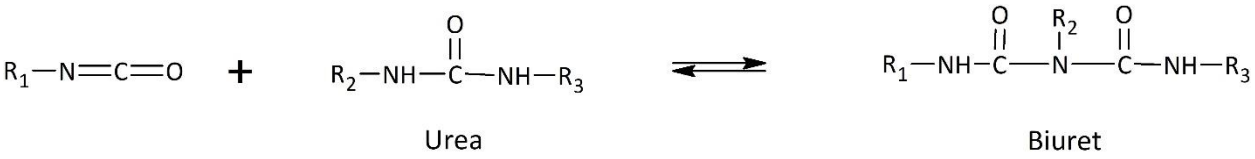

Figure 11: The reaction of urea with an isocyanate group to form biuret linkage

Hydrogen bonding was also considered in this work and improved the strength of the crosslinking matrix. Hydrogen bonding was typical in a crosslinked structure with urethane and urea. The N-H group acts as a proton donor while the carbonyl acts as a proton acceptor. Figure 12 displays hydrogen bonding between urethane groups. Hydrogen bonding between these groups increased the bonding strength of the adhesive [22].

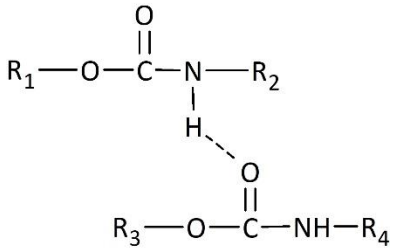

Figure 12: Hydrogen bonding between urethane groups

Urea also showed hydrogen bonding but can be in the form of monodentate (one hydrogen bond) or bidentate (two hydrogen bonds) (Figure 13).

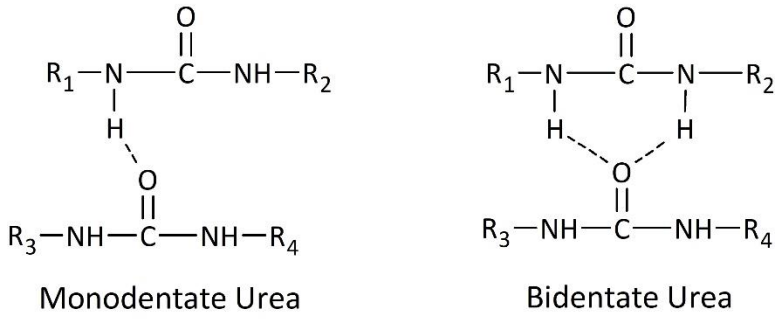

Figure 13: Hydrogen bonding between urea groups

Sonnenschein explained different pathways involved with isocyanates dimerizing and trimerizing. One example was the formation of carbodiimide groups [21]. The formation of carbodiimide is an irreversible catalyzed dimerization reaction of the isocyanate groups [23], [24]. The following shows the formation of carbodiimide in its simplest expression.

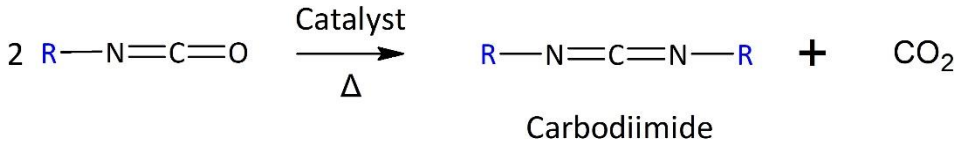

Figure 14: Catalyzed dimerization of isocyanate to form carbodiimide

Unintentional formation of carbodiimide from MDI stored in closed volumes can be a safety concern because of the release of carbon dioxide [21]. It has also been shown to form as a result of urethane degradation [25], [26].

The formation of uretidione (Figure 15) was described as a slow reversible reaction by Sonnenschein. This dimerization usually occurred due to long storage of pMDI and can further trimerize into isocyanurate(Figure 16) [21].

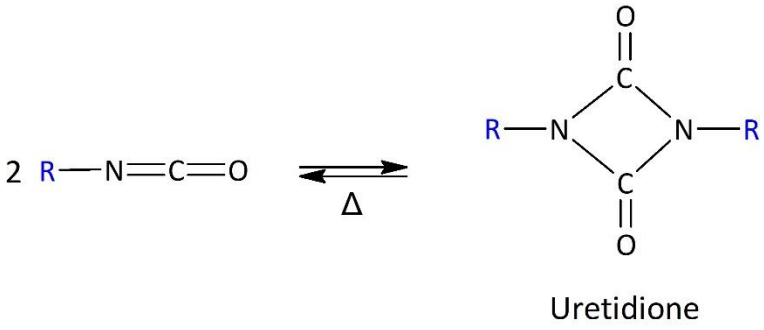

Figure 15: Dimerization of two isocyanates to form uretidione

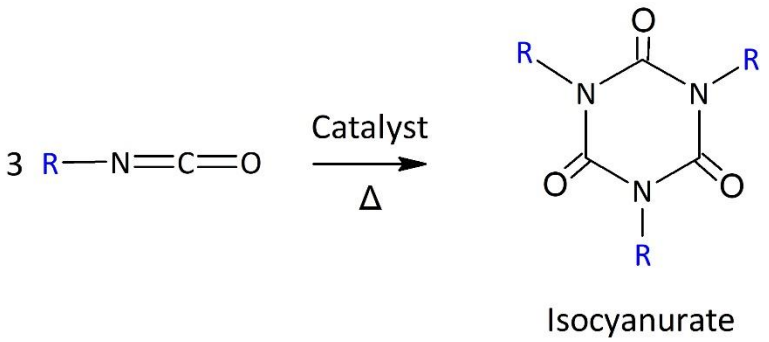

Figure 16: Trimerization of three isocyanates to form isocyanurate

pMDI has also been applied in conjunction with PF in OSB manufacture. In pressing PF in the surface layer and pMDI in the core layer, there can be a reaction between the alkaline PF and isocyanate group. The aqueous hydroxide anions react with the isocyanate yielding an amine similar to the reaction with water. The amines then react with additional isocyanates forming urea. Frazier explained that this can be counterproductive if the reaction rapidly occurred before hot-press compaction can occur [15].

Frazier discussed urethane modification of pMDI to help with gap filling problems associated with MDI. Low viscosity and a deep penetration propensity inhibit pMDI to be used in applications other than OSB production – like plywood, laminated veneer lumber, etc [15]. Further urethane linkage with components other than pMDI (e.g. soy flour) can open other markets for pMDI in the composite wood industry.

Soy Products

Soybeans were primarily harvested for their oil. There is considerable protein content in the soybean as well as carbohydrate content (Figure 17). The oil extraction process is usually

performed with hexane extraction. The defatted soy flakes or hulls could then be ground into a soy flour [27].

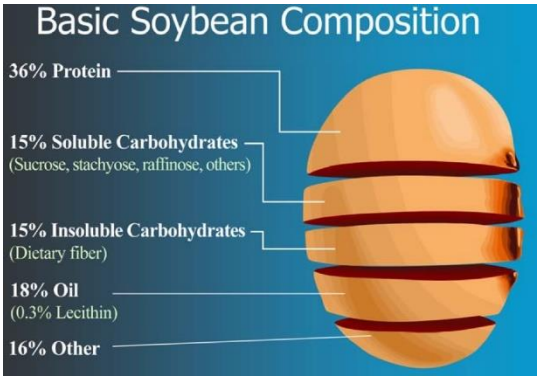

Figure 17: Composition of a common soybean before oil extraction [28]

This defatted soy flour consisted of about half protein. This protein was likely the primary source of adhesive strength from soybean flour [29]. The carbohydrates should not be overlooked as a possible adhesive source as well as the carbohydrate-protein Maillard reaction [7]. Further protein extraction from the soy flour can be performed to achieve higher protein contents of about 70% protein for soy protein concentrates (SPC) and about 90% protein for soy protein isolates (SPI) [29].

Soy-based adhesives have long been applied as wood adhesives historically and studied to a great extent in the 1920s and 1930s [30]. Denaturation of the soy protein using a caustic solution furthered the adhesive performance by exposing amide functional groups for better adhesion [31]–[33]. Petroleum based adhesives eventually replaced these soy adhesives in the 1940s due to improvements in durability, viscosities, pot-life, and eventually cost [34].

Soy protein is a linear, long chain polymer consisting of 18 different amino acids. These amino acids can be polar and nonpolar. The polar amino acids can be used to crosslink the protein to improve mechanical, thermal, water sensitivity, and hydrophobicity. They include

cysteine, arginine, lysine, histidine, and others. The polar functional groups can be carboxyl, amine, and hydroxyl groups capable of reacting. Carboxylic acid groups reacting with these polar functional groups in soy proteins form amide (from amine), ester (from hydroxyl), and anhydride linkages (from carboxyl). The crosslinked soy protein can be used as a resin in its own form or as a partial substitution with other petroleum-based resins. Soy protein adhesives have also exhibited other advantages in that it can be used as a fire resistant soy protein resin which aided in building materials requiring improved fire safety properties [7], [35].

Soy protein is primarily a globular protein, of which about 70% was consisted of globulin proteins. These globulins were primarily glycinin or conglycinin. Glycinin was comprised of six acidic and six basic protein subunits. These subunits alternate in two structural rings partially joined by disulfide bridges. Conglycinin, on the other hand, contains more neutral amino acids and less thiol groups to form disulfide bridges. Instead, the protein subunits were held together by hydrophilic interactions through the polar functional groups referred to above. These separated proteins can make a useful adhesive, but the isolation process can denature and eliminate some of the components needed to crosslink [11].

Potentially reactive side-chain amino acid groups in the proteins, glycinin and conglycinin have been shown to react with formaldehyde (Table 2) [36], [37]. These reactions improve the crosslinking density, but a disadvantage arises in the form of additional formaldehyde. The reaction was also easily reversed in moist environments.

Table 2: Amino acids in soy protein with potential to react with formaldehyde [38]

Amino acid	Structure	wt%
Lysine	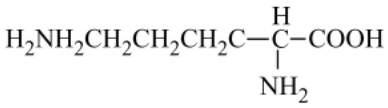	6.8
Histidine	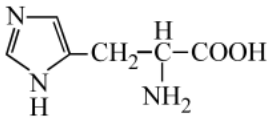	3.4
Arginine	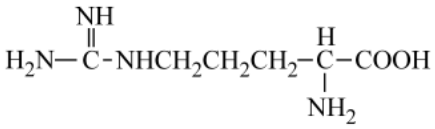	7.7
Tyrosine	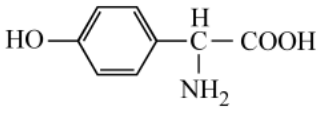	4.2
Tryptophan	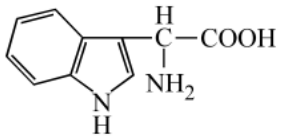	1.3
Serine	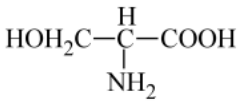	5.4
Cysteine	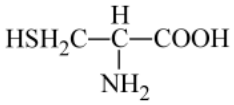	2.5
Total		31.3

Even though the backbone structure of the soy protein was always a 2-aminoacetic acid, the side chains can be aliphatic or polar (hydroxyl, thiol, carboxylic, and many nitrogen containing compounds). This varies with most adhesives in which there were only one to a few monomers.

The primary structure of the protein involved the linear polymer chain of amino acids (Figure 18 – bottom left). Crystallites form in the secondary structure due to intrachain and interchain interactions. These interactions form beta-sheets and alpha-helices (Figure 18 – bottom right). The tertiary structure is formed with the folding in of the protein structure due to the intrachain interactions (Figure 18 – top). This occurs in aqueous environments where non-polar side chains minimize their interactions with water by folding the structure in on itself. Interchain interactions also play a role in disulfide groups from thiols, acid-base interactions, salt bridges with multivalent cations, and hydrogen bonds. The quaternary structure is formed when

the globules formed in the tertiary structures interact with each other (Figure 18 – top left). These interactions were due to hydrophobic, hydrogen bond, salt, and disulfide formation [11].

The soy protein in its native state (quaternary structure) conceals a large amount of the active groups that contribute to adhesive bonding through disulfide bridges with thiols, polar bonds such as hydrogen bonds and acids, and bases as salt bridges. Denaturation can expose these groups by unfolding the protein structure to a certain degree. Denaturation breaks the quaternary structure which was followed by the opening of the tertiary structure providing more reactive sites contributing to adhesive strength. There was a challenge in not destroying too much of the tertiary structure as this improves the strength of the adhesive (Figure 18 – top right). There must be a balance between an open structure for reactive sites and a partially intact structure for stability. This can be very challenging when working with soy flour which only consists of about half proteins [11].

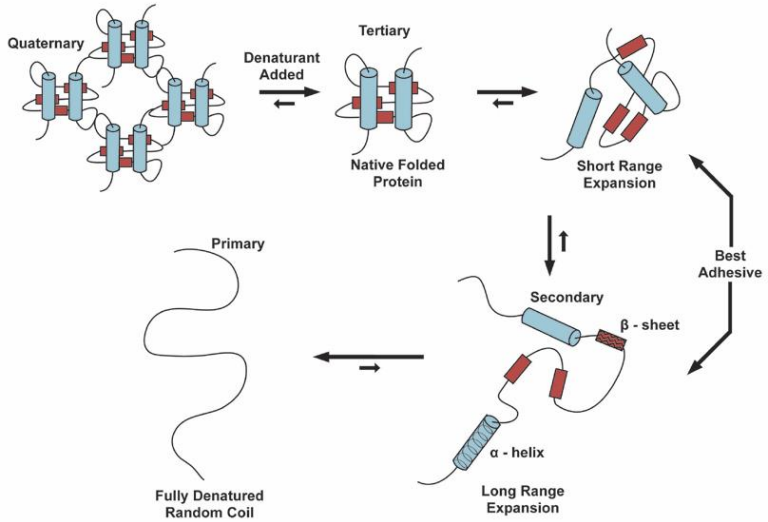

Figure 18: Denaturation of the protein structure [11]

Soy flour also contains soluble and insoluble carbohydrates. Insoluble carbohydrates play a minor role in strengthening the adhesive. The soluble sugars are made up about 30% of the

defatted soy flour. They are made up of glucose, fructose, sucrose, raffinose, and stachyose. The soluble sugars play a negative role in the use as an adhesive due to an increase in dispersion viscosity, consumption of some of the crosslinker, and increase in water absorption which softens the adhesive under high moisture conditions [11].

Adhesion theory

A background of adhesion theory was necessary to understand the objectives entailed in this work described previously. Marra described the chain-link analogy with a bond only being as strong as its weakest link [39]. There were three possible failure mechanisms with wood adhesives. The possible failure points were in the adhesive itself, the wood itself, or the wood/adhesive interface. Different zones associated with the wood and adhesive interaction were identified by Marra (Figure 19). The complications associated with the wood/resin interface were also explained. Region 1 represented the pure adhesive. It was considered cohesive failure in this zone, and the adhesive was deemed not acceptable if this was the point of failure. Regions 2 and 3 represented the adhesive boundary and was considered not homogenous and the beginning of the interphase region. This was the point where the local properties began to change from that of the bulk adhesive to the point where the local properties reflect that of the bulk adherend [40]. Regions 4 and 5 represented the interface of the boundary layer and substrate. This was where the primary adhesive mechanism was represented. The wood cells modified by the adhesive were represented in regions 6 and 7. This was the surface of the wood where resin penetration drove the mechanism. Regions 8 and 9 were unadulterated wood. The adhesive was considered acceptable if failure occurred here [39].

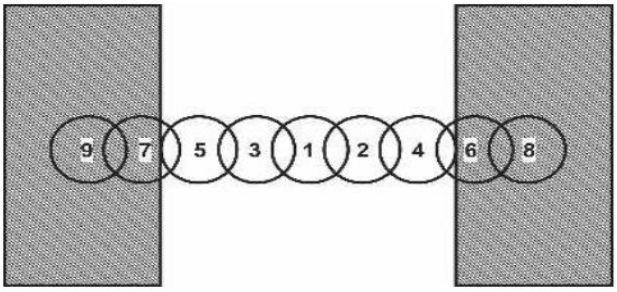

Figure 19: Chain link analogy for an adhesive bond in wood [39]

There are currently five theories of adhesion: mechanical entanglement/interlocking theory, diffusion theory, electronic theory, adsorption/specific adhesion theory, and the covalent bonding theory [13]. These theories can differ in their contribution to adhesion forces at the adhesive/substrate interface as well as differ according to the class of adhesive studied. Mechanical entanglement/interlocking theory of adhesion was heavily influenced through penetration, therefore a certain amount of adhesive penetration in the first few shallow layers of wood substrate was desirable. Bonded joint strength required two parameters: intrinsic adhesion and energy (viscoelastically and plastically dissipated around the tip of the propagating crack). Mechanical interlocking did not appear to be the main contributor to wood adhesion because thermosetting resins were brittle and cohesive by themselves [13].

Voyutskii [41]–[43] first promoted the diffusion theory of adhesion in the early 1960s which stated mutual diffusion of polymer molecules across their interface – a polymeric resin and a polymeric substrate (wood). There were two requirements of diffusion: similar solubility parameter values and being amorphous – a high degree of crystallinity tends to resist dissolving in a solvent, and there must be sufficient mobility [13]. Wood was not a homogeneous polymer; it was made up of three polymers. This meant that there were possibly three different solubility parameters with the resin. Cellulose was crystalline and amorphous while hemicellulose and

lignin were amorphous. Diffusion could be thought of as a molecular level of mechanical interlocking, but a small molecular weight was required to flow in the wood cell walls [44].

Anand et. al. [45]–[50] stated that the bond strength's dependence on time of contact and resin molecular weight could be explained by the effect of wetting of the substrate surface and that diffusion does not play a significant role in bond formation. The authors believed the increase in bond strength was due to an increase in interfacial contact. They believed the mechanism of adhesion depended on the formation of secondary, van der Waals forces across the interface of the adhesive and substrate (adsorption/specific adhesion theory). Polymers that were highly crosslinked (like thermosetting wood adhesives) and polymers that were highly crystalline (like wood cellulose) were highly unlikely to exhibit interdiffusion as a mechanism of adhesion [44]. The exception would be fiberboard where elevated levels of moisture, pressure, and long pressing time lower the glass transition temperature of lignin. Lignin would then be mobilized, and interdiffusion between lignin polymers would contribute to bonding fiberboard together. Secondary forces still appeared to be the primary contributors to adhesion [13].

Deryaguin et. al. [51]–[53] promoted the electronic theory of adhesion. There is likely an electron transfer upon contact if the substrate and adhesive had different electronic band structures – promoting a double layer of electrical charges at the interface – contributing significantly to adhesion. Weaver [54]–[56] claimed it was a result, not a cause, of high joint strengths. Roberts' [57] experiments displayed a contribution from the electrical double layer at a rubber-glass interface of about 10^{-5} mJ/m^2 – negligible to van der Waals forces at 60 mJ/m^2. Electrostatic forces were more likely to occur in debonding rather than bond forming [44].

The adsorption/specific adhesion theory claimed that an adhesive adhered to a substrate due to the intermolecular and interatomic forces between atoms and molecules of the two

materials [13]. This was originally coined specific adhesion [58]. Pizzi [13] termed this adsorption/specific adhesion theory but had a separate covalent chemical bonding theory.

The study of secondary bonds between resin and wood was coined the adsorption or specific adhesion theory proper. Hydrogen bonds, electrostatic interactions, and van der Waals interactions appeared to play a role in wood adhesion. Electrostatic interactions tended to be repulsive and quite insignificant compared to van der Waals and hydrogen bonds between PF and cellulose from the wood substrate (Table 3). The dielectric constant of water was considered due to the residual moisture of wood. Pizzi [13] concluded secondary chemical bonds were the dominant mechanism for bonding wood. PF to crystalline cellulose and UF to amorphous and crystalline cellulose adhesion had been modelled as physicochemical adsorption due entirely to a balance of attractive and repulsive secondary forces at the interface of the substrate and adhesive [59]–[62]. Similarity between these theoretical calculated results and experimental results confirmed adsorption/specific adhesion by secondary forces was the most relevant mechanism for wood adhesion.

Table 3: Relative contributions (kcal/mol) of van der Waals, hydrogen bonds, and electrostatic secondary forces to the adhesion of species from a PF resin to wood cellulose [13]

	Van der Waals	Hydrogen bonds	Electrostatic	Total energy of cellulose–phenol interaction
o-Monomethylol phenol	−12.60	−0.23	0.64	−12.190
p-Monomethylol phenol	−10.77	−0.46	0.66	−10.567
o,*o*-Dimethylol phenol	−10.45	−0.77	0.67	−10.550
o,*p*-Dimethylol phenol	−12.47	−10.00	0.65	+3.119
PF dimers				
o,*o*-Dimer	−5.34	−7.75	0.77	−12.329
o,*p*-Dimer	−7.00	−5.81	0.73	−12.080
p,*p*-Dimer	−6.51	−4.37	0.68	−10.203

[a]Negative values indicate attractive secondary forces; positive values indicate repulsive secondary forces.

In primary bonds, the covalent chemical bonding theory was the prevailing theory thought to be present with adhesives, but it was difficult to prove. Under normal conditions, formation of covalent bonds between an adhesive and wood substrates had never been observed [63]. It was either not present or undetectable because there was a low proportion of covalent bonds compared with other bonds. Therefore, the author concluded that covalent bonding between resin and wood was either absent or negligible. Pizzi [13] showed that the methylol groups of PF react much faster with the aromatic nuclei of the adhesive than with the nuclei of the lignin in the wood substrate. MDI had been assumed to covalently bond with the hydroxyls of the wood substrate, but Johns [63] concluded that there was no covalent bonding between pMDI and the wood substrate due to the more likely reaction of MDI with water. The reaction of isocyanates from MDI with water to form polyurea proceeded at 7.4×10^{-6} L mol^{-1} s^{-1}, while hydroxyls from wood carbohydrates to form polyurethane proceeded at 2×10^{-7} L mol^{-1} s^{-1}, and aliphatic hydroxyl groups such as is found in lignin to form polyurethane proceeded at 6×10^{-6} L mol^{-1} s^{-1}. This demonstrated that isocyanates were more likely to react with water to form polyurea rather than with hydroxyls from wood to form polyurethane [64]. MDI and water were shown by Frisch et. al. to form polyurea which adhered to the wood substrate by secondary forces alone [65]. Therefore, the adsorption/specific adhesion theory was the primary theory of adhesion assumed in this work with wood adhesives due to primarily van der Waals forces and occasionally hydrogen bonding.

The wood/resin interface had three stages of adhesion: bond forming, liquid to solid, and durability. Bond forming was dependent on thermodynamic wetting and rheological properties. The adhesive should have lower surface energy than the substrate and must make contact on the molecular level to form a bond. Penetration of the adhesive into the substrate was related to good

bond formation and was thought to occur in wood either through the lumen or cell wall. Filling lumens was the original concept [66]. Penetration in the lumen depended on the viscosity of the adhesive, applied pressure, temperature, and time. Penetration in the cell wall could occur when the cell wall was partially removed or possibly through pits in the cell – although this has not been demonstrated [44]. High viscosity adhesives may not wet well especially with substantial microroughness of the substrate [67].

Wetting of the adhesive must occur before higher viscosity from solidification of the adhesive hindered the wetting. The liquid to solid stage of adhesion involved polymerization, loss of solvent, and solidification from the melt. Durability involved the de-bonding process which was due to viscoelastic energy dissipation. This can occur in all portions of the product (not just the wood-adhesive interface) and was also influenced through dimensional changes in the wood [44]. Adhesion theory was difficult to characterize – especially in the wood/resin interface. This work focused on the adhesive in the bulk (cohesion) due to these complexities by characterizing the curing kinetics of the wood adhesives studied.

Pressing theory

Several types of presses can be used in the manufacturing of oriented strand board (OSB): batch or continuous, steam injection, plate, and/or radio frequency or micro-wave heated [68]. A Wausau lab and pilot scale hydraulic press manufactured for pressing composite wood was used in this work because the primary interest was in a batch process with plate heating. There were several coupled physico-chemical-mechanical phenomena present in the pressing process, and there has been work performed modelling this complex process in batch conditions [69]–[72].

Pressing strand board is primarily controlled by pressure and temperature for a specified time. Heat and mass transfer are the main transport mechanism in this process. The heated press platens evaporated the bound water of the strands at the surface during the initial stage of pressing. This built up vapor pressure that drove the evaporated water to the cold center of the mat. This vapor would then condense in the cold mat center. The core temperature would gradually increase, and the water in the core would eventually vaporize. The increased vapor pressure would then drive the vapor to the surface, or outside boundary, of the mat and exit the mat [73].

This steam flow assisted heat transport but would subside as the water content of the mat was depleted. The rate of moisture and heat transfer depended on the structure geometry of the mat and how it was altered during the compression. A void volume occurs as a result of the compression process and flake geometry that always varied and created a pathway for fluid flow. Thermal conductivity, permeability, and diffusivity of the mat are changing during the pressing process [73].

Variability existed between other pressing processes because of these complexities, and a simplified model was necessary to discover the specific control parameters (temperature, pressure, and time) for proper transfer of heat to manufacture a composite board comparable to industrially manufactured boards. The density of the mat had a direct influence on the void volume. A pressing procedure was determined to be employed for experiments to form strand boards for testing neat and soy substituted resins used in the process. This work only considered the affected core temperature due to the variability of the density of the mat, or board density. Volume of the finished board was held constant. Therefore, density was manipulated by adjusting the total mass of the board.

Contact angle and resin spread

This work studied contact angles of resin droplets with and without soy products substituted into them. The surface free energy of the solid and the interaction energy between the solid and liquid were beneficial to this work but were deemed outside of the realm of this study due to the heterogeneity of the wood substrate (e.g. cellulose, hemicellulose, lignin, and micro-roughness). Therefore, a homogenous solid was used to minimize the effects of the interaction of the solid and liquid on the surface tension of the liquid. A glass surface was used because of the relative smooth surface and non-reactivity with the resin as compared to a wooden surface. Contact angles of the liquid resin and the effect of the contact angle with soy substituted into the resin were related to the spread of the resin droplet. The resin droplet geometry was of interest because of the application of the resin during the blending process was affected by the resin spread of these droplets. A smaller resin spread would inhibit the coating of the strands and therefore decrease the coated strand contact area. Board density was also considered in the resin spread study.

Thermogravimetric Analysis (TGA)

In thermogravimetric analysis (TGA), the thermal analyzer measures the amount and rate of weight change in materials as a function of temperature and/or time in a controlled environment. The thermal analyzer could be used to measure both physical and chemical changes in a sample by studying responses due to increasing temperature (constant heating rate) or time (constant temperature or mass loss) [74]. Decomposition, oxidation and reduction, and sorption/desorption of volatiles could be detected via a material's weight change during these reactions due to thermal treatment. The weight change during these reactions can be correlated

with different characterization of the material such as chemical structure, processing, and end-use performance [75].

This work studied TGA data to analyze mass loss with a constant heating rate and mass loss at constant temperature. The mass loss at a constant heating rate of resins with and without SF substituted into them was analyzed to determine any variations in reaction kinetics. TGA data was also analyzed to determine new or missing mass loss events that could signify other reactions between SF and the resin. This data was also used in isoconversional kinetic analysis to describe the curing kinetic relationship between soy products and the resin by calculating the activation energy.

The mass loss data was referred to as TGA data throughout this work. This mass loss was also differentiated with respect to temperature and was referred to as derivative TGA (DTGA) data throughout this work.

The DTGA data was analyzed to define temperature zones of weight change events to characterize specific reactions occurring due to thermal treatment. The liquid PF contained water to aid in wetting during interface with the wooden substrate. Although the samples were vacuum dried, there was an expected amount of water bound in the sample. This water loss was expected in the lower temperature zone as well as low molecular weight monomers that were being released from the resin.

The DTGA data was expected to show peaks at certain temperatures representing the maximum amount of weight loss occurring at that temperature. This maximum weight change that occurred at that temperature represented the maximum reaction rate occurring for that weight loss event. This temperature was referred to as the DTGA temperature peak throughout this work.

Activation Energy was calculated using the Kissinger equation:

$$-\ln\left(\frac{\beta}{T_p^2}\right) = -\ln\left(\frac{AR}{E_\alpha}\right) + \frac{E_\alpha}{RT_p} \quad (1),$$

where β was the time rate of change of the temperature (temperature ramp), T_p was the temperature at which the maximum reaction rate occurred (DTGA temperature peak), A was the pre-exponential factor which accounted for both the rate of molecule collisions (when all component concentrations were 1 mol/L) and molecule orientation during collision [76], E_α was the activation energy, and R was the universal gas constant. Plotting $-\ln\left(\frac{\beta}{T_p^2}\right)$ versus $1/T_p$ at varying temperature ramp rates developed a linear relationship. The activation energy and frequency factor could then be solved for using the slope and y-intercept from that line [77]–[79]. An example of this using TGA data from PF was performed by Chen et. al [80].

Differential Scanning Calorimetry (DSC)

The differential scanning calorimeter (DSC) analysis uses temperature measurements of a sample and reference which were used to calculate the differential heat flow. The following equation was used for the DSC analysis performed in this work:

$$q = -\frac{\Delta T}{R_r} + \Delta T_0\left(\frac{R_r - R_s}{R_r R_s}\right) + (C_r - C_s)\frac{dT_s}{dt} - C_r\frac{d\Delta T}{dt} \quad (2),$$

where q was the sample heat flow, ΔT was the measured sample temperature (T_s) minus measured reference temperature (T_r), ΔT_0 was the measured base temperature of the sensor minus the measured sample temperature (T_0-T_s), T_0 was the temperature for the control, R_r was the reference sensor thermal resistance, R_s was the sample sensor thermal resistance, C_r was the reference sensor heat capacity, and C_s was the sample sensor heat capacity. The equation did not account for pan heat flow effects [81].

Even though DSC was described as the preferred analysis for reaction kinetics using the Kissinger equation in the prior section due to differential data, there were disadvantages to using DSC analysis for this work. The DSC instrument required a hermetically sealed sample due to the release of volatiles from PF that could affect the sensitivity of the machine. There was still a risk of exposure with the hermetically sealed pans since the standard TA pans were only rated to 300 kPa of pressure or lower. These pans also required a smaller sample size which led to less accuracy in the measurements. Higher pressure rated pans (up to 10 MPa) were more expensive and led to more resistance in the pan wall due to its thickness. As stated before, the pan heat flow was not accounted for in equation (2) used for the Q100 DSC.

The TGA thermal analyzer did not require a closed vessel for the material being tested. As stated before, weight changes attributed to reactions could be used alternatively. Reusable pans and ease of use also led to a larger sample size attaining higher accuracy in the results.

Fourier Transform-Infrared (FT-IR) Analysis

The FT-IR spectrometer is used to obtain an infrared spectrum of the absorption or emission of a solid, liquid, or gas. This infrared spectrum can be analyzed to characterize the chemical structure of a substance. A solid sample was analyzed in most cases in this work. Liquid samples were analyzed when possible.

The attenuated total reflectance (ATR) accessory was employed in this work. Prior published literature using FT-IR analysis with resins commonly used the ATR accessory which reflects the infrared beam off of the sample rather than transmits the infrared beam through the sample [82]. The machine used was a PerkinElmer Spectrum 100 FT-IR Diamond ATR. This allowed the infrared beam to reflect off the sample rather than pass through it. This work analyzed the spectra from PF and pMDI samples to observe peaks associated with functional

groups. SF substituted into PF and pMDI samples were also analyzed. The neat resin spectral analyses were compared to the soy substituted resin spectral analyses by measuring the magnitude, area, and location peaks associated with a chemical structure. Varying thermal treatments were employed to all samples to analyze the polymerization reactions occurring in the samples.

Phenol Formaldehyde and Soy Product Reactions

Prior published work has been performed on soy product substitution in PF [34], [83]–[86]. Wescott, Frihart, Lorenz, et. al. had shown the most promising application with soy flour substitution in PF. They showed that the adhesive mechanism change occurred in the bulk adhesive due to crosslinking between the SF and PF – cohesion. The soy flour required modification through denaturation followed by exposure to formaldehyde. The mixture was then subjected to phenol and more formaldehyde in the synthesis of the soy flour substituted resin. The soy flour likely reacted with the excess formaldehyde rather than the methylated phenol present in the PF resin. The authors also noted that the possibility that the soy flour being trapped in the PF crosslinking network could not be ruled out [11], [34], [84], [85], [87].

Kuo, et. al. showed work with a modified aqueous soy flour with a crosslinking agent added to it. One possible crosslinking agent described was PF, but the PF had to be conditioned to a neutral pH instead of an alkaline pH which was typical for commercial PF resins to extend pot life. This treatment had also assumed longer curing times than what was needed for industry performance – 10 minutes compared to 2-3 minutes of press time that was typical in industry. There was mention of shorter press times (7 minutes) by implementing a powder form of the soybean-based adhesive, but costly freeze-drying or spray drying was needed. The formaldehyde:phenol ratio of the prepared PF used in the Kuo, et. al. work was also very high

(2.4:1) which increased the formaldehyde content of the finished product. There was likely a reaction with excess formaldehyde methylating the soy flour as was described in the Wescott, Frihart, Lorenz, et. al. work [11], [34], [84], [85], [87] instead of the reaction described by Kuo, et. al. between methylated phenol and soy flour. The blending process also required a 7% adhesive loading (dry weight basis) of the soybean-based adhesive resin which was compared with a lower 5% adhesive loading of commercial PF resin. Both adhesive loadings were higher than typical adhesive loadings used in industry (2-4%). The wood flakes also had to be dried to about 6 weight percent moisture due to the extra water in the soybean-based adhesive [27].

This work differed from the prior published works in that it incorporated defatted soy flour with a commercial PF in the strand board forming process. This was a more industry friendly approach. The existing materials were used (commercial PF), and there would be minimal new equipment needed since the soy flour could be incorporated during the blending process. There was a decreased cost involved with this work due to no pretreatment of the soy flour and the use of the cheaper defatted soy flour. Decreased pot life also occurs with the pretreatment of soy products and their incorporation into the PF resin before the board forming process.

The hypothesis for the work with phenol formaldehyde (PF) and defatted soy flour (SF) was that SF chemically interacted with PF to modify the overall adhesive in the bulk (cohesion) to a higher degree than the wood/resin interface (adhesion). Frihart, Wescott, Lorenz, et. al. had shown that SF crosslinked with PF and assumed the chemical interaction occurred through amino acid side chains in the soy protein becoming methylated due to reaction with formaldehyde [11], [34], [84], [85], [87]. One likely reaction pathway would involve a methylated soy protein to react with free ortho and para sites in phenols and methylol groups

from PF. Another possible condensation reaction pathway would involve methylene linkage or ether linkage with hydroxyls from the soy protein reacting with either an open site or a methylol group on a methylated phenol (Figure 20). Another possible condensation reaction could occur between both methylol groups from soy protein and PF (methylated phenol) to form a methylene bridge or an ether bridge (Figure 21).

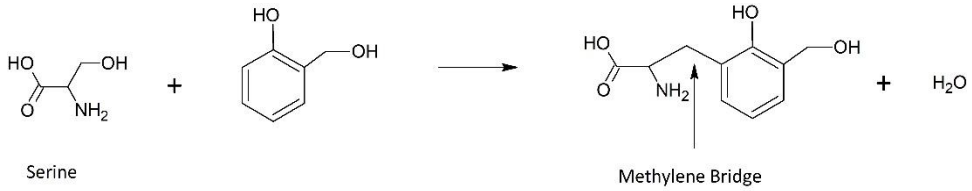

Figure 20: Possible reaction between serine from soy protein and PF forming methylene bridge

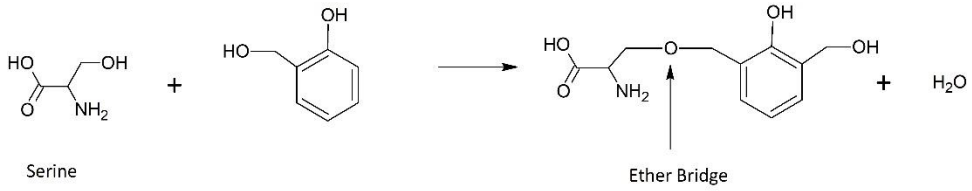

Figure 21: Possible reaction between serine and PF forming ether bridge

Verifying or disproving this hypothesis either corroborated the assumption that PF and soy flour crosslink during the curing process as had been suggested in prior published work or refuted the hypothesis thereby showing little to no crosslinking between PF and SF under the conditions set forth in this work. In the case of disproving the hypothesis, the primary adhesive mechanism altered due to SF interaction with PF would be assumed in the wood/resin interface. There were only two possible mechanisms that could be altered due to adhesive modification – adhesion or cohesion (a failure in unadulterated wood was not considered since there was no adhesive interaction).

Verifying or disproving the hypothesis in this work expanded on the knowledge of the interaction with PF and SF. The scientific community could employ this knowledge to better engineer soy products designed to interact with PF. A modification of PF could be engineered to better interact with the SF during the pressing process. Verifying or disproving the hypothesis would also aid in showing how soy product substitution could influence a change in either crosslinking in the bulk or interactions in the wood/resin interface. Prior modelling studies that had been published with wood adhesives could be used with this data [73], [88], [89].

pMDI and Soy Product Reactions

There has been little past published work incorporating soy products with pMDI and most have used modified soy products. Amaral-Labat, et. al. used glyoxalated soy flour with tannin and pMDI. This process decreased the amount of formaldehyde by incorporating glyoxal to functionalize the soy flour, but this soy flour was not a defatted soy flour (25.4% lipids) [8]. Zhang, et. al. showed work using denatured SPI and small amounts of MDI in resin formulations, but this required the higher protein containing SPI and modification for use [90], [91]. Zhong and Sun worked with SPI, polycaprolactone, and very small amounts of MDI (up to 5%) [92].

This work differed from the prior published works in that it incorporated defatted soy flour with a commercial pMDI in the strand board forming process in a similar fashion as the PF and SF in this work. It was also more industry friendly due to using existing resins and minimal equipment upgrades. There was also a decreased cost involved with this work due to no pretreatment of the soy flour and the use of the cheaper defatted soy flour. Decreased pot life was also considered a disadvantage to processes mixing soy products with the pMDI resin before the board forming process.

The hypothesis for the work with pMDI and defatted soy flour (SF) was that SF chemically interacted with pMDI to modify the overall adhesive in the bulk (cohesion) to a higher degree than the wood/resin interface (adhesion). A possible reaction pathway between pMDI and SF would involve urethane linkage due to the isocyanate group from pMDI reacting with a hydroxyl group from SF. This hydroxyl group could come from numerous sources in the SF (i.e. proteins or carbohydrates). A possible reaction was given in Figure 22 as an example with one of the amino acid side chains, arginine. It was not considered to be the only reaction occurring to produce urethane linkage in this work. Another possible reaction pathway between pMDI and SF could involve urea linkage due to the isocyanate group from pMDI reacting with an amine group from the SF. Again, a possible reaction was given in Figure 23 as an example with the amino acid side chain, serine, but it was not considered the only reaction occurring between pMDI and SF.

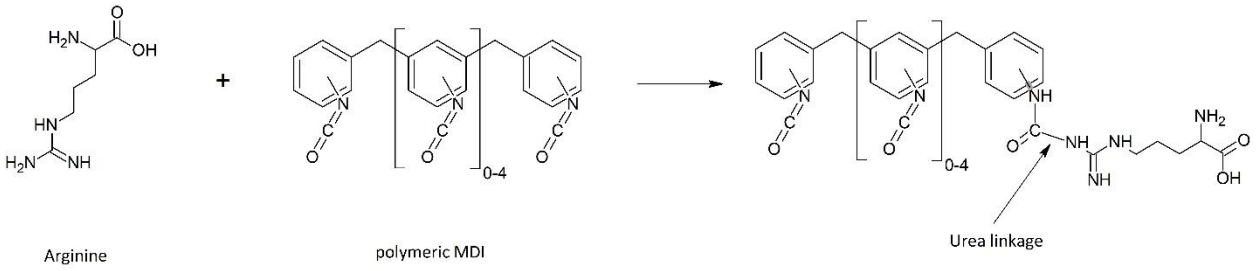

Figure 22: The reaction between a primary amine of arginine and polymeric MDI

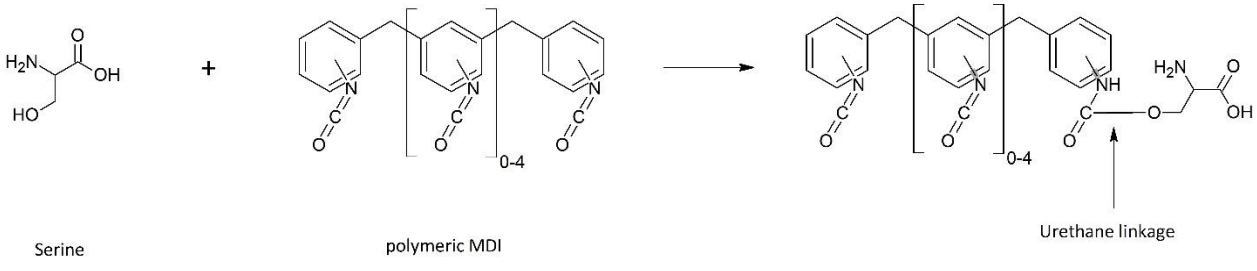

Figure 23: The reaction between a hydroxyl of serine and polymeric MDI

Verifying or disproving the hypothesis with pMDI and SF, like the PF and SF work, would corroborate the assumption that pMDI and soy flour crosslink during the curing process as the primary mechanism or would refute the hypothesis thereby showing little to no crosslinking between pMDI and SF under the conditions in this work. In the case of disproving the hypothesis, the primary adhesive mechanism altered due to SF interaction with pMDI would be assumed in the wood/resin interface.

Verifying or disproving the hypothesis in this work expanded on the knowledge of the interaction with pMDI and SF. The scientific community could employ this knowledge to better engineer soy products and pMDI for use in the strand board forming process as well as better model the pressing process, similar to the PF and SF work.

Chapter 2: Screening Experimental Set-up

Introduction

Experiments were designed to test the hypotheses pertaining to SF substitution in synthetic wood adhesives and pressing conditions. Initial experiments were required to verify testing methods to properly compare SF substituted resins with their neat resin counterparts. A lap shear test was conducted to observe the effect of soy protein on phenol formaldehyde without the complexities of the strand board produced. Strand board formation was involved with most of the experiments in the first phase of this work. Proper strand board formation was required to compare the resins. A temperature profile experiment was performed to model the heat and mass transfer to the center of the mat during pressing so that control parameters could be determined for best pressing conditions. Strand boards were then formed at differing densities to determine the effect of either neat or SF substituted resin on flexural strength and modulus. Contact angles were measured to relate them to droplet geometry and thusly resin spread of neat and soy substituted resins. Finally, a design of experiment was performed on strand boards to measure the modulus of rupture and elasticity and its effect from varying soy substitution and total adhesive loading.

Experimental

Materials

The liquid phenol formaldehyde (aqueous) used was a commercial GP® 240C11 RESI-STRAN® intended for bonding Oriented Strand Board (OSB) supplied by Louisiana Pacific Corp. that was used in all experiments using liquid PF (Table 1). The powder Phenol Formaldehyde (PF) was a GP 190C80 Woodweld® intended for bonding Oriented Strand Board resin supplied by Huber Corp. that was used in all experiments using powder PF.

Table 4: Properties of Phenol Formaldehyde Adhesive [93]

Characteristics	Liquid PF Adhesive
Appearance	red to brown
Specific gravity	1.21
pH	10.6
Boiling point	100 °C
Solids content	52%
Free formaldehyde content	<0.1% by weight

The polymeric methylene diphenyl diisocyanate (pMDI or MDI) used was MONDUR 541, Materials #: 5212146 and supplied by Bayer Material Science LLC. Moisture content was assumed zero for mixing applications. All uses of the acronym MDI were intended to refer to polymeric MDI unless specifically noted – this includes the use of neat MDI referring to neat pMDI.

Soy protein isolate (SPI) was used in the form of Pro-cote 4200 soy and was donated by Solae, LLC. SPI contained about 90% protein [29]. Moisture content was assumed zero for mixing applications. Defatted soy flour (SF) was provided by Archer Daniels Midland. This soy

flour was labeled 7B meaning it was minimally heat processed and most nearly resembles the native defatted raw soybean [94]. It was labeled as having a very fine grind. Soy protein constitutes about half of the mass of soy flour [29]. Moisture content was assumed zero for mixing applications.

The emulsified wax (aqueous) used was a Hexion Bord'N-Seal(TM) FMH-XD and was provided by Huber Corp. Solids content was reported as 47%. Wood strands were supplied by Huber Corp. and taken from storage in the Forest Products Laboratory at Auburn University. These were Southern Yellow Pine variety or more specifically, loblolly pine (Pinus taeda).

Wooden laps were cut from loblolly pine (Pinus taeda) 2”x4” boards acquired from Lowe’s Department Store to be used in the lap shear test. The wood samples were cut according to standard DIN EN 205 with the dimensions 80 mm long, 20 mm wide, and 5 mm thick [95].

Lap Shear tests

Lap shear or tensile testing is a method of testing an adhesive by pulling bonded layers apart along the plane of adhesion. Lap shear tests were used to find the tension at maximum force of the adhesive. The tension was an indicator of the adhesive strength when the test was performed properly and could be used to calculate the shear stress of the adhesive. These tests were performed to characterize the strength of the adhesive with and without soy protein substituted. A higher protein containing soy product, SPI, was used to focus on the effect of protein on the adhesive and negate the effects of other components of soy – such as carbohydrates.

Wooden laps were used in lap fashion to hold the adhesive during the shear test. The wood samples were cut according to European standard DIN EN 205. The standard DIN EN 205 was used because of the smaller lap shear overlap area, or glue line, compared with other

standards (10 mm X 20 mm). The smaller area decreased the possibility of wood failure which increased the possibility of total adhesive failure for better test results [95].

The wood specimens were cut so that the grain was parallel to the length to ensure complete failure in the adhesive only. All laps were conditioned at 65% RH and 22 °C. The dimension for the overlap area to where the adhesive would be applied was 20 mm wide by 10 mm long (Figure 24). 0.05 g of the resin was applied to the overlap area on a wooden lap. This equated to 125 g/m^2 adhesive loading. Another lap was pressed on the overlap area to distribute the adhesive evenly over the area of both laps. The laps were then wrapped with aluminum foil.

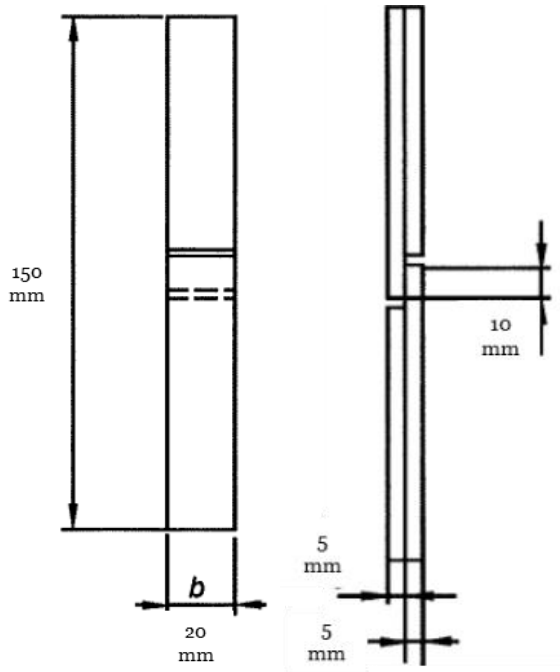

Figure 24: Overhead (left) and side (right) view of lap shear samples [95]

Lap shear samples were then pressed in a 23 cm x 23 cm press (Figure 25) with platens heated to 150 °C and 1.38 MPa for 10 minutes. The gauge pressure was calculated with the following equation.

$$P_{gauge} = P_{sample} \frac{A_{sample}}{A_{piston}} \quad (3),$$

The area of the piston was calculated with a 47.6 mm diameter piston, and area of the sample was calculated as the total overlap area of 6 samples (6x10mmx20mm). The gauge pressure was calculated at 135 lb/in^2. The samples were then put into a mechanical convection oven at 100 °C for 4 hours to cure the adhesive.

Figure 25: Press used for lap shear samples

This cured sample was then mounted in a material tester. A shear force was then applied to the lap shear sample intended to test the shear strength of the adhesive. The lap shear test was performed on a Zwick/Roell Z010 Static Material Testing Machine. The samples were loaded vertically with a grip to grip separation of 90 mm. The rate of traverse used was 6 mm/min. The operation of the equipment and the analysis of the data was performed by the testXpert® II software.

Figure 26: Zwick Roell static material testing machine with a lap shear sample

The adhesive shear strength of the resin mixture for the wood-to-wood system was found by measuring the shear stress by the single lap-shear method and compared with that of untreated phenol formaldehyde resin following standard DIN EN 205. The shear stress was found by the following formula:

$$\tau = \frac{F_{max}}{A} \quad (4),$$

where τ represented the shear stress, F_{max} represented the maximum force that the sample underwent, and A represented the adhesive overlap area [95].

Resin Contact Angle Measurement

Contact angles of the resin were measured to describe the droplet geometry. This experiment primarily focused on the measurement of the contact angle of the liquid PF resin and its effect with soy product substituted into it. This information was needed to describe the droplet application during the blending process, but more importantly it was needed to describe the resin spread during the pressing process.

An experiment was set up to measure the contact angle of resin droplets with and without soy addition to liquid PF resin. The objective of the experiment was to describe a relationship between contact angle and resin spread. The resin spread was investigated due to its influence of adhesive application which was assumed to change during the pressing process due to higher and lower board densities. Contact angles of resin droplets on glass were measured by the sessile drop method with PF resin containing 0-10% ProCote. The soy protein isolate (SPI) was used in place of soy flour to remove the contribution of undissolved material to surface roughness. Ideally, the base surface should be wood, but the effect of ProCote on the contact angle was expected to be small, and surface roughness and the inhomogeneity of wood would add to measurement uncertainty [96], [97].

SPI was added to PF at a rate of 10% SPI substitution in the PF (dry weight basis). The mixture was mechanically stirred with a glass stirring rod until visually uniform and homogenous. Approximately 100 μL of adhesive was then dropped on a glass slide with a micro-pipet in the sessile drop fashion. Images were taken with a high-resolution camera. Contact angles from both sides of the drop were calculated with Drop Image software. The slide was cleaned with acetone between each sample. A total of 25 replicates were taken for each group.

Adhesive mixing

Liquid PF and soy flour or soy protein isolate (SF or SPI) were weighed out according to their representative dry wt. % for the total adhesive. Mixtures were labeled throughout this work with the amount of soy product substituted in them: dry wt. soy product (SPI or SF)/total dry wt. resin (PF and soy product). The soy was added to the PF, and the liquid PF mixtures were mechanically mixed in a glass beaker with glass stirring rod until the sample was visually uniform and homogenous.

Strand Board Forming

The Wausau lab and pilot scale hydraulic press manufactured for pressing composite wood was used for all pressing of strand boards. This press was used for batch processes and used heated platens. Ingredients were gathered by calculating the percentage dry weight of the total product. Wood strands were dried at 100 °C until the desired moisture content of the strands was achieved (~6-10%).

There were two methods used in this work for the adhesive application onto the strands or blending step. The first involved putting enough strands for two boards in a large plastic garbage bag and distributing the adhesive (liquid or powder) uniformly onto the strands. The bag was then closed and shaken until the adhesive was distributed onto the strands. This was referred to as the "bag" method throughout the paper.

The other method involved using a concrete mixer (Figure 27) and a paint sprayer. Enough strands for two boards were deposited into the cement mixer and covered with a vinyl covering to reduce spray drift. A paint sprayer was then used to apply an emulsified wax while the chips were tumbled in the concrete mixer. The wax was applied at 1% dry wt./dry total board wt. This step was skipped for experiments not using wax. The adhesive was applied between 2% and 6% dry wt. adhesive/dry total board wt. This percentage application was referred to as total adhesive loading and was specified in each experiment.

Figure 27: Cement mixer used for adhesive application [98]

Liquid resins were applied in short bursts using the paint sprayer evenly over the strands as they were tumbled in the concrete mixer. Dry resins (e.g. powder PF) were applied while the mixer was stationary for safety reasons. About a fifth of the powder resin was distributed evenly over the strands each time the mixer was stopped. The mixer was allowed to tumble the strands for approximately 1 minute between each application of powder resin. The application process was repeated until all resin was applied. The mixer was allowed to tumble the strands for approximately another 10 minutes after all resin was applied to ensure full distribution of either liquid or powder resin. This was referred to as the "concrete mixer" method throughout the work.

The coated strands were then transferred to a forming box (Figure 28 – left) placed on a metal sheet and distributed evenly in the box. A board with the same dimensions as the inside of

the box was pressed on top to compress the mat and test the distribution of the strands. If there was not a uniform distribution, strands were redistributed in a way to compensate for a better distribution. When the strands were distributed evenly, the board was pressed onto the strands again while the forming box was lifted. The board was taken off, and any fallen strands were placed on top of the mat. Another metal plate was then placed on top of the other plate "sandwiching" the formed strands between the two plates. Aluminum foil was used between the strands and metal plates in the cases of pMDI resins to aid in the release of the board from the metal plates after pressing. The formed strands were then pressed between the two metal plates in the Wausau hydraulic press (Figure 28 – right). Two metal bars were used on either side of the pressed strands as guides to maintain the targeted thickness of 11 mm. The temperature of both platens of the press was 204 °C with a total pressing pressure sufficient to reach the thickness guides. A pressure setting of 2.0 MPa was used to ensure the mat was compressed enough to reach the guides. Target density ranged from 0.48 to 0.64 g/cm^3 for total board weight. The press time varied from 2.5 to 4 minutes.

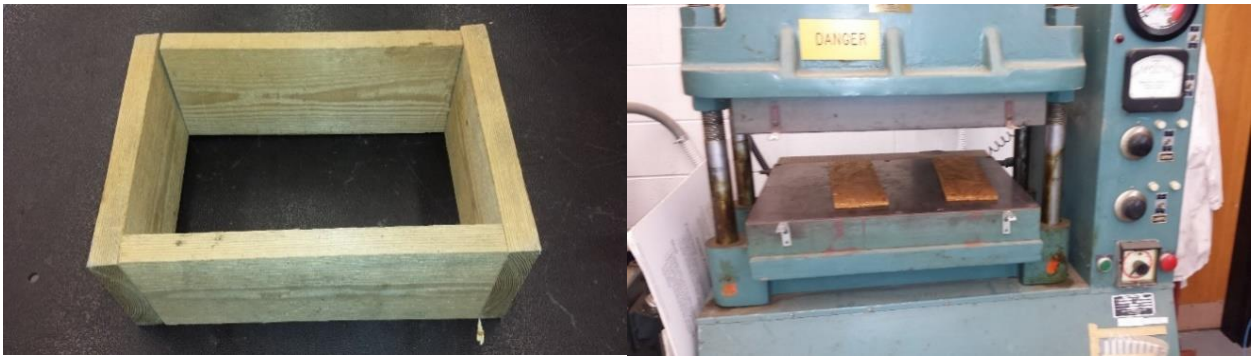

Figure 28: Forming board (left), 21 cm X 31 cm. Wausau press used for strand board pressing (right)

The "sandwiched" metal plates were then taken out of the press where the top plate was taken off. The formed board was taken and weighed. This weight was compared with the

expected weight for the target density since all volumes were the same. Adjustments in density were made to next samples if needed. These boards were then stacked on top of each other as the cure still proceeded. The samples were left stacked for 24 hours since stacking them inhibited heat loss that aided in further curing – referred to as “hot stacking”.

The sample boards were then cut into samples for testing according to ASTM D1037-12. Density was calculated for all cut samples by measuring mass, length, width, and thickness according to the standard [10]. An example of cut samples can be seen in the following figure.

Figure 29: Testing strips cut from strand boards

Strand Board Testing (ASTM D1037-12)

All cut samples were tested according to the ASTM D1037-12 standard [10]. The Zwick/Roell Z010 Static Material Testing Machine was used to test physical properties unless otherwise stated.

Strand board samples referred to as wet boards were soaked for 24-hours continuously (method B) according to the ASTM D1037-12 standard. The samples used for thickness swell (TS) and water absorption (WA) were cut in 152x152 mm sections and laid horizontally while soaking. The samples used for wet MOR and MOE were cut according to the testing method and laid horizontally while soaking. Water was maintained at a level of 25 mm above the specimens while soaking [10].

Thickness of the strand board was measured at four points midway along the board (one on each side) 25 mm into the board using a caliper before and after the soak. Weight was also recorded before and after the soak. Samples were allowed to drain on a rack for 10 minutes after the soak before wet measurements were taken. Thickness swell was taken as the difference between the average thickness before and after the soak (%). Water absorption was calculated as the difference in mass before and after the soak (%). Wet MOR and MOE samples were tested after the 10-minute drain [10].

Standard ASTM D1037-12 [10] was used to prepare the strand board samples and perform the tests to measure the flexural strength and flexural modulus of the boards. Flexural strength and modulus of rupture (MOR) were used interchangeably in this work because they represent the same measurement. Similarly, flexural modulus and flexural modulus of elasticity (MOE), or modulus of elasticity, were also used interchangeably in this work.

The samples were loaded with longer strands facing down to ensure maximum breaking force was achieved. Modulus of rupture and elasticity were tested on the Zwick/Roell Z010 Static Material Testing Machine. The MOR and MOE were calculated from one experimental run during a three-point bending test described in detail later in the chapter. An example of a sample being tested for MOR and MOE can be seen in the following figure:

Figure 30: Strand board testing strip being tested in the Z010 static material tester

Dry samples were referred to as dry MOR and MOE and were not subjected to any soaking treatment. Wet samples were also tested and specified as wet MOR or MOE when performed. Samples were soaked according to the 24-hr soaking method described above. TS and WA measurements were taken before MOR and MOE tests were performed. Wet boards were then tested in the same fashion as dry MOR and MOE [10]. MOR was calculated using the following equation:

$$R_b = \frac{3P_{max}L}{2bd^2} \quad (5),$$

where b was the width of the specimen (mm), d was the thickness of the specimen (mm), L was the length of span (mm), P_{max} was the maximum load (N), and R_b was the modulus of rupture (MPa) [10].

The modulus of elasticity (MOE) was a measure of stiffness. By measuring the MOE, one can characterize the deformation that the sample has. Higher MOE shows plastic deformation while lower MOE shows elastic deformation. Higher MOE was desired in wood composites. MOE was calculated using the following equation:

$$E = \frac{L^3}{4bd^3}\frac{\Delta P}{\Delta y} \quad (6),$$

where *ΔP/Δy* was the slope of the straight-line portion of the load-deflection curve (N/mm) and *E* was the modulus of elasticity (kPa) [10]. Calculations for MOR and MOE were performed by the testXpert® II software.

Internal bond was measured according to the ASTM D1037-12 standard and described as a tension test perpendicular to the surface of the specimen. Samples were cut 50 mm square. Aluminum blocks were glued to each of the square faces of the specimen. The sample was then loaded into the loading fixture on the Zwick/Roell Z010 Static Material Testing Machine for testing [10]. An example of the fixture schematics can be seen in the following figure.

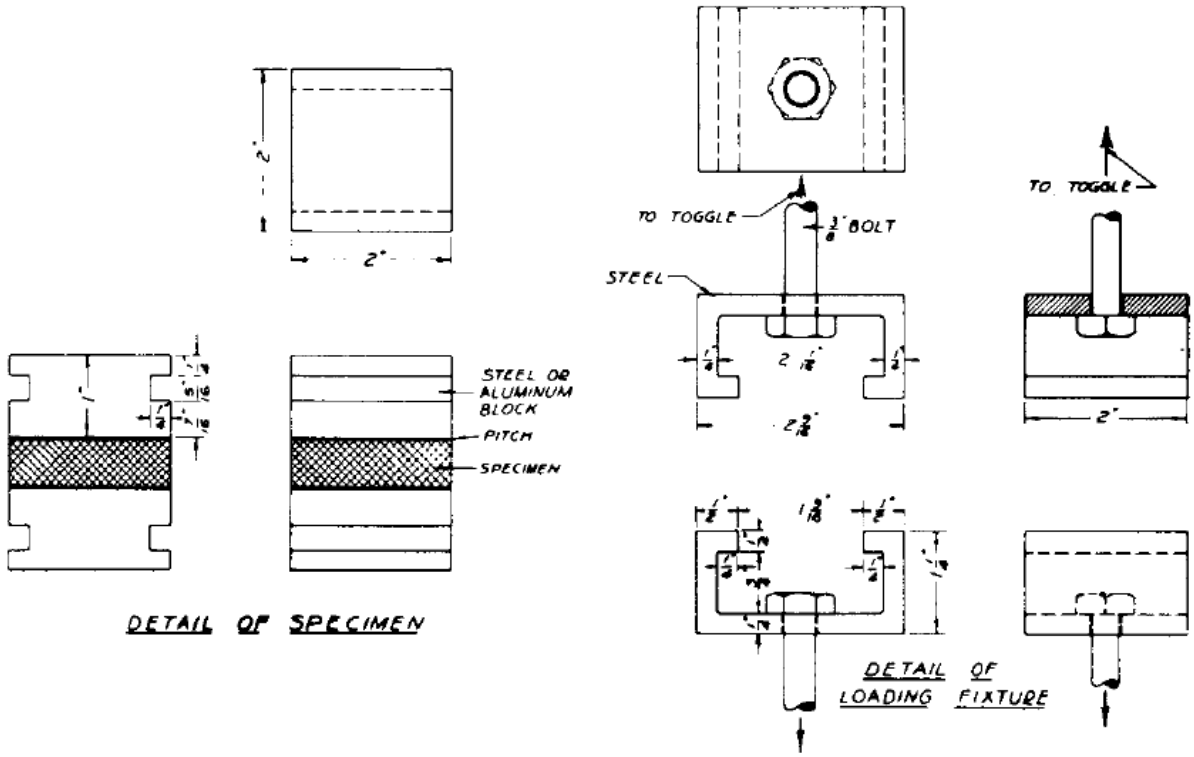

Figure 31: Detail of specimen and loading fixture for internal bond measurement [10]

The internal bond was calculated using the following equation:

$$IB = \frac{P_{max}}{ab} \quad (7),$$

where *IB* was the internal bond strength (MPa), P_{max} *was* the maximum load (N), *a* was the width of the specimen measured in dry condition (mm), and *b* was the length of the specimen measured in dry condition [10]. Calculations were performed by the testXpert® II software.

Design of Experiment: vary adhesive loading and SF

A design of experiment was performed by varying the total adhesive loading and substituted SF in the resin. The objective of the experiment was to test whether more adhesive present in the mat influenced the strength and stiffness of the board – especially in wet properties. An optimum operating range for adhesive loading with and without soy substitution in the resin was also determined in the process.

The Box-Behnken Surface Response design of experiment [99] was used as opposed to a full factorial design. The Box-Behnken design focused on the midpoint of operating parameters which carried an advantage when operating at high or low conditions which could be detrimental to the process (e.g. operating at an elevated temperature which could degrade the equipment). It was also useful in cases of difficulty in producing a high number of samples needed for a full factorial design.

The higher board density of 0.64 g/cm^3 (40 lb/ft^3) was chosen because it was normally used for specialty boards requiring higher physical characteristics in manufacture of OSB. The 0.48 g/cm^3 (30 lb/ft^3) density was chosen for the lower range because a higher void volume would occur in the wood structure leading to dimensional failure of the board. The adhesive loading low range of 2% (dry wt. adhesive/dry wt. board) was used because this was the lower limit used in industry. The upper range was used because 6% had been used in some works but

was typically lower in the industry. The soy substitution upper range of 10% was used because prior tests showed that wet properties would fail without wax addition when compared with the control PF (0% soy – lower range). The following parameters were used in the design:

- Board Density: low-0.48 g/cm^3 (30 lb/ft^3), mid-0.56 g/cm^3 (35 lb/ft^3), high-0.64 g/cm^3 (40 lb/ft^3)
- Total Adhesive Loading: low-2%, mid-4%, high-6%
- Soy Substitution: low-0%, mid-5%, high-10%

Liquid PF and SF substituted into liquid PF were used as the resins for this experiment. Dry and wet flexural strength and flexural modulus were measured as the response. The boards were prepared according to the blending procedure described as the "bag" method. Sample boards were tested according to the methods described in the strand board testing procedure.

The Box-Behnken Surface Response design of experiment was fashioned according to the work of Myers and Montgomery [99]. There was a total of 30 boards formed with 13 variations of parameters (6 boards were formed with all midpoint parameters). The design layout was randomly listed using Minitab software, so the samples could be tested without bias.

Temperature Profile for Strand Board Pressing

A pressing procedure was required in the development of the experimental design which involved forming strand boards for testing neat and soy substituted resins. There were several coupled physico-chemical-mechanical phenomena present in the pressing process, and these were primarily controlled by pressure and temperature for a specified time.

A simplified model was necessary to define the specific control parameters (temperature, pressure, and time) for proper transfer of heat to manufacture a composite board comparable to industrially manufactured boards. The density of the board formed had a direct influence on the

void volume, or the space between strands. The temperature profile experiment applied the core temperature affected by the density of the mat to describe the heat transfer during the pressing process.

A strand board sample was formed without adhesive added. Three densities were employed: 0.46, 0.53, and 0.60 g/cm^3. A temperature probe was inserted into the center of the strands. The sample was then pressed while the temperature was recorded at intervals of 10 seconds.

Results and Discussion

Lap Shear Experiment

The first experiment involved a lap shear test using soy protein isolate (SPI), which has a protein content higher than soy flour (~90% versus ~50%), substituted into liquid PF. It was observed that the 30% soy substituted into liquid PF was thick compared with the other formulations although viscosity was not measured. Soy protein substitution in phenol formaldehyde has been shown to increase the viscosity in Wescott and Frihart's work [84]. The thickness of the PF with the added soy was cause for concern as there was a viscosity limit on spinning disc atomizers used to distribute the adhesive in the manufacturing blending process. Wescott and Frihart also described soy-based resins as thixotropic [84]. The thickness observed could be misleading as the high shear of the atomizers could lower the viscosity enough to be used. Temperature must also be considered as higher temperatures were likely to lower the viscosity.

It was expected that the SPI substituted resins would have equal to higher shear stress than SF substituted resins because of the higher protein content. It was also expected that the

heat from the lap shear press as well as the water content from the liquid PF would hydrolyze the soy protein to increase adhesive performance.

The following figure displays the shear stress measured from lap shear tests using neat PF and SPI substituted into PF at 10, 20, and 30%.

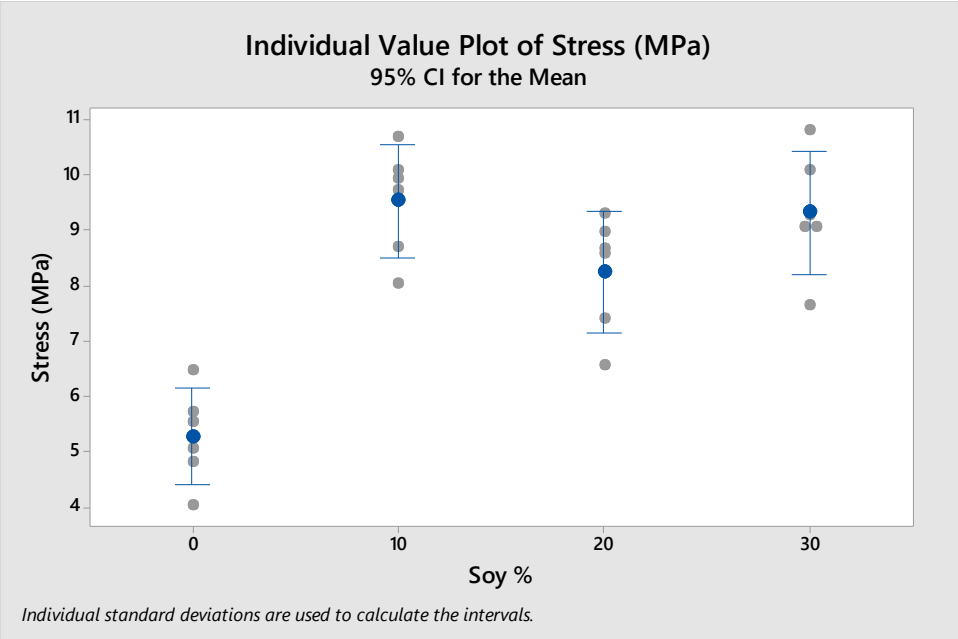

Figure 32: Lap Sheer stress of PF (control) versus different percentages of SPI substituted into PF

This initial test showed an improvement in shear stress of about 80% with just 10% SPI substituted into PF. There were not any significant increases in strength with additional soy substituted.

This supported the assumption that soy did hydrolyze from the heat from the press, but no significant increase of shear stress was observed with higher SPI substitutions than 10%. In the case of affecting the wood/resin interface, perhaps there was a limit to the ingress of the adhesive which was met at 10% SPI substitution affecting the adhesiveness to the wood substrate. This prompted more experimentation necessary to confirm this.

Temperature Profile for Strand Board Pressing

An experiment was performed to measure the temperature of the center of a strand board being pressed as a function of time and density. This experiment was performed to measure the time needed to reach full vaporization of the water in the center of the mat determined at different densities. An optimum pressing temperature of 140 °C has been reported by Lee, et. al. for a continuous press in the manufacture of OSB [100]. This temperature was also observed in the temperature profile experiment.

It was expected that the lower density would increase in temperature at a higher rate than the higher density mats because of the lower mass of water. It was also expected to observe a plateau of the temperature change with respect to time due to the vaporization of water in the board to steam (referred to as plateau temperature). It was also expected that this plateau temperature would be slightly above 100 °C due to the pressure exhibited on the strands from the press.

The pressed mat reached vaporization temperature at about 80 seconds after pressing for all densities (Figure 33). This was not expected. The higher densities contained more wood and water mass. Water flashed to steam at the surfaces, and higher vapor pressures transferred heat to the center of the mat. The high density mats contained more water. Therefore, more water could transfer more heat as steam increasing the heat transfer at a higher rate. This higher heat transfer could increase the temperature of the high density mats at approximately the same rate as the low density mats. This was ruled out because of the behavior of the temperature increase of all boards after 80 seconds. It was suspected that the time intervals of 10 seconds between the temperature measurements were not sufficient in detecting the differences.

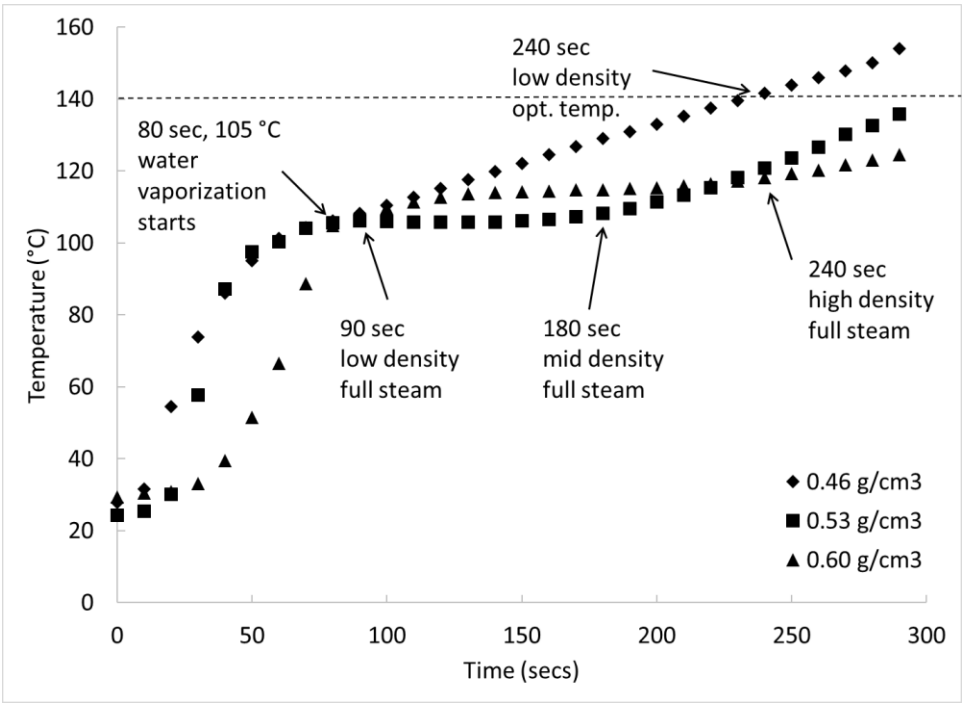

Figure 33: Temperature profile for low, medium, and high density strand board

The vaporization temperature is maintained for a brief period of time while all water in the mat was converted to steam. The temperature rose again signifying that all water had been converted to steam after the following times for each density: about 10 seconds with the lower density of 0.46 g/cm^3, about 100 seconds with the medium density of 0.53 g/cm^3 density, and about 160 seconds with the higher density of 0.60 g/cm^3.

The high density (0.60 g/cm^3) had a plateau temperature of about 114 °C while the medium density (0.52 g/cm^3) maintained a plateau temperature of about 106 °C. The minute time interval for the low density to vaporize the water prohibited an observed plateau temperature, but it was expected to be slightly lower than the medium density plateau temperature. These higher temperatures for higher densities were related to the amount of wood mass in the samples causing a higher pressure from the press to reach the guides that controlled board thickness.

Overall, the temperature profile analysis of the range of board densities tested showed that 4 minutes pressing time at normal pressing conditions was sufficient to vaporize all water even in the high density boards. The low density board reached the 140 °C optimum pressing temperature after 4 minutes of pressing described by Lee, et. al [100]. The time at which the full vaporization occurred was the point deemed sufficient for full curing. The pressing time of 4 minutes was not long enough for the higher density boards to reach the optimum temperature of 140 °C, but the temperature continued to climb in the center due to the higher temperature of the surface layers. The surface layer cannot be maintained at 204 °C for an extended amount of time due to adverse effects of the adhesive degradation (temperature confirmed in TGA work) and discoloration of the wood strands. The pressing time used for all future experiments using liquid and powder PF for medium to high density boards was therefore determined to be 4 minutes.

Comparison of different densities with 5% soy substitution in liquid PF

After determining the temperature profiles due to differing densities and the press time needed for cure for lab made strand board, another experiment was designed to observe how board strength was affected with liquid PF with and without substituted soy at differing densities. The objective of the experiment was to find the correlation between density and MOR and MOE using a control PF and a 5% soy substituted PF. Strand boards were constructed at differing densities of 0.51, 0.55, and 0.58 g/cm^3.

The correlation between density and the flexural strength and modulus of both the control and 5% soy substituted liquid PF was analyzed (Figure 34). It was observed that flexural strength and modulus both trended positively with increasing density which was expected. At lower densities the control PF and 95/5 PF/SF appear comparable. The trend lines of each adhesive can be seen intersecting at about 0.51 g/cm^3. As the density of the board increased there was an

increasing trend of both flexural strength and modulus observed in the control PF than the 95/5 PF/SF.

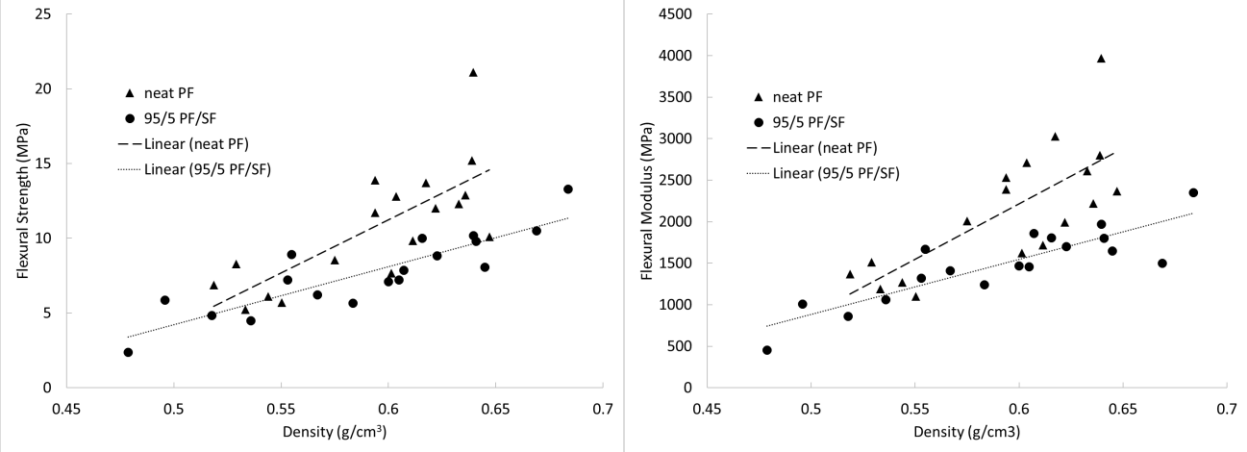

Figure 34: Flexural strength (left) and flexural modulus (right) of different density strand boards made with a control liquid PF and 5% soy substituted into PF

One possible explanation was that there were two different modes of failure that occurred at lower and higher density boards. As mentioned before, adhesive or cohesive failure could dominate as a primary mode of failure. Adhesive failure occurs at the wood/resin interface while cohesive failure occurs in the bulk of the adhesive [101].

It was believed that the form of failure at the lower density boards was due to adhesive failure due to the wood/resin interface and cohesive failure in the higher densities. It was observed that the soy substitution thickened the liquid PF to a certain degree which could affect resin droplet geometry affecting the resin spread of the resin in the strands when pressed. The density would have an influence on the manner in which this resin spread occurred. Higher density boards would inhibit resin spread to a degree if the resin was thicker. The lower density boards allowed for the thicker soy substituted resins to exhibit increased resin spread and therefore coat more strands with adhesive [101]. This prompted another experiment to understand the resin droplet geometry.

Resin Contact Angle Measurement

The next experiment examined the contact angle of the resin and its relation to resin spread. The experiment was designed to measure the contact angles of neat PF and soy substituted into PF to establish a relation to the resin spread and how soy substitution affected that. A homogenous surface was necessary to control the variability and accuracy of the comparison measurements; thus, a homogeneous glass surface was employed. A wood surface introduced experimental error due to surface micro-roughness and a heterogeneous interface (cellulose, hemicellulose, and lignin components).

The following figure shows the results of the contact angle measurement performed on neat PF and 90/10 PF/SPI superimposed on an example image for each.

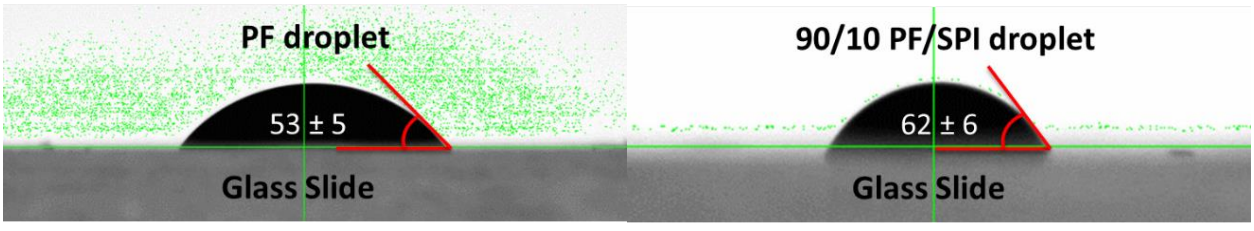

Figure 35: neat PF (left) and 90/10 PF/SPI (right) droplets on glass slides with mean contact angles for each shown with standard deviations

A substitution of 10% SPI in PF showed a 17% increase in the contact angle of the resin droplet on glass. This increase in the contact angle was most likely an artifact of an increase in viscosity. Wescott and Frihart showed a dramatic increase in viscosity when soy flour was substituted into PF [84]. This increase in viscosity would reduce resin spread because viscosity is the resistance of a liquid to flow. This reduction in resin spread would inhibit the bonded area between adjoining strands. The resin spread would likely change due to higher temperatures which would be the case during pressing. Nevertheless, the higher trends of the PF/SPI should be maintained.

The blending process was also performed at a lower temperature to which the resin droplets would be applied to the strands.

If the slopes of the trending lines in the differing densities are observed (Figure 34), the meaning becomes clear to the findings from the contact angle experiment and its relation to resin spread. Contact area between strands at low densities was relatively low inducing a lower applied pressure. Resin spread was limited because of this lower applied pressure. The strength of the composite comes from the resin itself present at the points of contact between the strands. When the density increases, there was more contact area between the strands which increased the applied pressure increasing resin spread. The soy substituted resin spreads at a lesser extent than the neat PF. This results in a lower relative bonded area and thus a weaker bond [101]. An increase in density increased the influence of resin spread on adhesive failure between the strands and resin.

Design of Experiment: vary adhesive loading and SF

An experiment was designed to analyze the effect of SF substituted into liquid PF on the modulus of rupture and elasticity in strand boards when varying density and total adhesive loading. The Box-Behnken design was used instead of a full factorial because of the difficulty in preparing the number of samples required for a full factorial.

The lower adhesive loading boards were analyzed first (Figure 36). Even though 5% SF showed lower flexural strength and modulus of the boards, the results were comparable between the control neat PF (0% soy) and 10% soy substituted into PF. Higher adhesive loading increased the flexural strength and modulus for both as was expected. The SF substituted resin did not increase as fast as the neat PF in the flexural strength – more so in the flexural modulus. It was more favorable to substitute SF in PF at lower total adhesive loadings. Resin spread influenced

adhesive bonding when excess resin was applied because a more spreadable resin will reach more points of contact between strands [101].

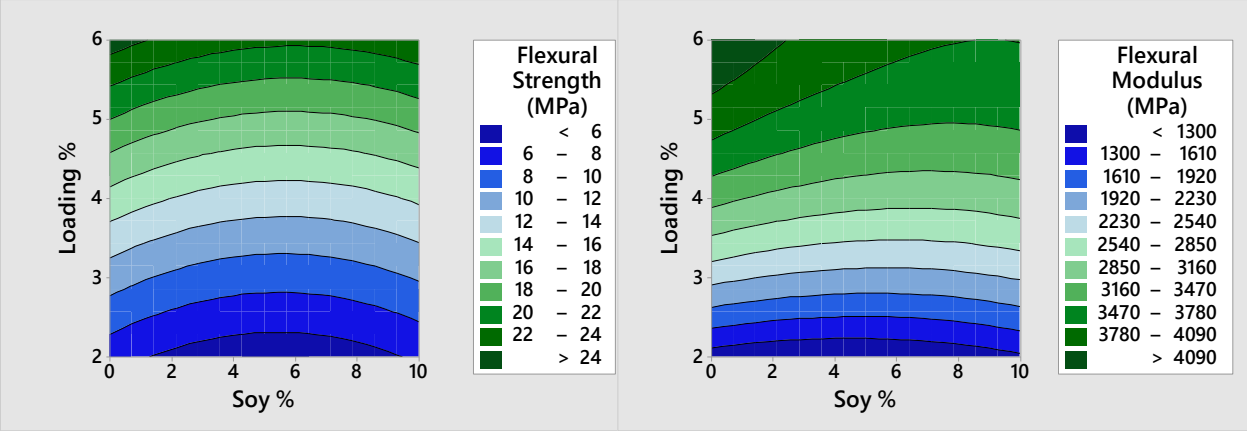

Figure 36: Flexural strength and modulus shown with varying adhesive loading and SF (soy %) for dry boards

The following figure shows the flexural strength and modulus of boards soaked in water for 24 hours with varying SF substitution and total adhesive loading.

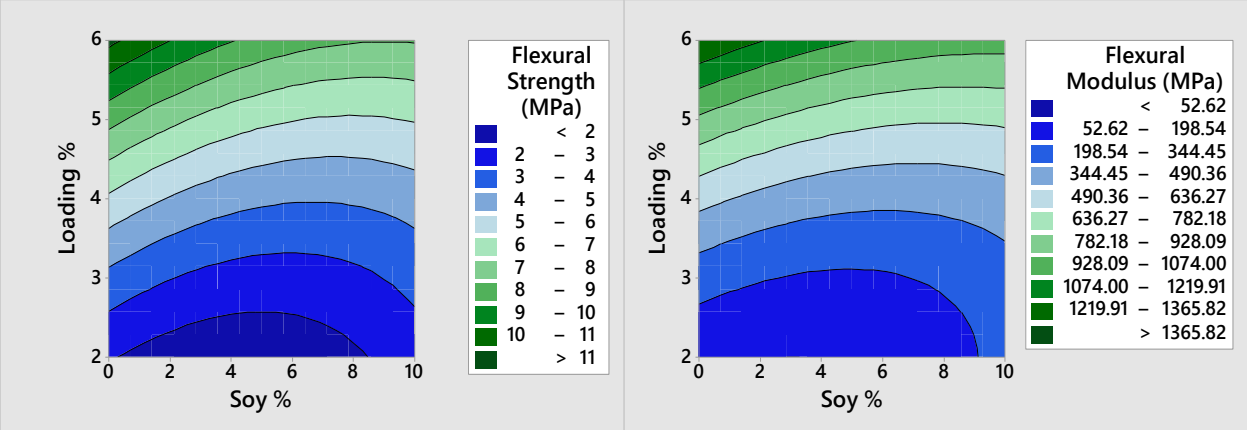

Figure 37: Flexural strength and modulus shown with varying adhesive loading and soy % for wet boards

The analysis observed in the dry boards translated to a higher degree in the wet boards. More favorable flexural strength and modulus at lower total adhesive loadings was observed in the 10% SF substituted resin boards at lower adhesive loadings. The rate of increase of both the flexural strength and modulus with increasing adhesive loading improved at a higher rate in the

neat PF than the SF substituted resin, but there was more of a difference in the wet boards. The higher adhesive loading exposed more adhesive in the bulk that had not penetrated the interfacial area of the wood substrate. This led to more exposure of the bulk adhesive to water. The more viscous soy substituted resin also did not penetrate into the contact area of the strands to as high of a degree as the neat PF leaving more resin exposed with higher loadings. The lower adhesive loadings allow for enough resin to spread and create an optimum resin/strand contact area [101].

Conclusions

The lap shear experiment using soy protein isolate (SPI) showed an 80% increase in shear strength with a 10% addition of SPI. This supported the assumption set forth in the work that soy products do appear to hydrolyze with the heat from the press. It was possible that there was a SPI substitution limit met at 10% SPI substitution limiting the ingress of the adhesive in the wood affecting the wood/resin interface. It was observed that the 30% SPI substituted into liquid PF was thick compared with the other formulations although viscosity was not measured.

The temperature profile for strand board forming showed that four minutes was a sufficient amount of time for strand board pressing to vaporize bound water in the center of the mat, even in the higher densities.

Low density strand board was more favorable with regard to flexural strength and modulus with SF substitution in PF. Cohesive failure possibly dominated the failure mode in higher densities due to more applied pressure from higher strand contact. This higher strand contact affected the spread of the resin to a higher degree in the high density boards. The thicker soy substituted resin would not have spread as much as the neat PF thereby lowering the contact area of the resin on the strands. Contact angle was measured for neat PF and 10% SPI substituted

into PF and showed a decrease in resin spread with higher SPI substitution confirming the findings in the experiment involving varied board densities with resin spread.

The design of experiment with varying adhesive loading and SF substitution showed that lower adhesive loading favors SF substitution in PF up to an SF substitution of 10% with respect to flexural strength and modulus. The higher adhesive loading exposed more adhesive that had not ingressed into the wood strands which would be more susceptible to water intake weakening the bond of the SF substituted resin. This was confirmed with the wet boards for high adhesive loading for both flexural strength and modulus.

Chapter 3: Liquid Phenol Formaldehyde and Defatted Soy Flour in Strand Board

Introduction

The first phase of this work was the screening stage and determined whether defatted soy flour (SF) could be substituted into the wood resin in the forming of strand board and to what extent SF could be substituted. The Chapter 2 determined the parameters needed to conduct the work in this section and partially explained some mechanisms of adhesion with the mixtures. It also determined that SF substitution was possible. This chapter determined that SF could be substituted at a rate of 10 to 14% in liquid phenol formaldehyde (PF). All substitution percentages for SF and an adhesive were reported in dry weight of SF/dry weight of adhesive.

Experimental

The detailed procedures for constructing the strand boards in this chapter are found in the experimental section of Chapter 2. Any modifications to the experiments in this section were specifically explained for each experiment. Defatted soy flour (SF) was the only soy product used in this chapter.

Variation of SF at 7, 14, and 21%

An experiment was performed to analyze board strength with higher amounts of SF substitution to determine the upper limits of SF substitution in PF since 10% SF substitution in

strand boards performed as well in flexural strength and modulus as neat PF in the previous experiment detailed in Chapter 2. SF was substituted at a rate 7, 14, and 21% in liquid PF. Two boards were made for each group including a group formed with a neat PF control. One of the two boards was prepared for dry sample testing while the other was prepared for wet sample testing. The boards were formed according to the "bag" procedure described in the previous chapter. A total adhesive loading of 6% was used. A target density of 0.56 g/cm^3 was used. There was no wax addition to the blending step for this procedure. Flexural strength, flexural modulus, and internal bond were measured for the dry samples while flexural strength, flexural modulus, thickness swell, and water absorption were measured for the wet samples. All test procedures were carried out using the ASTM D1037-12 standard [10].

Liquid PF Sequential Experiment

An experiment was designed to analyze the strength of boards formed with SF substituted in liquid PF using a different blending methodology involving sequential addition of components as well as addition of wax. The addition of components during the blending process onto the strands were as follows: wax, then SF, then liquid PF. The SF substitution rate for each group was 0, 20, and 30% dry soy weight/dry PF weight. Wax loading was 1%. Total adhesive loading was 6%. Target density was 0.56 g/cm^3.

The "cement mixer" blending procedure was used. The SF was applied in the same fashion as the powder PF procedure described in the previous chapter since it was applied separate from the liquid PF. This involved applying about a fifth of the SF while the cement mixer was not turning. The mixer was powered on for one minute and stopped. Another fifth of the SF was applied, and the process was repeated until all the SF was applied. The mixer was turned on again to distribute the SF on the strands uniformly for five minutes before the liquid

PF was applied. Press time was 4 minutes. The pressed boards were then cut into samples to be tested for wet and dry flexural strength and modulus, water absorption, thickness swell, and internal bond all measured according to ASTM D1037-12 [10].

Results and Discussion

Variation of SF at 7, 14, and 21%

This experiment was designed as a screening experiment intended to define how much SF could be substituted into liquid PF without compromising performance of the formed strand boards. An SF substitution rate of 7, 14, and 21% was used because 10% SF substitution had already been confirmed as possible in liquid PF in experiments performed in Chapter 2.

There was considerable variability in the dry flexural strength and modulus results (Figure 38) due to the small sample size, but some inferences could be made as there appeared to be a downward trend with higher SF substitutions. An SF substitution of 7% appeared to have comparable flexural strength and modulus, but both flexural strength and modulus drop with 14% and more so with 21% substitution.

There was also high variability seen in the results for internal bond (Figure 39) due to the low sample size although SF substituted boards showed less variability than the neat PF boards. The internal bond showed a rise in internal bond with 7% soy substitution, but there was a drop with 14% and more so with 21% mirroring to a degree the flexural strength and modulus.

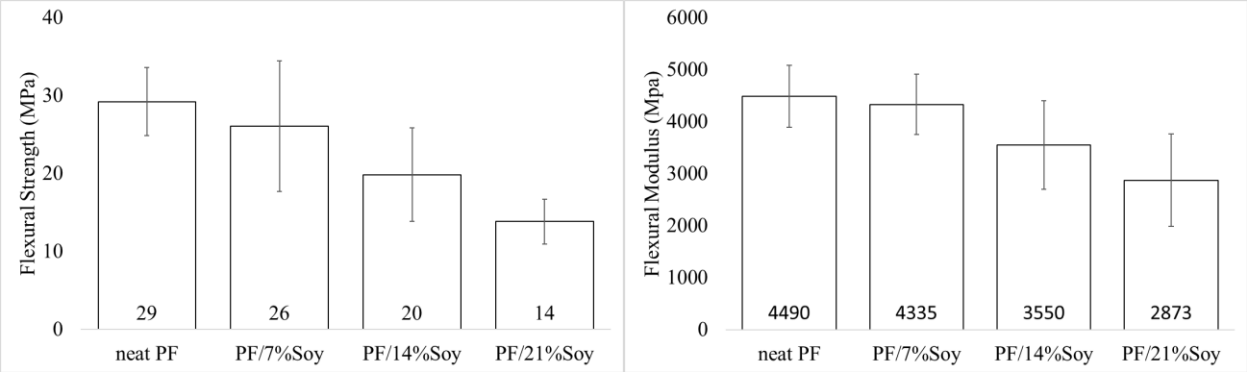

Figure 38: Flexural strength (left) and modulus (right) of dry strand boards made from 0, 7, 14, and 21% SF substitution

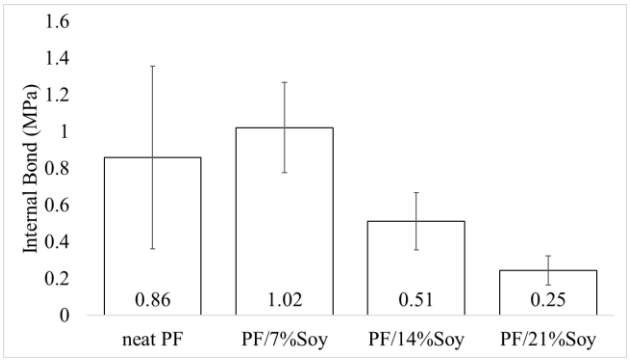

Figure 39: Internal bond of dry strand boards made from 0, 7, 14, and 21% SF substitution

This appeared to follow a similar trend observed in the lap shear test with SPI substitution in the previous section in that there was a maximum strength achieved with a certain amount of soy substitution (7% in our case). There was a drop in strength in the 20% SPI substituted lap shear test which could display the limitation of soy substitution in the resin inhibiting ingress into the wood substrate described in Chapter 2. A similar phenomenon was possible with the strand board. The resin ingress likely achieves an optimum amount of penetration due to the thicker SF substituted resin at 7% but negatively affects the adhesion bonding between the SF substituted resin and wood substrate with higher SF substitution. There was enough resin that had penetrated into the strands to positively affect the adhesion to the

strands and more resin to contribute to the cohesiveness of the adhesive in the bulk. A thicker adhesive (14% and 21% SF substitution) had more resin present to contribute to the cohesiveness, but the adhesion to the wood strands was likely detrimented due to less penetration into the wood substrate. To further understand what was occurring, the wet properties were analyzed.

The wet flexural strength and modulus, thickness swell, and water absorption worsened for boards with increasing SF substitution (Figure 40). Because there was more adhesive present in the bulk with the thicker SF substituted resins (less ingress into the strands), there was more adhesive exposed to water during the soak. Due to the higher solubility of SF with water, it negatively affected the strand board's wet properties when there was too much adhesive present in the bulk. It should be noted that there was no wax addition in this experiment which would negatively affect the wet properties as well.

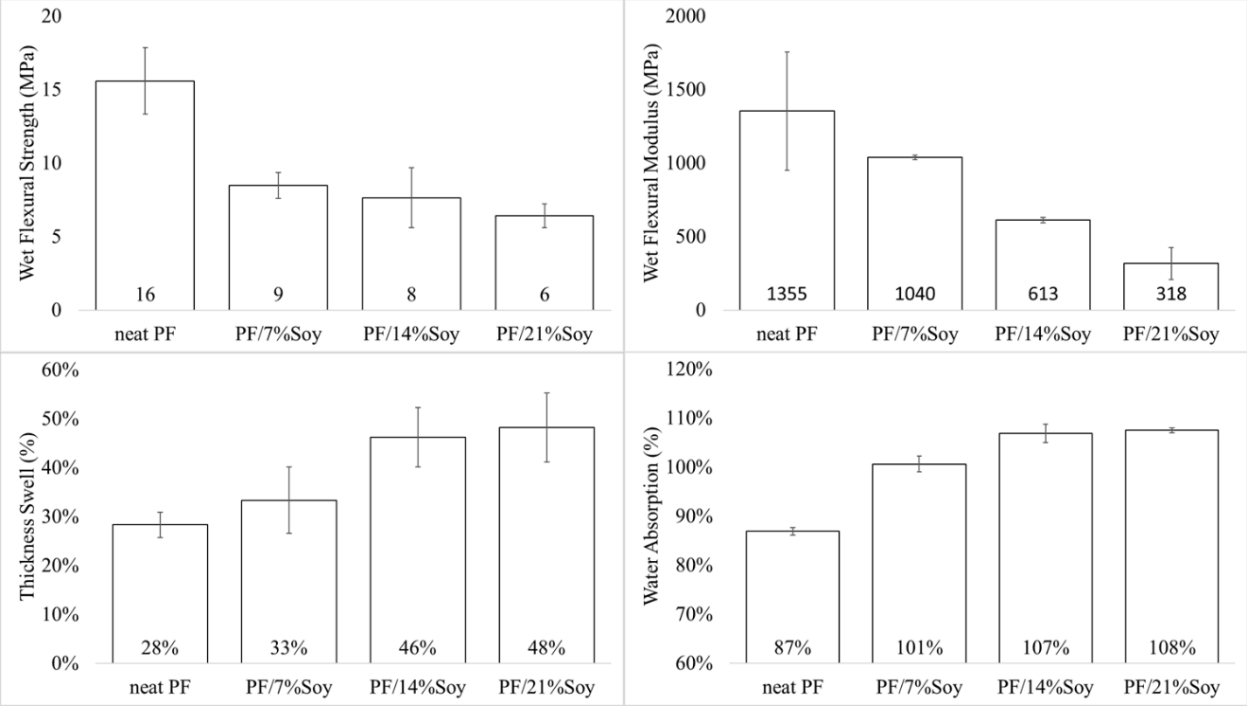

Figure 40: Wet flexural strength (top left) and modulus (top right), thickness swell (bottom left), and water absorption (bottom right) of 24 hour-soaked strand boards made from 0, 7, 14, and 21% soy flour substitution

Variability was still high for the PF in the wet flexural strength and modulus compared to the soy substituted resins, but thickness swell and water absorption showed more control with neat PF boards than the SF substituted resin boards. The water absorption was the limiting factor when better wet properties were preferred, and internal bond was the limiting factor when dry properties were preferred. Based on these results, an SF substitution rate between 10 and 14% may be possible in liquid PF, but the board would be better suited in a dry environment for its intended purpose such as an interior structural board.

Liquid PF Sequential Experiment

It had been shown that resin spread can affect the mat forming process in a negative way with soy product substitution in higher density boards (Chapter 2). It was also shown in prior works [84] that soy product addition to liquid PF dramatically increased viscosity. Work with

pMDI showed that it was possible to adjust the blending process to a sequential one (Chapter 5) – in particular, applying the SF and liquid resin sequentially in the blending process. This experiment was designed to test the effects of sequential addition to physical tests of strand boards formed with the SF substituted liquid PF. Wax addition was also implemented as other experiments had shown a significant advantage to board wet properties which could benefit the SF substitution process to a higher degree.

An SF substitution rate of 20% and 30% in liquid PF was compared with a control liquid PF in this experiment by measuring physical properties of the boards formed with these resins. An SF substitution rate of 20% soy substitution was possible with powder PF without compromising properties (Chapter 4), and the liquid PF resin spread was not compromised due to SF substitution since the components were applied separately. It was also desired to observe the effects of a higher SF substitution at 30% to determine if there was a drop in properties with higher SF substitution since it was observed with higher SF substitution in the last experiment. The results of the flexural strength and modulus of dry strand boards can be seen in the following figure.

Again, there was significant variability in the dry flexural strength and modulus results (Figure 41) due to the variability of the test and low sample size, but there was more control observed in the SF substituted flexural strength results. Overall the results were comparable with the control at all substitutions of soy. It was probable that the liquid PF and the SF interacted with the strands separately since they were added separately.

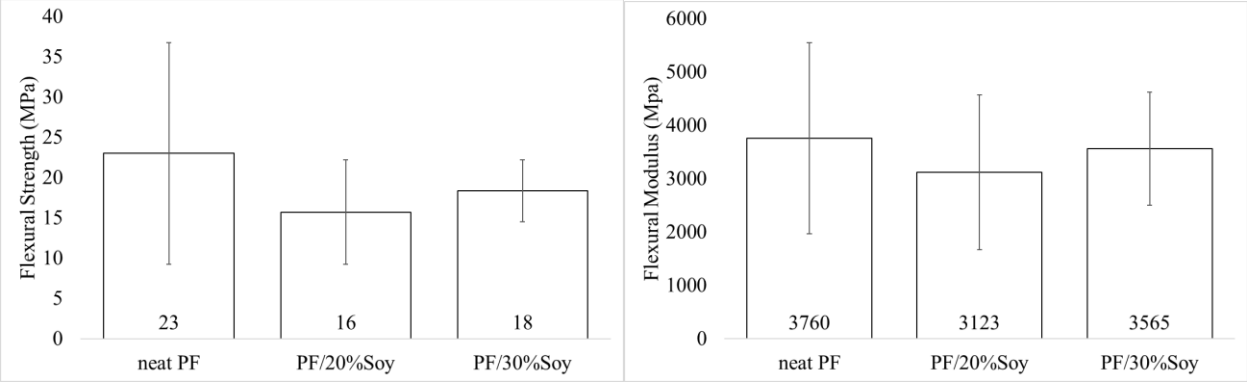

Figure 41: Flexural strength (left) and modulus (right) of dry strand boards made from 0, 20 and 30% SF substitution with sequential addition

If a separate interaction was the case, then the adhesive strength could be a simple summation of liquid PF's and SF's adhesive strength. The slight drop seen in the strength at 20% substitution could be the contribution of 80% of the liquid PF found in the control plus a smaller contribution of hydrolyzed soy flour.

The SF had the same amount of water to help hydrolyze it as the experiments where the SF was premixed with the liquid PF before adding it to the blending process, but there was not as complete of an interaction between the SF and the water from the PF compared with the mixing process of the SF and liquid PF. This could have affected the soy hydrolysis. This unhydrolyzed soy flour would then act as an inert ingredient having no effect on the adhesive strength of the strand board. It was not probable because more SF substitution would result in worse strength if this was the case. An SF substitution of 30% was statistically no different in flexural strength and modulus of the boards. Therefore, it was probable that the SF still hydrolyzed despite the lessened interaction with the water from liquid PF.

This summation of adhesive contributions from SF and liquid PF does not explain why the SF substituted resin performed better in board properties than the 21% SF substituted resin in the prior experiment not blended sequentially. If the resin spread was an issue with the non-

sequential blending experiment and not an issue in the sequential addition experiment, it would explain the drop in strength that was observed in the non-sequential experiment.

Internal bond was also measured, and the results can be seen in the following figure.

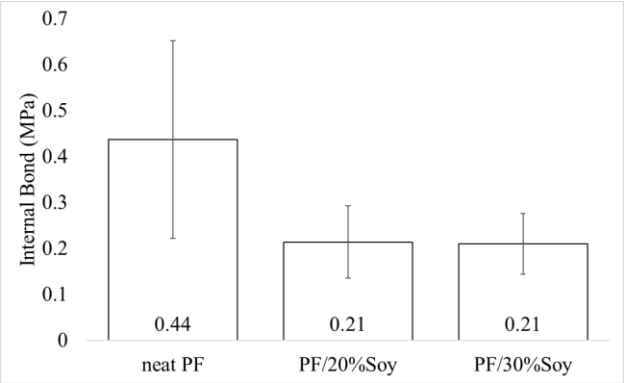

Figure 42: Internal bond of dry strand boards made from 0, 20 and 30% SF substitution with sequential addition

The variability in the neat PF control was observed again in the internal bond. There was a drop in internal bond for boards formed with 20% SF substitution, and 30% SF substitution results were comparable with the 20% substitution results. Again, internal bond prohibited additional SF substitution regardless of the order of addition of the components during the blending process. It appeared that the hydrolyzed soy does not perform well in internal bond whether sequential or not. If there was a chemical interaction between PF and SF, it did not benefit internal bond. If it was assumed that the contributions of PF and SF were summative like was assumed with the flexural strength and modulus, the contribution of hydrolyzed SF did not contribute as much as it did for the flexural strength and modulus. Unfortunately, internal bond prohibits SF substitution as high as 20% substitution with sequential addition. Perhaps it could be higher than the 10-14% determined before with sequential addition.

The results for the wet properties of the sequential addition experiment can be seen in the following figure.

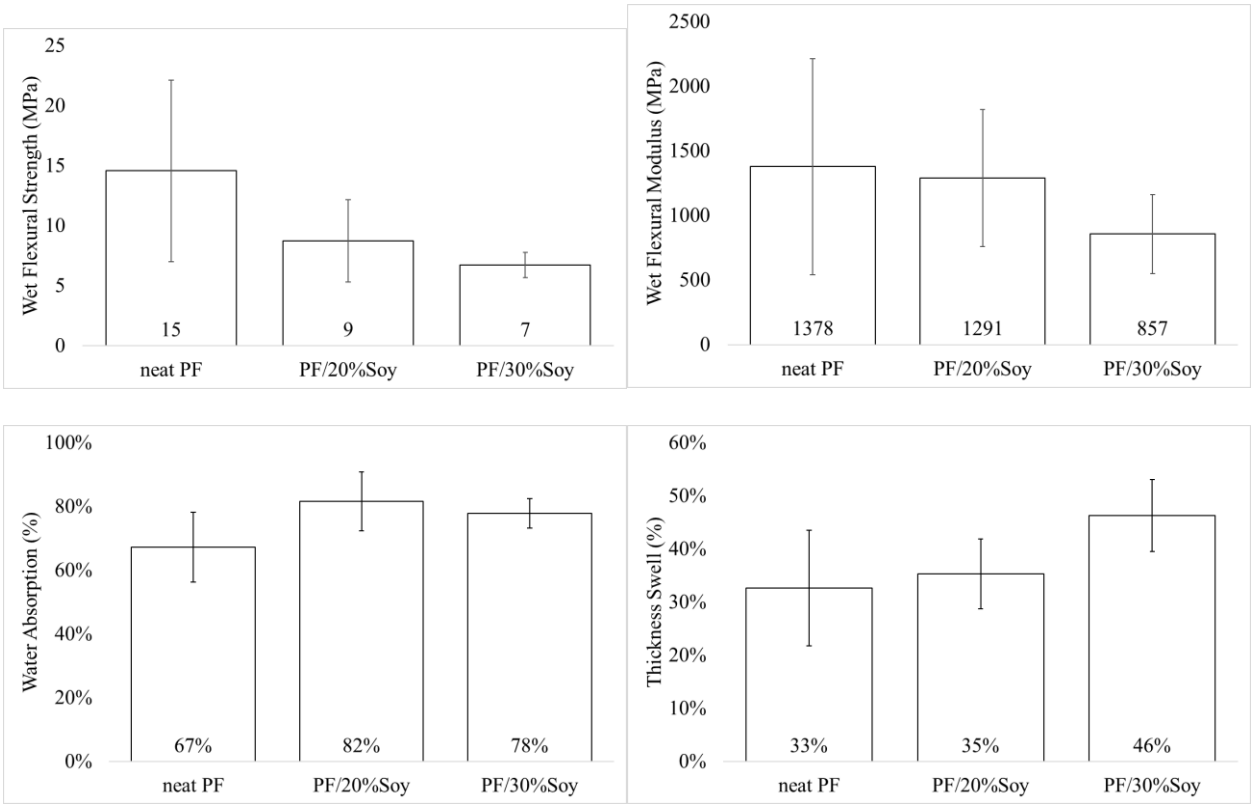

Figure 43: Wet flexural strength (top left) and modulus (top right), thickness swell (bottom right), and water absorption (bottom left) of 24 hour-soaked strand boards made from 0, 20 and 30% SF substitution with sequential addition

Although the wet flexural modulus and thickness swell was comparable between the control boards and 20% SF substituted boards, the wet flexural strength and water absorption properties were worse with SF substituted PF boards. Water absorption was the limiting wet property for SF substituted resin boards with sequential blending. It was probable that the SF mixed with the liquid PF would have penetrated into the strands more than the sequentially added SF. More sequentially added SF would then be exposed in the strand board matrix being susceptible to water soaking. This would explain slightly worse wet properties than the premixed PF/SF. Regardless, the SF substitution that would be probable in liquid PF without compromising board properties was still between 10 and 14%. It was possible that sequential addition may raise the substitution rate slightly but not considerably.

Conclusions

Overall, SF substitution was shown to be substituted in liquid phenol formaldehyde between 10 and 14% without compromising formed strand board properties. There was more variability in the control PF as compared to the SF substituted resin boards in all dry tests. There was considerable variability in all tests because of the variability of the tests conducted and the small sample size. Both experiments showed that internal bond was the limiting dry property and water absorption was the limiting wet property when substituting SF in liquid PF formed boards.

The first experiment showed that 7% SF substituted PF in boards had either a positive effect on physical properties or comparable properties. However, 14% SF substituted resin in boards showed a considerable drop in performance for internal bond and water absorption. It was believed that there was a minimum amount of penetration into the strands needed to contribute to the adhesiveness of the resin/strand interface without adhesive failure of the boards. This minimum was found between 7 and 14% in this experiment (10 and 14% if you consider the design of experiment from the prior section showing 10% SF substituted resin in boards had comparable or better properties). The extra resin that had not penetrated contributed to the cohesiveness of the adhesive bulk. Higher SF substitutions thickened the resin and therefore lowered the penetration to a point that the wood/resin interface was affected causing the point of failure to be adhesion. The wet properties confirmed this because more adhesive was available to interact with the water during the soak. The higher water solubility of SF compared with PF along with more adhesive to interact with the water explained the lower wet properties.

Sequential addition of the blending components was performed for the second experiment with higher soy substitutions since resin spread and ingress into the wood would likely not be inhibited with the liquid PF. The possibility that the SF was not hydrolyzing was

eliminated because of the higher SF content not being more detrimental to the dry flexural strength and modulus of the formed boards. It was believed that the contributions of the hydrolyzed SF and liquid PF were summative, and that the contribution of the hydrolyzed soy was not as much as the liquid PF. The internal bond showed that the hydrolyzed soy does not contribute as much if this was the case ultimately limiting SF substitution below 20% for sequential addition. Wet properties were worse for SF substituted resins in the sequential experiment. This was believed to be because of more liquid PF penetrating into the strands leaving more hydrolyzed soy to interact with water debilitating the contribution of the soy.

Chapter 4: Powder Phenol Formaldehyde and Defatted Soy Flour in Strand Board

Introduction

It was desired to determine if and to what degree soy could be substituted into phenol formaldehyde (PF). This was achieved in liquid PF, but the oriented strand board (OSB) manufacturing process also uses powder PF as an adhesive. Powder PF was usually liquid PF manufactured the same way and spray dried to eliminate the water content [102]. The following section investigates soy substitution as it pertains to powder PF and attempts to satisfy the first objective of the research by determining if and how much soy substitution was possible.

Experimental

The materials and methods of forming strand boards for the experiments of this chapter were given in detail in Chapter 2. Any modifications to the experiments in this section were specifically explained in the chapter. Defatted soy flour (SF) was the only soy product used in this section. Powder PF was the only form of phenol formaldehyde used in this section.

SF Substitution in Powder PF

An experiment was designed to test the effect of substituting SF into powder PF and its use in strand boards by comparing the differences between SF substituted in powder PF at the following rates: 0% (control), 21%, and 30%.

The same procedure defined for strand board forming in Chapter 2 was used with the following changes. The “concrete mixer” method was used. Wax was applied before the adhesive in the blending process. The adhesive was prepared before adding to the strands. SF was substituted into the powder PF at varying percentages. All reported SF percentages were dry weight soy/dry weight adhesive (SF and PF). The SF and PF were assumed to be at 0% moisture for mixing steps.

The SF and PF were mixed by adding the components to a Ziploc bag and shaken for 5 minutes to ensure that it was well mixed before application to the wax coated flakes. The adhesive was applied during the blending process as described by the dry resin application in the Chapter 2. The adhesive loading was 6% dry weight adhesive/dry weight strand board.

Results and Discussion

SF substitution in Powder PF

Strand boards were formed using a control powder PF and SF substituted into powder PF at 21 and 30%. This was done to test whether SF substitution was possible with powder PF and to what degree that substitution was possible without compromising performance of the strand boards formed with the adhesives. The results for the can be seen in the following figure.

Variation was still an issue with the flexural strength and modulus results (Figure 44) of strand boards similar to the liquid PF study. The variation was likely because of the small sample size and test variation. There was a clear increase in both flexural strength and modulus with SF substituted resins. There was no resin spread to consider since both PF and SF were dry, but powder PF was known to melt during the pressing process which allowed for flow and penetration into the strands [103]. Perhaps the PF and the hydrolyzed soy interacted during the

melt. This could either be a chemical crosslinking interaction or an interaction that affected the wood/resin interface. There was evidence that there was an interaction of some kind although this experimental analysis could not conclude on which.

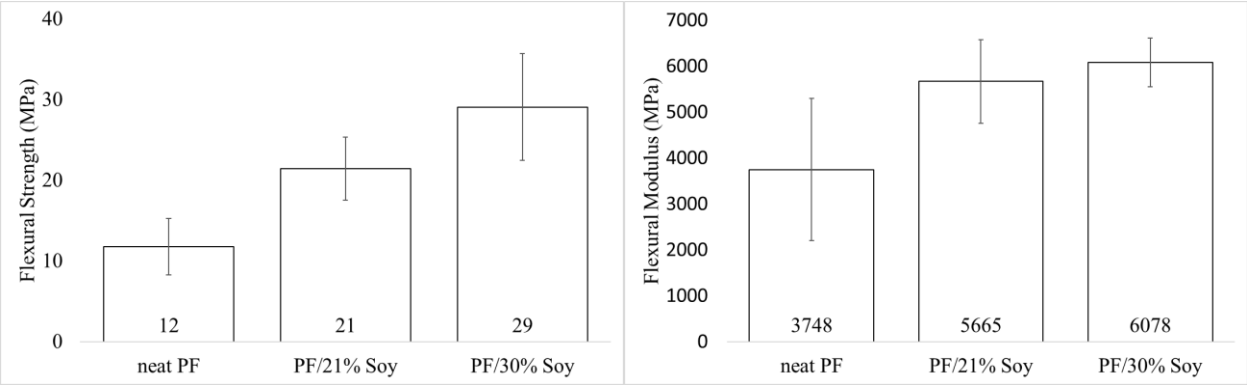

Figure 44: Flexural strength (left) and modulus (right) of dry strand boards made from 0, 21, and 30% SF substitution in Powder PF

If it was assumed that the contributions of PF and SF were additive like it was for liquid PF, then the contribution of hydrolyzed soy flour was more than powder PF. This does not follow the sequential liquid PF results. It was more likely that there was an interaction between the two that affected the flexural strength and modulus in a positive way. The following results of the internal bond show a similar picture.

Unlike the liquid PF, the powder PF formed board internal bond results (Figure 45) showed a rising trend in internal bond with more SF substitution even with 30% SF substitution. Again, it was believed that the SF interacted with the powder PF in a way to increase the bonding strength of the adhesive.

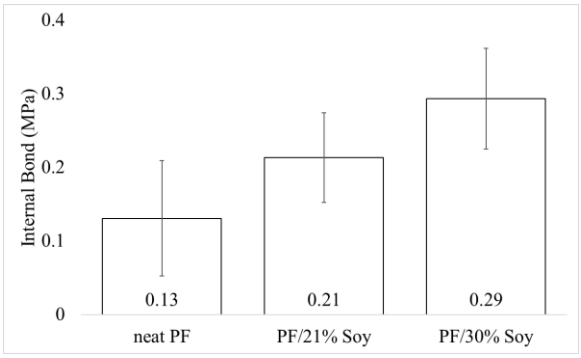

Figure 45: Internal bond of dry strand boards made from 0, 21, and 30% SF substitution in Powder PF

The SF substituted wet flexural strength and modulus showed more control in variation than the neat powder PF samples (Figure 46). There was no loss in properties with SF substituted resin boards when comparing wet flexural strength and modulus with the neat PF. In fact, the 21% SF substituted resin board samples showed a higher wet flexural modulus. Thickness swell showed comparable properties for the 21% SF substituted resin and the neat PF boards, but the 30% SF substituted resin samples showed worse thickness swell properties. The water absorption appeared to be the limiting board property with the amount of SF substitution allowed in powder PF. There was an upward trend with higher amounts of SF substitution for water absorption.

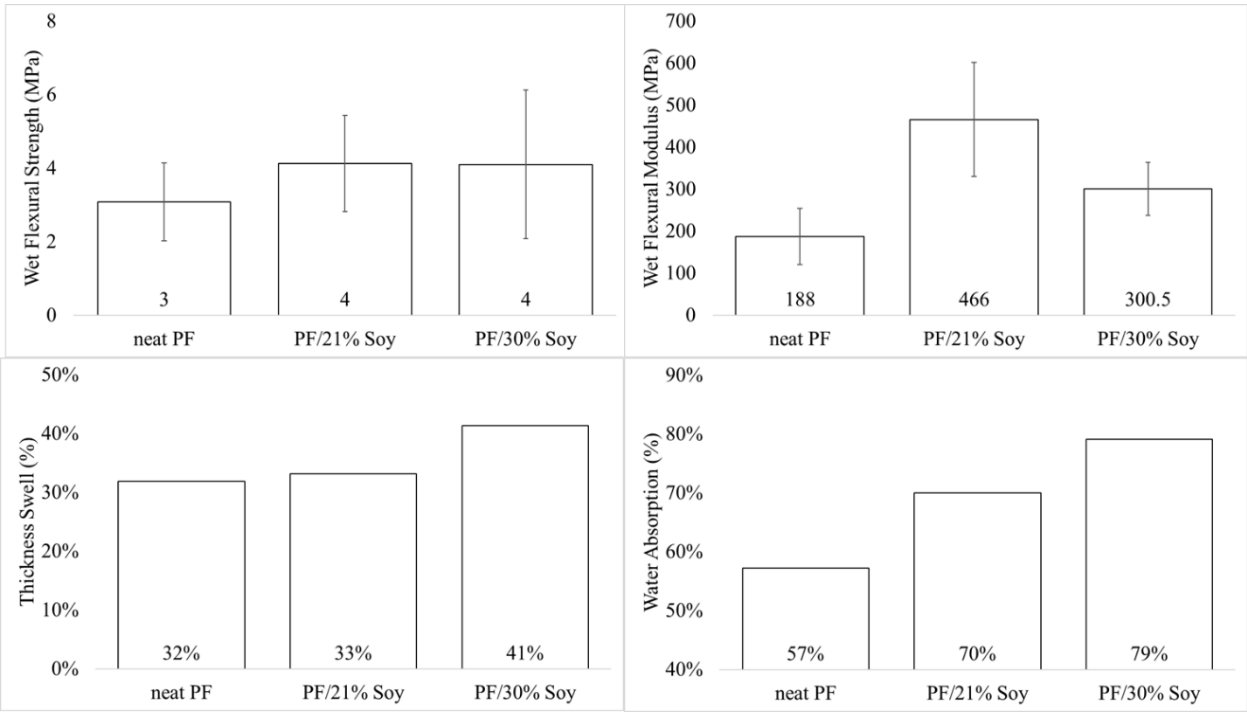

Figure 46: Wet flexural strength (top left), flexural modulus (top right), thickness swell (bottom left), and water absorption (bottom right) of 24 hour-soaked strand boards made from 0, 21, and 30% SF substitution in Powder PF

When one considered an interaction between PF and soy as was done for the dry properties, it would favor wet properties more if this interaction affected the wood/resin interface. If more SF was allowed to penetrate into the wood strands because of its interaction with powder PF during the melt, there would be less SF to interact with water during the 24-hour soak. It was believed that this was the case, but more experimentation was needed to confirm this. These results showed that SF substitution in powder PF was possible and could be substituted between 21% and 30% with the limiting board property being water absorption.

Conclusions

SF substitution in powder PF was possible between 21% and 30% without compromising board properties. Water absorption appeared to be the limiting property when soy substitution

was considered. Thickness swell also played a minor role in limiting the SF substitution. It was thought that the SF does interact with the powder PF in a way to strengthen the adhesive bonding of the strand boards formed. It was thought that this interaction may affect the wood/resin interface since wet properties were not as detrimental as expected. The liquid PF/SF resins were believed to have less penetration due to a thicker resin inhibiting the wet properties because of more water exposure to the adhesive. The powder PF could show the opposite affect by allowing more hydrolyzed SF to escape water exposure through ingress into the strands.

The next phase in the research of SF substituted in phenol formaldehyde was to determine the mechanism of adhesive that was affected by the substitution of SF. The original hypothesis was that this interaction was a chemical one. There was evidence to both accept and refute this hypothesis in the work of the first phase, but a thorough study in curing kinetics was required to confirm this.

Chapter 5: Methylene Diphenyl Diisocyanate and Defatted Soy Flour in Strand Board

Introduction

Methylene diphenyl diisocyanate (MDI) was is as a wood adhesive and is seen as becoming more and more dominant in the OSB industry. It reacts very aggressively with hydroxyl groups which was of great benefit to the wood adhesive industry as there were so many hydroxyl groups in which to react with in wood. There was also reactivity with amines. Both amine and hydroxyl functional groups were present in soy protein [13]. The objective of this chapter was to determine if SF could be substituted into polymerized MDI (pMDI) and if so to what degree.

Experimental

The materials and methods of forming strand boards for the experiments of this chapter were given in detail in Chapter 2. Any modifications to the experiments in this section were specifically explained in the chapter. Defatted soy flour (SF) was the only soy product used in this section.

Materials

The polymeric methylene diphenyl diisocyanate (pMDI or MDI) used was MONDUR 541, Materials #: 5212146 and supplied by Bayer Material Science LLC. All uses of the acronym MDI were intended to refer to polymeric MDI unless specifically noted – this included the use of neat MDI meaning neat pMDI.

Strand board formation using pMDI and SF

SF was substituted at 0% (control), 20% and 30% into pMDI. The soy was mixed with the pMDI prior to application in a glass beaker mechanically with a glass stirring rod until the mixture was visually uniform. The "concrete mixer" blending procedure was used with 2.5 minutes for press time, 4% total adhesive loading, and 1% wax addition.

Results and Discussion

Strand board formation using pMDI and SF

All work performed to this point had involved phenol formaldehyde and its use with SF. This experiment focused on pMDI and its use with SF. It was believed that the SF would interact chemically increasing the bonding strength of the resin.

Although there was more variation in the 30% SF substituted resin board results (Figure 47) for both dry flexural strength and modulus, there was an increase in both flexural strength and modulus compared to the control pMDI. The 20% SF substituted resin showed comparable flexural strength and modulus results with the neat pMDI formed boards. The internal bond mirrored these results except with more variability (Figure 48).

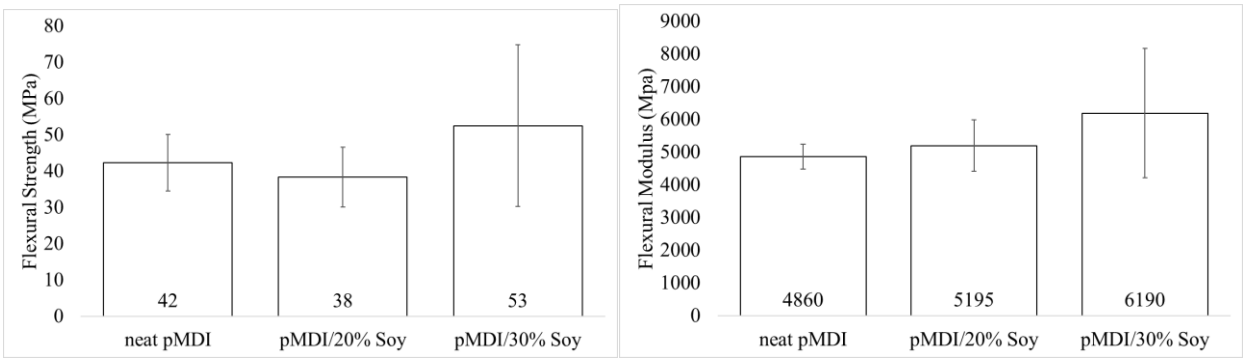

Figure 47: Flexural strength (left) and modulus (right) of dry strand boards made from 0, 20, and 30% SF substitution in pMDI

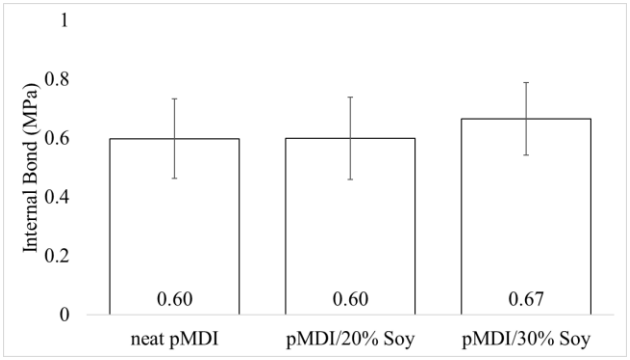

Figure 48: Internal bond of dry strand boards made from 0, 20, and 30% SF substitution in pMDI

An observation was made in this experiment to the thickness of the resin when SF was added to pMDI. It had been shown with prior work that pMDI resin penetrated deeper into wood than PF resins due to the low molecular weight (~50% monomer) and low surface tension of pMDI [103]. Perhaps the SF substitution allows more resin to be present in the bulk due to less penetration into the wood similar to what was suspected with the liquid PF. With more likelihood of the pMDI resin penetrating than PF, perhaps this would be more beneficial to pMDI if that were the case.

It was also possible that the pMDI and SF were interacting chemically by crosslinking between the two. It was likely that both adhesion and cohesion interactions were occurring, but it could not be deduced from the results of the strand board dry tests.

There was a slight improvement in wet flexural strength and modulus, thickness swell, and water absorption with increasing SF substitution in pMDI formed boards (Figure 49), and there was an improvement in the flexural modulus of the 20% SF substituted boards. There was an increase in thickness swell and water absorption with increasing SF substitution in pMDI formed boards, but the 20% SF substituted resin boards were comparable with the control.

It appeared wet properties were not significantly limited due to SF substitution as it was with phenol formaldehyde. Thickness swell was the limiting property, but it was still comparable with the control at SF substitution rates of 30%. It was determined that SF could be substituted into pMDI up to 30%.

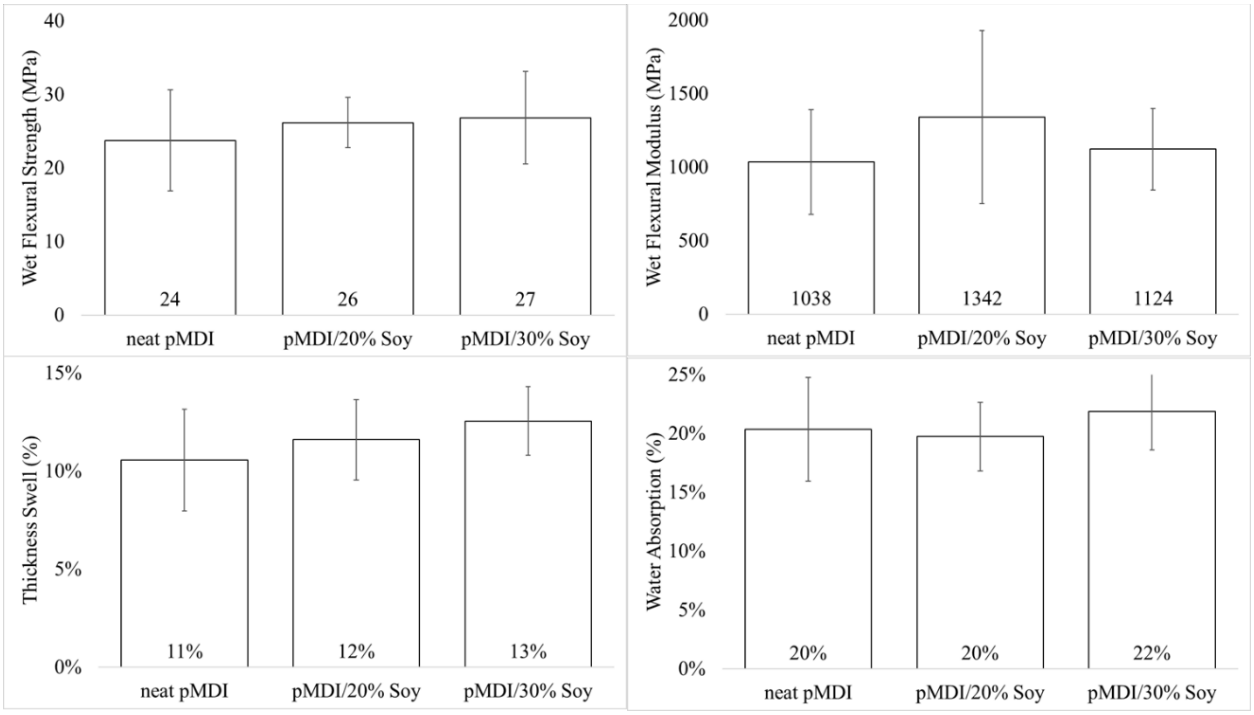

Figure 49: Wet flexural strength (top left) and modulus (top right), thickness swell (bottom left), and water absorption (bottom right) of 24 hour-soaked strand boards made from 0, 20, and 30% soy flour substitution in pMDI

The better wet properties did not explain what the primary mechanism of adhesion that had been changed with SF substitution in pMDI. It was possible that more amine groups in the soy flour reacted with the isocyanate group to create urea linkage which would have better water resistance, but more experimentation was necessary.

Conclusions

SF substitution in pMDI was possible up to 30% without compromising board properties. Thickness swell appeared to be the limiting property when SF substitution in pMDI was considered. It was believed that the SF was interacting with the pMDI in two possible ways: a chemical crosslinking one affecting the bulk of the resin mixture and the wood/resin interface affecting the adhesion of the resin to the wood substrate. It was not known which interaction was primarily affected with SF substitution in pMDI. Urea linkage does improve wet properties which would be evidence of crosslinking, but thickening the resin to alter the wood/resin interface would allow more resin to contribute to the bulk. There was evidence to both accept and refute the hypothesis of crosslinking in the work of the first phase, but a thorough study in curing kinetics was required to confirm this.

Chapter 6: Phenol Formaldehyde and Soy Product Curing Kinetics

Introduction

The work in this chapter was focused on understanding the interaction between soy products and the wood adhesive, phenol formaldehyde (PF). Understanding the interaction aided in determining whether soy products affected the overall resin to a higher degree in adhesive failure or cohesive failure. The curing kinetics were studied in neat PF and compared with the curing kinetics of mixtures of various soy products with PF to understand how the overall adhesive was affected. These soy products included defatted soy flour (SF), soy protein isolate (SPI), and denatured, defatted soy flour (soy-D).

The work in this chapter was considered the next successive phase in research of the substitution of SF in phenol formaldehyde. It followed the screening work performed showing SF substitution was possible in liquid PF between 10 and 14% (Chapter 3) and powder PF between 21 and 30% (Chapter 4) without loss of properties in the formation of strand boards. The work in this chapter was based on the hypothesis that the primary interaction affected with soy product substitution in PF was a chemical crosslinking one affecting the overall adhesive in the bulk. The objective of this work was to either refute or support the hypothesis.

Thermogravimetric analysis (TGA) was implemented to characterize the curing reaction of each of the resins. TGA was also performed to characterize degradation pathways to understand the products produced from the PF/soy product mixtures as well as compare them with the neat PF resin. The experimental activation energies of the curing reactions of the PF/SF mixtures and the neat PF were also calculated using data obtained from thermal treatment of the resins. Data obtained from Fourier transform-infrared (FT-IR) spectroscopy of the cured and non-cured PF/SF mixtures and the neat PF were analyzed through spectral interpretation. Identified wavenumber bands of importance through examination of prior published work or identification of appearing or disappearing bands were analyzed.

Materials and Experimental Method

Soy protein isolate (SPI), ProCote 4200, was donated by Solae, LLC. Defatted soy flour (7B) was provided by Archer Daniels Midland, of which about half of the mass of soy flour was constituted of soy protein [29]. The liquid PF resin used was GP 240C11 RESI-STRAN intended for OSB manufacturing (aqueous solution – 58.9% solids content) donated by Louisiana-Pacific Corporation. The powder PF was GP 190C80 Woodweld intended for OSB manufacturing donated by J. M. Huber Corporation. The denatured SF (soy-D) was prepared according to the Wescott/Frihart method [34].

Pre-Treatment of Soy Flour (Soy-D)

Defatted soy flour (SF) was denatured in an experiment to compare with untreated (not pre-treated) SF substituted into PF to compare properties obtained from TGA and FT-IR data. The Wescott/Frihart method was used [34]. The amount was reduced to a fourth of the mass that the published paper used.

The initial ingredients of 194.5 g of tap water, 7.00 g of NaOH, and 1.325 g of ethylene glycol were added to a three-neck round bottom flask. A thermometer and condenser were attached to the flask which was suspended in an oil bath. The mixture was stirred with a magnetic stirrer while heated to 70 °C. 87.5 g of SF was added to the rapidly stirring mixture at a rate of about 5 g/min to maintain a proper dispersion. The mixture was then heated to 90 °C over a 15-minute period with rapid agitation and held between 88 and 92 °C for 2 hours while rapidly agitating the mixture. The mixture was then cooled in an ice bath to 35 °C.

The solids content calculation of the mixture referred as soy-D in all future experiments was performed by placing a sample in a mechanical convection oven at 105 °C. Samples were weighed before and after to determine the solids content. The sample was heated until there was no difference in weight observed. The solids content of the sample in the convection oven after 18 hours was determined to be 30.1%.

PF and soy-D samples were also prepared. PF solids content was calculated as 58.9%. The wet Soy-D was added to the liquid PF in the proper ratio to obtain a 70/30 PF/soy-D ratio according to the calculated solids weight. The mixture was then dried in a vacuum oven to prevent curing at 24” Hg vacuum. The temperature was set at 31.5 °C for two days and 34.0 °C for 3 more days for a total of five days of vacuum drying.

Thermogravimetric Analysis (TGA)

Thermogravimetric Analysis (TGA) was applied on data from resin samples thermally treated using the TA Instruments Q5000 IR thermal analyzer. This thermal weight-change instrument was operated in conjunction with the TA Instruments Universal Analysis 2000 program version 4.5A.

Thermal treatment was administered to various samples containing PF and/or soy products during a constant temperature increase (dynamic TGA or ramp) or constant temperature (isothermal) treatments while measuring mass loss, temperature, and time. Ramp thermal treatments were administered to characterize volatile evaporation, curing reactions, and degradation reactions.

The isothermal TGA experiments were used to calculate the amount of time required to fully cure different mixes of PF and soy products. This experiment was performed using a constant temperature based on prior observations of TGA ramp data. The times of cure were then compared between the different mixes.

Weight and temperature calibration was performed on the thermal analyzer at least every two days of testing. The chamber was purged with 90/90 mL/mL of N_2/N_2 in the balance/sample for 30 minutes if there was a period of non-testing. Longer intervals of inactivity on the thermal analyzer required 200/200 mL/mL of N_2/N_2 in the balance/sample for 12 hours.

TGA Sample Preparation

Prior to thermal treatment, samples were prepared of uncured, vacuum dried samples of neat liquid PF and mixtures of PF and soy products. The following resin ratios were prepared: 70/30 (dry weight/dry weight) PF/SF, 70/30 PF/SPI, and 70/30 PF/soy-D. Neat samples of SF, SPI, soy-D, and powder PF were also prepared as is. Mixtures of 80/20 PF/SF were also prepared for both liquid PF and powder PF.

The liquid PF mixtures containing soy products were mechanically mixed in a glass beaker and glass stirring rod until visually uniform. The SF and SPI were in powder form and assumed dry when mixed with PF. The soy-D samples were not dry and prepared as described in the Wescott/Frihart procedure [34] with the same water content when mixed with liquid PF.

The samples were then placed in a vacuum oven set at about 20” Hg of vacuum and about 40 °C until there was no change in weight (four days) to remove as much moisture as possible without applying enough heat to cure the sample. The solid uncured samples were then filed using a bastard file into a powder for use in the thermal analyzer.

Approximately 15 mg of the powder sample (neat PF or PF/soy product mixture) was weighed out into a tared platinum-HT pan. The pan was then loaded into the TA Instruments Q5000 IR thermal analyzer. A purge rate of 10/90 mL/mL of N_2/N_2 in the balance/sample was used.

The thermal analyzer was programmed to increase the temperature at a constant rate (i.e. ramp) to a certain final temperature (500 °C in most cases) or immediately jump to a specified temperature (130 °C in most cases) for isothermal experiments. The temperature ramp consisted of constant rates of 2.5, 5.0, 10.0, 15.0, or 20.0 °C/min from room temperature to the desired temperature.

The isothermal treatments were applied to samples at a constant temperature. The time required to fully cure different mixes of PF and soy products at a specified temperature was measured. This experiment was performed using a constant temperature based on prior published work and observations of dynamic TGA data. The times of cure were then compared between the different samples.

The initiation of the time for the time intervals measured in the isothermal experiments commenced at the start of the temperature jump from room temperature to the specified temperature. The time to reach the specified temperature was typically 5-10 seconds depending on the final temperature and was included in the measured time interval. The final time was analyzed by identifying the time at which the same amount of mass fraction remaining matched

the end of cure identified in the dynamic TGA data. This time interval measured was referred to as the time of cure.

TGA data was also observed and compared between neat PF, neat SF, neat SPI, neat soy-D, 70/30 PF/SF, 70/30 PF/SPI, and 70/30 PF/Soy-D using data from dynamic thermal treatment at a ramp rate of 5 °C/min for all samples.

A comparison was also made between liquid and powder PF with and without SF substitution to note any differences since liquid PF was primarily used in this study. Powder PF required no processing as it was already dried and powdered. Powder PF was manufactured by spray drying a resole liquid phenol formaldehyde resin [102]. Mixing of powder PF and SF was achieved by adding both components in a plastic bag, sealing the bag, and mixing the contents by shaking the bag for five minutes to assure uniform mixing. The powder (neat PF or PF/SF mixture) was treated to the same procedure in the thermal analyzer as the samples containing liquid PF after grinding the dried liquid samples into a powder.

There was a minimum of five replications per temperature ramp per sample. These five replications were required to produce data that contained no noise in the TGA data. The DTGA temperature peaks were also required to have no outliers when compared with each other. Grubbs and Dixon's ratio outlier tests were used with the Minitab® 18.1 software to eliminate any outliers.

Activation Energy Calculation

The DTGA data was employed to identify temperatures at which the maximum amount of mass loss occurred during each of these characterization events, referred throughout this work as DTGA temperature peaks. These temperature peaks were identified for each event at various ramp rates, and a temperature range was identified containing these temperature peaks for each

event, referred throughout this work as reaction events or zones. The DTGA temperature peaks were used to calculate activation energy for each of those events.

The following shows a plot of typical TGA and DTGA data for a neat PF sample thermally treated at a ramp rate of 2.5 °C/min.

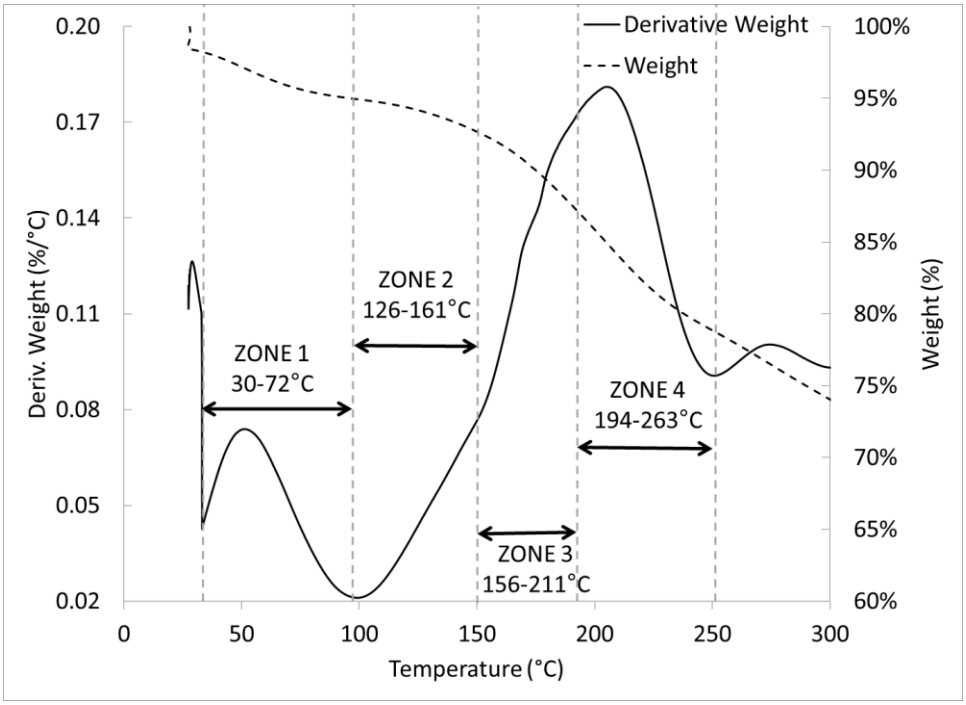

Figure 50: TGA and DTGA data showing five temperature ranges (or zones) of reaction events that were analyzed

Figure 50 was shown as a visual aid to help identify temperature ranges (or zones) of the DTGA temperature peaks found for all ramp rates for each mass loss event. Zones 2 and 3 were of particular interest because it contained the curing reaction.

There was a wide temperature distribution for each of the events because of the range of ramp rates (2.5, 5.0, 10.0, 15.0, and 20.0 °C/min). These events were identified for neat PF and all PF/soy product resin mixtures. The temperature ranges included data for each event from all resins: neat PF and the PF/soy product mixtures.

Each of the DTGA temperature peaks in the curing reaction temperature range (or zone) for a sample with their respective ramp rates (K/min) were used to calculate the activation energy for the curing reaction. This was performed using the Kissinger method by plotting $-ln\left(\frac{\beta}{T_p^2}\right)$ versus $1/T_p$, where T_p was the DTGA temperature peak and β was the ramp rate. The data had a linear relationship, and the slope and y-intercept of the plotted line were used to solve for the activation energy. Microsoft® Excel® software was used to calculate the activation energy.

Differential Scanning Calorimetry (DSC)

Differential scanning calorimetry (DSC) analysis was performed using data from the TA Instruments Q100 Differential Scanning Calorimeter. The data from the DSC was analyzed using the TA Instruments Universal Analysis 2000 program version 4.5A. DSC analysis was performed on PF and 70/30 PF/SF samples. The data was used to corroborate the thermogravimetric analyses – in particular the curing reaction analysis.

The samples were prepared in the same manner as the TGA experiments for the liquid PF and liquid PF/SF mixtures that were dried and ground into powder. Approximately 1-5 mg of the powder was then loaded into a pan bottom. A pan lid was then applied to the pan bottom and pressed in a T-zero press. The sample weight was recorded for each of the samples.

T-zero hermetically sealed aluminum pans were used because of the volatile gases given off during the curing cycle. The hermetically sealed pans were rated to a pressure of 300 kPa. A reference pan with no sample was used as a comparison which was also a T-zero hermetically sealed pan.

The sealed pan with the sample was then loaded into the DSC along with an empty pan as reference. A constant temperature increase (ramp) at rates of 5, 10, 15, or 20 °C was performed for each sample to a final temperature of 240 °C. A purge gas of nitrogen was used at a rate of 50

mL/min. Some samples were given a cool down at the same ramp rate as the temperature increase. The cool down occurred until ambient temperatures were achieved, and the sample was heated back up to 240 °C at the same ramp rate. This was done to confirm the presence of volatile gases given off.

Fourier Transform-Infrared (FT-IR) Analysis

Spectral analysis was performed on PF and PF/soy product samples using Fourier transform-infrared (FT-IR) spectroscopy. Chemical structures were identified and compared for the samples through spectral analysis to determine the characteristics of cure. An experiment was designed to acquire spectrum data from samples heated in the TGA at varying temperatures and compare the data with each other – primarily at the curing point found in the TGA and DSC work. The data was used in conjunction with the TGA and DSC data to determine whether chemical crosslinking occurred due to this heat treatment process and to what degree that the curing reaction was affected with soy product substitution.

TGA samples scanned with the spectrometer were prepared in the same fashion as indicated in the TGA experiments performed prior to this experiment through mixing, vacuum drying, and grinding into powder. Previous dynamic TGA data was analyzed at the ramp rate of 2.5 °C/min to find the temperature of full cure as well as other transitional points. The transition temperature points were defined as the point at which there was a minimum mass change occurring between zones. The temperature of each of the transitions was the point at which the DTGA data reached a minimum after the DTGA peak temperature found for that reaction event. The minimum was found using the TA Instruments Universal Analysis 2000 program version 4.5A.

An example of the transition temperature analysis for PF using the software can be seen in the following plot.

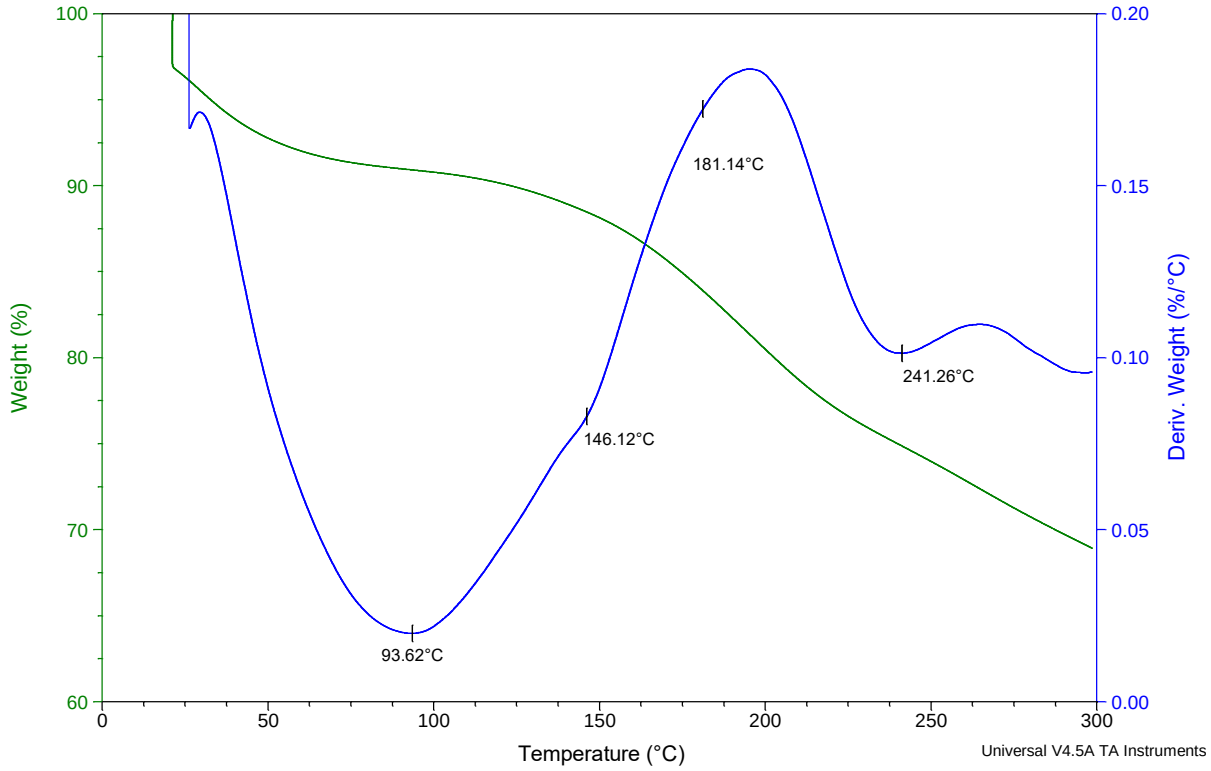

Figure 51: TGA and DTGA of PF sample at 2.5 °C/min displaying DTGA minima analyzed for end of reaction events (e.g. end of cure)

The above example displays the temperatures at which the DTGA minima that followed the four DTGA temperature peaks of each reaction event. These temperatures were recorded for each replication. These temperatures were then averaged to calculate the setpoint temperature that the dynamic TGA experiment was set to ramp at 2.5 °C/min for the transition experiment. These samples were referred to as transition samples in the rest of the chapter. The calculated transition temperatures can be seen in the following table.

Table 5: Transition temperatures calculated for end of each zone and each material

Transition Temperature	1st (°C)	2nd (°C)	3rd (°C)	4th (°C)
PF	94	147	182	242
70/30 PF/SF	101	143	195	257
70/30 PF/SPI	104	148	201	244
70/30 PF/Soy-D	107	139	181	300

Ground samples were then heated in the TGA to the specified temperature for the transition identified at the same parameters as the prior experiments in a nitrogen environment. The samples were then collected from the thermal analyzer and scanned by the FT-IR spectrometer where the spectrum data was collected by the PerkinElmer software. FT-IR spectra were collected using a PerkinElmer Spectrum 400 Imaging System spectrometer. Two scans were performed for each sample. One was performed after pelletizing the powder sample using a PerkinElmer pelletizer. The other sample was placed on the ATR crystal and pressed with the pressure apparatus attached to the machine. No noticeable difference in absorbance due to sample preparation technique was observed.

There were four replicates collected for each transition for each material: PF, 70/30 PF/SF, 70/30 PF/SPI, and 70/30 PF/Soy-D. The first transition was defined as between the lowest temperature reaction event (i.e. volatile release) and the subsequent reaction event occurring at a higher temperature (i.e. curing reaction). The second, third, and fourth transitions were found in an analogous manner with increasing temperature. Each material transition temperature was calculated separately.

Samples with no thermal treatment were also scanned on the FT-IR spectrometer and termed “no cure” or “uncured”. SF with no thermal treatment was scanned on the FT-IR spectrometer. A sample of SF mixed with the same amount of water content as the liquid PF was

heated in a mechanical convection oven for 60 minutes at 130 °C to simulate the thermal treatment of the SF in the PF/SF thermal treatments. This sample was also scanned on the FT-IR spectrometer.

Area calculation of the band intensity was attempted but was deemed too complex because of overlapping curves. Deconvolution, as pointed out by Myers, et. al., was also deemed too complex to attempt [104]. Prior published work from Myers, et. al. showed success in the use of the magnitude of the highest intensity peak at the identified wavenumber of 1600 cm^{-1} to be used as the normalization technique. Normalization was performed using the magnitude of the peak obtained at the wavenumber of 1605 cm^{-1} for the uncured PF [104]. Therefore, quantitative analysis of the FT-IR spectra was not attempted. A qualitative study was performed instead.

Results and Discussion

TGA/DTGA work

Curing and degradation reaction kinetic data was examined to compare characteristics of weight loss due to thermal treatment with and without the substitution of soy products in PF. TGA and DTGA data for the thermal treatment of neat PF, neat SF, 70/30 PF /SF, neat SPI, 70/30 PF /SPI, neat Soy-D, and 70/30 PF /Soy-D at a heating rate of 5 °C/min under nitrogen were shown in the following figures.

The main thermal degradation for defatted soy flour (Figure 52 a & b) began at the onset temperature of about 210 °C where the cleavage of glucoside units occurred [105]. The DTGA data displayed two peaks associated with the degradation in this temperature range (peaks at 248 °C and 300 °C). Guettler's work with soluble sugar extract from SF suggested that the lower

temperature degradation peak (most thermally sensitive fraction of SF) was the soluble sugar fraction whereas the peak at the higher temperature was the insoluble soy [106].

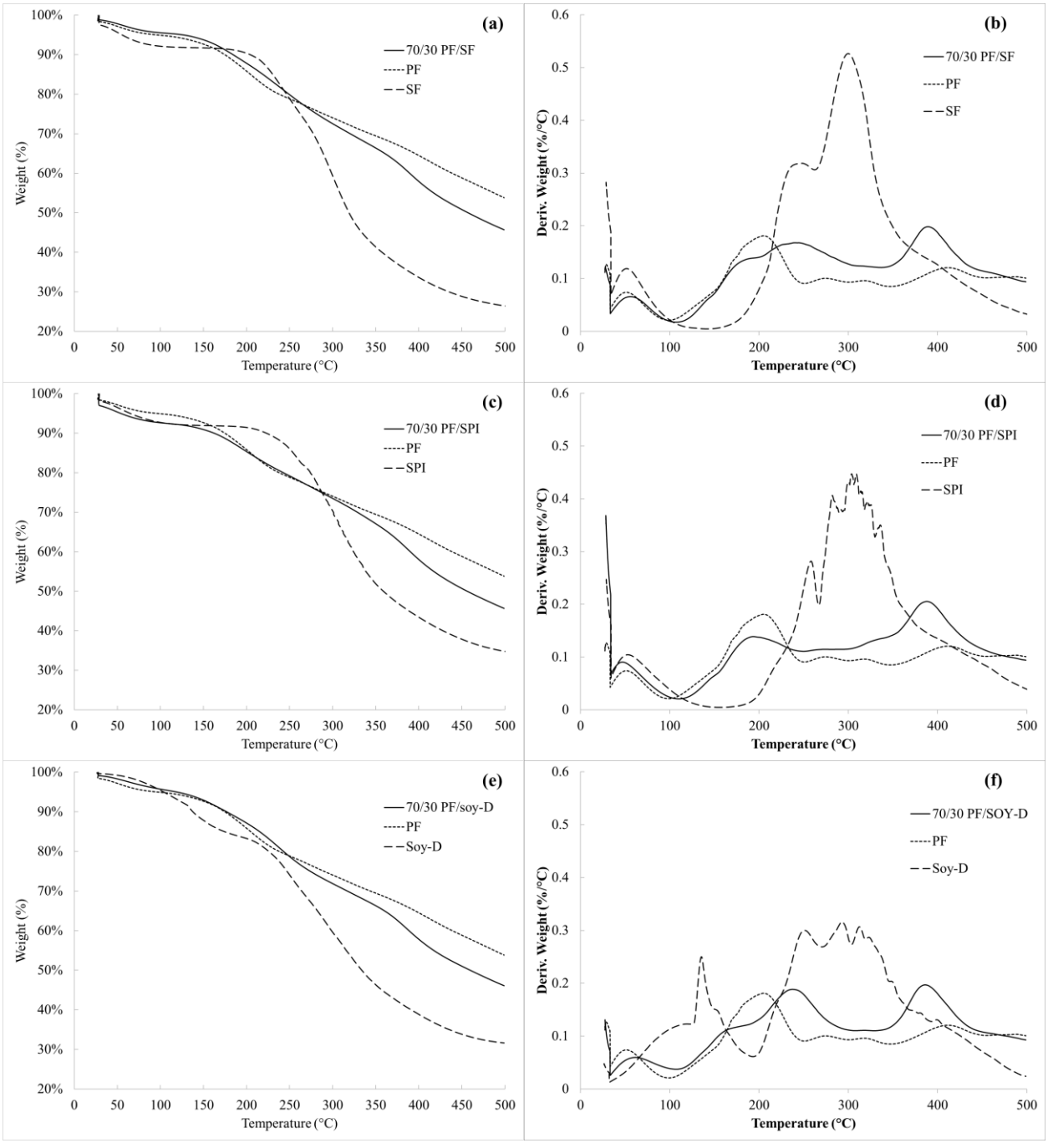

Figure 52: Dynamic TGA (left) and DTGA (right) data for neat PF, neat SF, and 70/30 PF/SF (a&b); neat PF, neat SPI, and 70/30 PF/SPI (c&d); neat PF, neat Soy-D, and 70/30 PF/Soy-D (e&f)

The SPI TGA data (Figure 52 c & d) indicated a similar range of degradation temperatures as the SF. A smaller amount of mass was lost at the lower temperature degradation peak in the SPI as compared to the SF, but there was a higher onset temperature of 232 °C and higher DTGA peak of 258 °C indicating that this was not part of the soluble sugar fraction as in SF. This was expected with the isolate as the soluble sugars had been extracted [106]. The degradation in the temperature range of 200-400 °C was a degradation of the soy protein [107]. This involved the breaking of hydrogen bonds (intramolecular and intermolecular), electrostatic bonds, and cleavage of the peptide bonds of amino acids in the protein structure [108].

The soy-D TGA data (Figure 52 e & f) also displayed a similar range of degradation temperatures as the other soy products. An onset temperature (224 °C) and DTGA peak (251 °C) for the soy-D degradation region lied between the SF and SPI onset temperatures and DTGA peaks suggesting there were still soluble sugars present, but the denaturation process had eliminated a partial amount of these soluble sugars. Qi and Sun performed TGA on a modified soy flour and showed protein degradation between 208 and 400 °C [107]. This TGA data followed closely with the soy-D thermal degradation in the same temperature range. The higher amount of mass lost as compared to the other soy products between room temperature and 190 °C was attributed to the large water content of the soy-D.

The neat PF TGA data (Figure 52 - short dash) showed five clear mass loss events. The lowest temperature event occurred between room temperature and about 100 °C and was attributed to the release of low molecular weight monomers and other volatiles (such as moisture) [109]. The next concurrent event occurred between about 100 °C and 250 °C. Khan and Ashraf described this region as a post-curing [110], but upon further observation this event showed that it was the sum of multiple events. The region between temperatures of 100 °C and

150 °C can be described as the main curing reaction. Katović and Kombinat described the free phenol groups and ortho-methylol phenol groups reacting in the condensation reaction to form the methylene bridge between the two phenols. The next concurrent curing reaction occurred in the temperature range of about 150 °C and 175 °C and represented the formation of ether linkage between the phenol groups. This was characterized as the disappearance of the methylol group and the appearance of the ether group [111]. The next event occurred in the temperature range of 175 °C and 250 °C. Although Khan and Ashraf described the temperature range of 100 °C to 250 °C as post-curing, Katović and Kombinat pointed out the loss of ether groups at 210 °C and therefore the cleavage of the ether bridge between the phenols [110], [111]. There had also been oxidation (even in inert environments) of methylol groups to (1720 cm^{-1}) carboxyl groups [111], [112]. The temperature range after 175 °C was considered degradation in this work. The focus of this work will be on the two events of methylene and ether bridge formation which was part of the polymerization process expected in the PF resin, or the curing reactions. All regions between 250 °C and 400 °C were described as thermal degradation of hydrocarbon chains and distillation of volatile degradation products [109], [113].

The substitution of SF in the 70/30 PF/SF mixture (Figure 52 a & b) showed multiple peaks in the DTGA data. The TGA and DTGA data appear to be a combination of the events of neat PF and SF upon initial observation. The curing reaction was observed in the same general temperature range as the neat PF between 100 °C and 175 °C. The soluble sugar fraction was represented in the DTGA peak temperature of about 250 °C. This peak disappeared in the PF/SPI mixture (Figure 52 c & d) due to the absence of soluble sugar in SPI. The peak was present in the PF/soy-D mixture (Figure 52 e & f) indicating that there were still soluble sugars present in the denatured SF. Overall, the mass loss events for the PF/soy product mixtures during thermal

treatments appeared to be a combination of PF and the soy product. No new events were observed.

Residue Analysis

A residue analysis was performed to confirm that there were no new thermal treatment events due to the substitution of soy products in PF. The residue analysis was performed by comparing an actual residue of the PF/soy product mixture to an expected residue to test if it was indeed a combination of components. The expected residue of the PF/SF due to the combination of the neat PF and SF was calculated by using the following equation:

$$m_{mix} = 70\% m_{PF} + 30\% m_{SF} \quad (8),$$

where m_{mix} was the calculated mass percentage of the residue left that would be expected in the mixture if the components lost the same amount of mass, m_{PF} was the mass percentage of the residue left of the PF at that temperature, and m_{SF} was the mass percentage of the residue left of the SF at that temperature. The expected residue for the PF/SF mixture left after thermal treatment to 500 °C was less than 1% different from the actual residue. The PF/SPI actual residue was 5% lower, and the PF/soy-D actual residue was 2% lower than the expected residue.

Residue analysis was also performed after the curing reaction for each of the PF/soy product mixtures, the results of which were displayed in Table 6. There was not a considerable difference in the PF/soy product mixtures between the actual and expected residues left after the curing reaction.

Table 6: Actual versus calculated residues left after the curing reactions for PF/soy product mixtures

Resin Mixture	m_{mix} *actual (%)*	m_{mix} *calculated (%)*	*percentage difference (%)*	*Temperature at end of event (°C)*
70/30 PF/SF	87%	87%	1%	203
70/30 PF/SPI	85%	88%	-3%	200
70/30 PF/soy-D	88%	86%	2%	192

Powder PF DTGA

A study was performed to compare powder PF and liquid PF and the effect of SF substitution on each. Powdered PF was used in the manufacturing of oriented strand board as well as the liquid PF. Therefore, the work towards defining the contribution of SF to liquid PF found in this study could be transferred to powder PF if the thermal treatment properties were comparable.

The TGA/DTGA data for neat liquid and powder PF (Figure 53 a & b) were acquired from a dynamic thermal treatment of 2.5 °C/min. The TGA/DTGA data indicate comparable weight loss events due to thermal treatment. All observable DTGA temperature peaks complemented each other.

The TGA/DTGA data for neat liquid and powder PF (Figure 53 c & d) were acquired from a dynamic thermal treatment of 2.5 °C/min for the powder PF/SF mixture and 5.0 °C/min for the liquid PF/SF. The TGA/DTGA data also indicate comparable weight loss events due to the thermal treatment. The 80/20 PF/SF mixtures also show complementing DTGA temperature peaks. However, the temperature peaks for the liquid mixture were slightly higher than the powder due to the liquid mixture being subjected to a 5.0 °C/min temperature ramp instead of a 2.5 °C/min ramp like the powder mixture. Soy product influence on liquid PF as compared with

powder PF does not show significant differences when comparing TGA/DTGA data. It was therefore assumed that all results from the liquid PF TGA experiments apply to the powder PF as well.

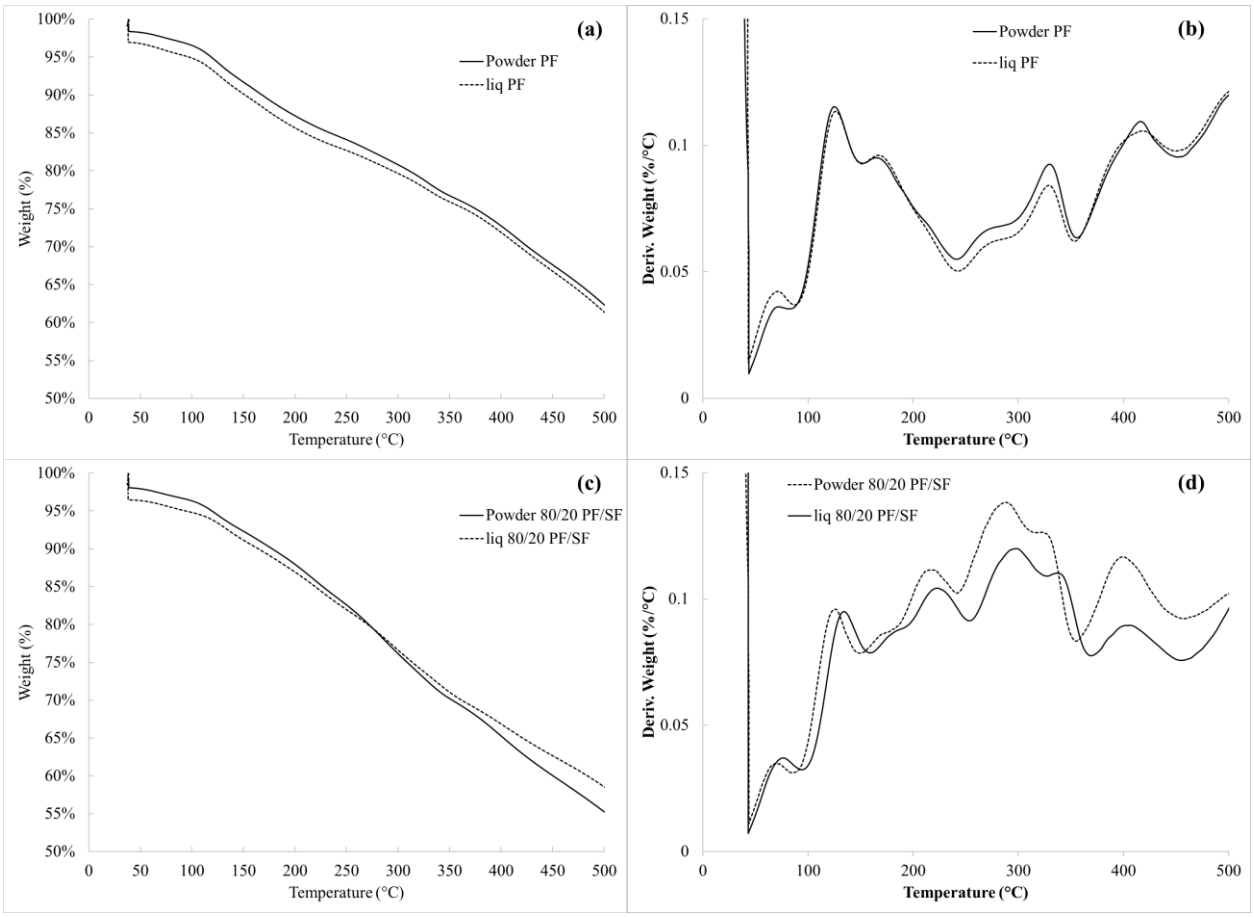

Figure 53: Dynamic TGA (left) and DTGA (right) data for neat powder PF and neat liquid PF (a&b); 80/20 powder PF/SF and 80/20 liquid PF/SF (c&d)

Differential Scanning Calorimetry (DSC)

Heat flow data from dynamic DSC scans of PF and 70/30 PF/SF (dry weight/dry weight) at 5, 10, 15, and 20 °C/min ramp rates were analyzed and used to corroborate TGA data used in the TGA/DTGA study of PF and soy products. The curing reactions were identified in the DSC data to confirm the findings in the TGA/DTGA study. The validity of using the vacuum drying procedure to avoid curing of the liquid PF samples was also verified.

The exothermic peak could be attributed to the heat release of the curing reaction. This peak was identified in the DSC data from the thermal treatment of a vacuum dried PF sample (Figure 54 – left). A DSC scan was performed on a sample of PF that had been cured at 130 °C for 60 minutes to represent a full cure (Figure 54 – right). The heat flow data for the non-cured and fully cured samples were compared to validate the vacuum drying process.

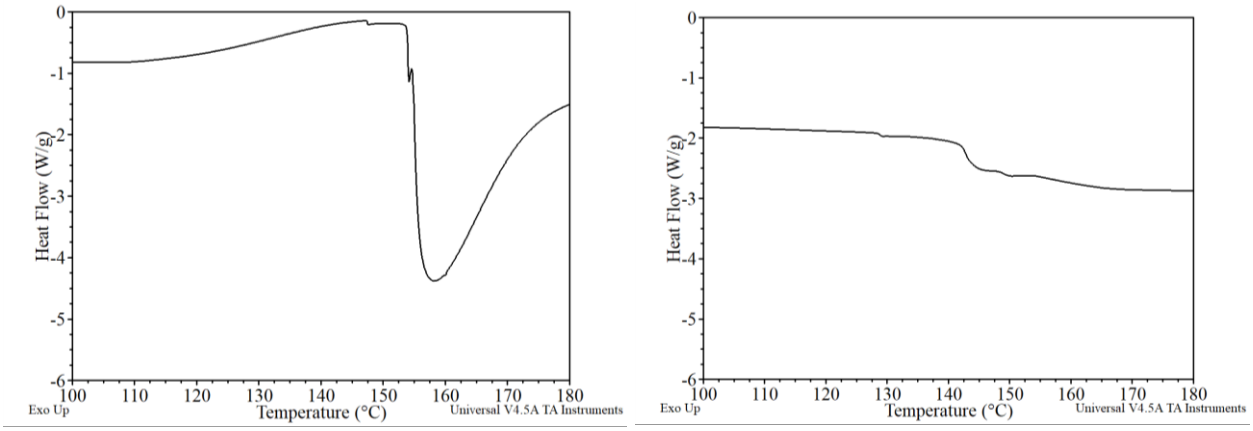

Figure 54: Dynamic DSC scan data of PF vacuum dried (left) and fully cured (right) at 20 °C/min

The vacuum dried PF data showed an exothermic curve in the temperature range of about 120 °C to 150 °C. This exothermic curve was immediately followed by an endothermic curve in the temperature range of about 150 °C to 180 °C. This endotherm was believed to indicate the release of moisture from the condensation reaction of the formation of methylene bridges during the first curing reaction. This followed the same pattern as all dynamic DSC scans of non-cured, vacuum dried PF and PF/SF samples. One could also observe a glass transition around 147 °C.

The fully cured PF data showed no exothermic or endothermic curve. This was further evidence that the exothermic curve followed by the endotherm was indicative of the curing reaction for methylene bridge formation. It should be noted that a glass transition also occurs in the fully cured sample around 143 °C.

The endothermic peak (Figure 54 – left) can be attributed to a volatile gas release. Figure 55 displayed the dynamic DSC heat flow data for both PF and 70/30 PF/SF where the temperature had been increased, decreased, increased, and decreased again all at a constant rate of 10 °C/min.

The first ramp showed the glass transition (~145 °C), exothermic curve (~120-150 °C), and endothermic curve (~150-160 °C) displayed in Figure 54 (left). There was also another endothermic curve towards the end of the first temperature increase. This could be attributed to moisture given off due to two methylol groups forming an ether bridge in the condensation reaction of the second curing reaction [114], [115]. There was also the possibility that this could be formaldehyde given off due to ether bridge degradation to a methylene bridge, but there was no indication of a formation of ether bridges at a lower temperature. Therefore, it was assumed this higher temperature endotherm represented the second curing reaction of ether bridge formation.

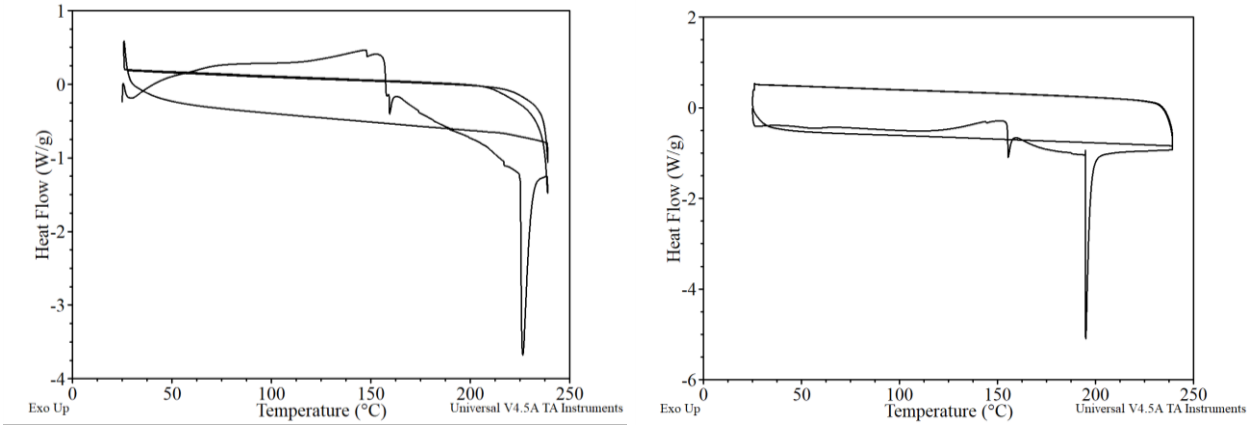

Figure 55: DSC scan data of PF (left) and 70/30 PF/soy flour (right) with a ramp up, cool down, ramp up, then cool down at 10 °C/min

In Figure 55, The samples go through a cool down cycle depicted by the flat line above the first temperature increase. The constant temperature increase was then repeated and can be

depicted by the flat line in the same area as the first temperature increase. A flat line for the second temperature increase was indicative of volatile substances given off in the endothermic curves observed in the first temperature increase. Therefore, it was assumed that the lower temperature endothermic curve represents the first curing reaction of methylene bridge formation, and the higher temperature endothermic curve represents the second curing reaction of ether bridge formation.

The heat flow data from dynamic DSC scans of PF and 70/30 PF/soy flour at 5, 10, 15, and 20 °C/min ramp rates were analyzed and used to corroborate TGA data (Figure 56). The temperature peaks attributed to the lower temperature DSC endothermic curve data for the release of volatile gases during the first curing reaction (DSC-endo), the DSC exothermic temperature peak for the first curing reaction (DSC-exo), and the DTGA temperature peak data used for the calculation of activation energy for the first curing reaction (DTGA) were compared with each other. The data was separated by ramp rate since ramp rate affects the heat flows and mass losses attributed to the thermal treatment rate in DSC analysis and TGA. The temperature data were both from PF and 70/30 PF/SF because both showed similar exotherms and endotherms.

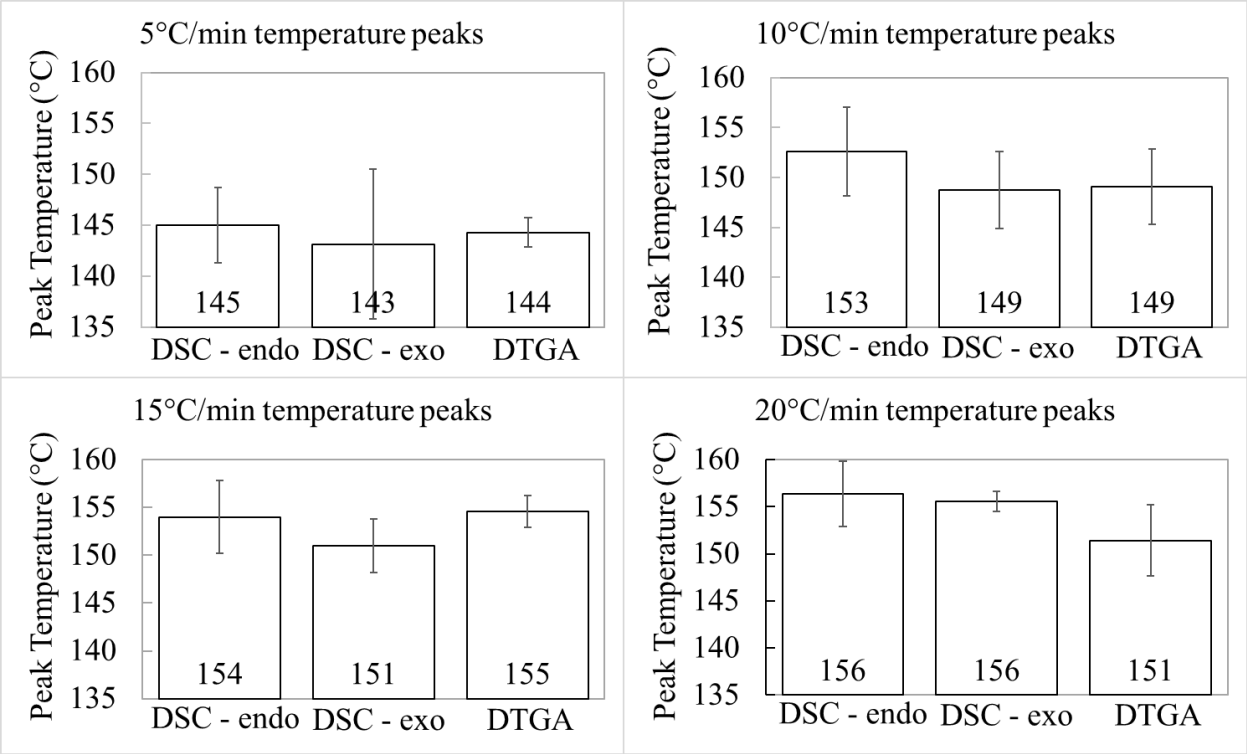

Figure 56: Comparison of peak temperatures for dynamic DSC and TGA data at different ramp rates

The endothermic peak temperature average was slightly higher than the exothermic peak temperature average which follows what had been shown with previous DSC data. The DTGA temperature peak data fell within the standard deviations of the temperature peaks of the endothermic and exothermic curve observed in the DSC data. This evidence suggested that the DTGA temperature peak data followed well with the reaction kinetics of the condensation reaction that occurred during the polymerization of PF and PF/SF mixtures and was sufficient in calculating the activation energy of the curing zone using the DTGA temperature peak data.

The DSC/TGA corroboration along with some disadvantages to using DSC analysis versus TGA for thermal analysis showed that the TGA/DTGA was favorable to DSC analysis. The disadvantages of using DSC over TGA included the following: using a hermetically sealed pan versus an open pan which led to risk of volatile contamination of the sensitive equipment on

the DSC if the pressure rose above the 300 kPa rating; the overlaying of the endothermic curve over the exothermic curve data during the curing reaction resulting in temperature peak identification difficult; using a smaller sample amount decreasing the accuracy of the results; and the difficulty of use compared to the TGA leading to smaller number of samples decreasing the accuracy of the results. Higher pressure rated pans than the hermetically sealed pans were available but were costlier and less accurate due to pan heat flow. However, the combination of DSC analysis and TGA was essential to defining the curing reactions.

Activation Energy Calculation through Thermogravimetric Analysis

The DTGA temperature peaks of thermal weight loss events were used to calculate activation energy for each reaction event using the Kissinger method. The following shows the results for activation energies for the release of volatiles in the lower temperature event for neat PF and all PF/soy product mixtures.

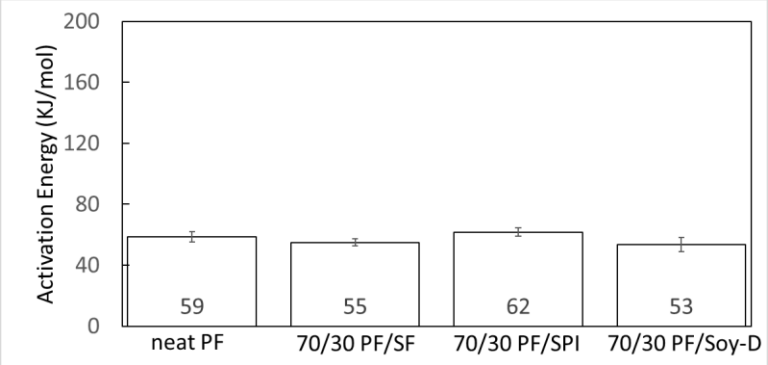

Figure 57: Calculated activation energies for the release of low molecular weight volatiles

The activation energies closely resembled each other for all materials. The energies were low compared with the other reactions because this reaction represented low molecular weight monomers that were being released from the PF and soy product substituted PF mixtures [109]. These results verified the accuracy of this procedure to calculate activation energy. The variation

was very low, and the results were expected to be similar to each other in this reaction because of the PF containing the low molecular weight volatiles.

The following shows the results for activation energies for the first curing reaction forming methylene bridges between the phenols.

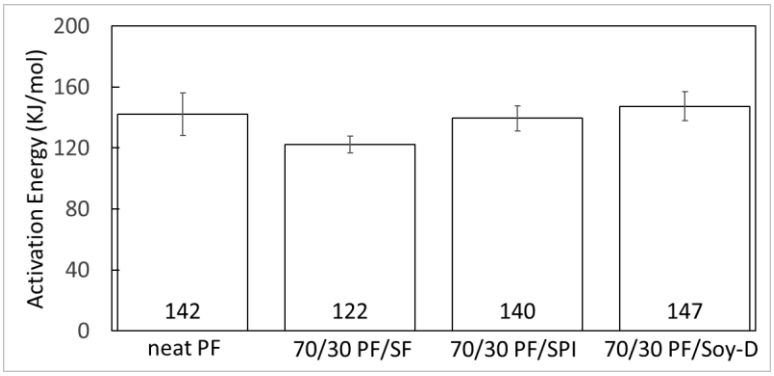

Figure 58: Calculated activation energies for the formation of methylene bridges (first curing reaction)

Overall the activation energies for the methylene bridge formation were similar. One would expect to see more contrast between activation energies for curing if the mechanism that was altered due to soy product substitution was a chemical crosslinking one. There was a small drop in the 30% SF substituted resin in activation energy, but the activation energy for the PF/SPI mixture having a higher protein content would have trended down for the first curing reaction if the protein from the soy flour was interacting chemically with the PF matrix.

The activation energies for the second curing reaction forming ether bridges between the phenols was calculated (Figure 59). As in the formation of the methylene bridges, there was no significant difference in the activation energies for the second curing reaction involving ether bridge formation.

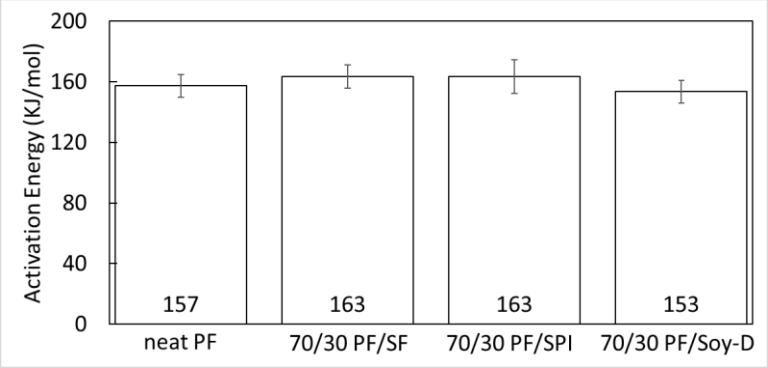

Figure 59: Calculated activation energies for the formation of ether bridges (second curing reaction)

The evidence from the TGA/DTGA study and the activation energy corroborate each other in suggesting that if there was a change in the crosslinking mechanism due to the interaction of soy products with PF, it did not play as significant of a role as its interaction with the wood/resin interface. The work from the screening sections was therefore corroborated to more of a degree in refuting the hypothesis for SF and PF.

Isothermal Thermogravimetric Analysis

Isothermal TGA was used to further characterize the first curing reaction involving methylene bridge formation. An example of the identification of the end of the cure was explained through the dynamic TGA data for a PF sample used in the TGA study using a constant temperature increase of 5 °C/min. The analysis was performed using the TA instruments software as seen in the following figure.

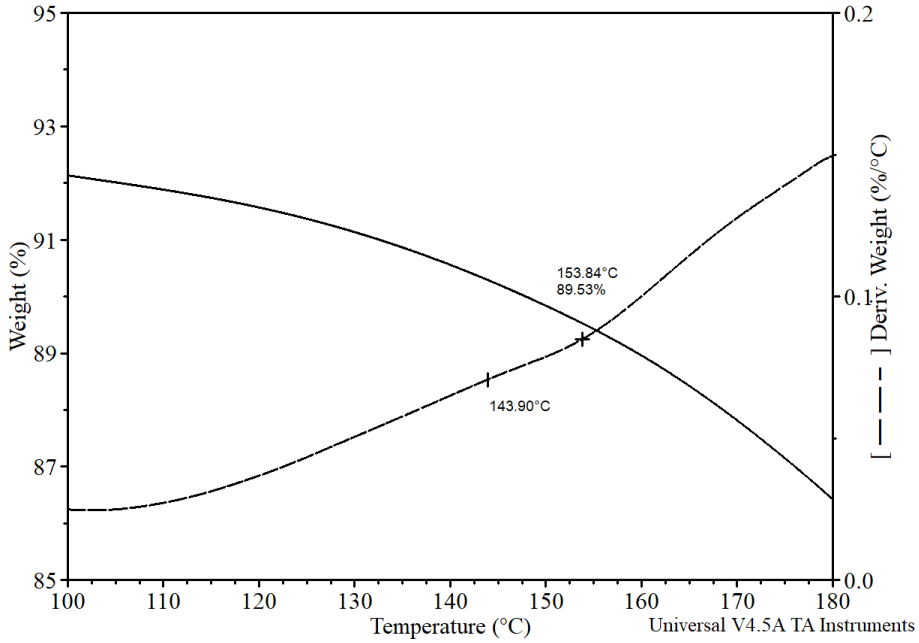

Figure 60: TGA (solid) and DTGA (dash) data of PF ramp (5 °C/min) showing curing peak and point of full cure

The first temperature identified (144 °C) was the DTGA temperature peak of the first curing reaction. The second temperature (154 °C) was the DTGA inflection point at which it was assumed that the cure was complete. This was assumed because it was the temperature at which the smallest amount of weight change was occurring between the first and second curing reactions and therefore represented a transition between these.

The following was a plot of the DSC heat flow data of neat PF taken at the same ramp rate as the TGA sample shown above.

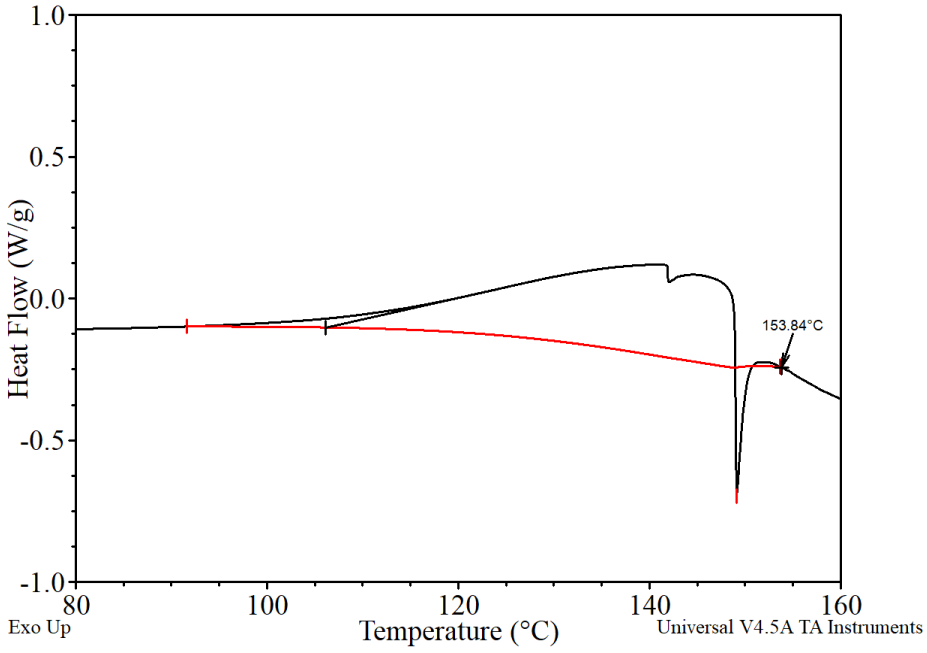

Figure 61: DSC data showing curing region for PF at a ramp rate of 5 °C/min with DTGA inflection point identified

The temperature from the DTGA point of inflection, where it was thought that the point of full cure occurred (154 °C), was identified in the DSC data above. The point occurred directly after the endothermic curve indicating the release of water from the condensation reaction. This evidence suggested that the point of inflection in the DTGA data was sufficient in estimating the temperature of the end of the first cure for that ramp rate. This also fell within literature values of PF curing [109]. Therefore, the mass percentage left at the point of inflection in the DTGA data signified full cure. DTGA point of inflection data was used as the method for identifying transitions between each of the mass loss events (or zones) identified earlier.

The DTGA temperatures of full cure of the first curing reaction were analyzed for all TGA temperature ramp rates to estimate the mass percentage left at full cure. The mass percentage data was then compared with each other by using one-way ANOVA (α=0.05). There

was no significant difference when comparing ramp rates of all samples (p=0.792). The mass percentage left at cure was therefore not dependent on the ramp rate.

The data did show significant differences between the type sample (PF, 30% soy, 30% SPI, or 30% soy-D) (Figure 62).

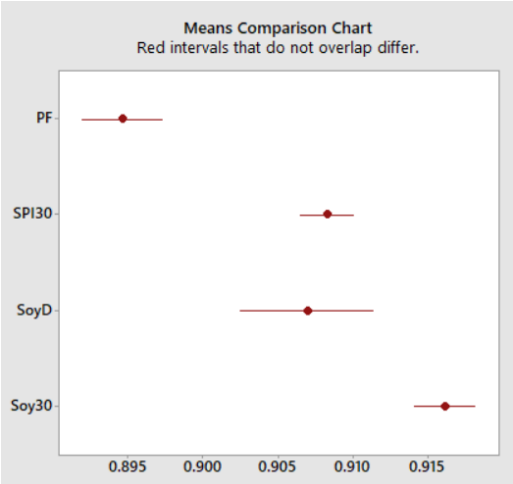

Figure 62: Comparison of mass left after full cure of the first curing reaction for neat PF (PF), 70/30 PF/SPI (SPI30), 70/30 PF/soy-D (Soy-D), and 70/30 PF/soy flour (Soy30)

The chart above shows that PF had the least amount of mass left over at full cure. This showed that PF required the most mass loss to achieve a full cure. The 70/30 PF/soy flour mixture showed the least mass loss to achieve full cure. This was significant in that approximately 2% more adhesive was left in any wood composite using the PF/SF mixture than neat PF. The PF/SPI and PF/soy-D showed similar mass losses – less than PF but more than PF/SF. An explanation for the higher mass left for the PF/soy product mixtures was that the extra soy product residue was not reacting with the PF therefore not releasing moisture from the condensation reaction. This further refuted the hypothesis that soy products were altering the PF to a higher degree in cohesion rather than the wood/resin interface.

The mass loss data was then used with isothermal TGA data to estimate the time of cure for each sample. The TGA data was plotted, and the time was found when each sample achieved a mass loss equal to the mean of the mass loss for the type of sample.

An example of the time of cure analysis can be seen in the following plot of an isothermal TGA run of PF at 130 °C.

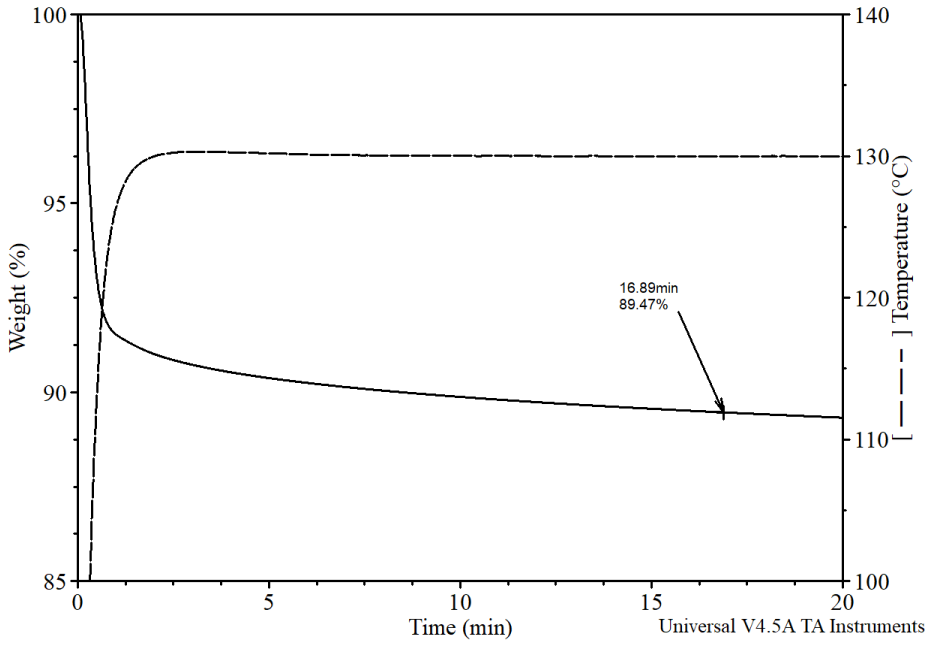

Figure 63: Isothermal TGA run of PF at 130 °C showing point of cure

The isothermal TGA runs were heated at a constant temperature for two hours to collect mass loss data sufficient enough to compare to the mass loss data of the dynamic TGA for the first curing reaction. The mass loss at the end of the two-hour cycle varied considerably which caused variation in the time of cure measurements. When the time of cure was compared with the mass loss of that same sample after two hours, there was a linear relationship between the two. The following normalization equation was used.

$$X = \left[a + \frac{(x - A)(b - a)}{B - A}\right] \times 100 \quad (9),$$

where *x* was the time of cure, *X* was the new data point, *a* was the minimum mass loss after two hours, *b* was the maximum mass loss after two hours, *A* was the minimum time of cure, and *B* was the maximum time of cure in the dataset.

This data was then compared with each other according to mix using either a one-way ANOVA (α=0.05) for all or a 2-sample t test (α=0.05) for direct comparison between two mixes (Figure 64).

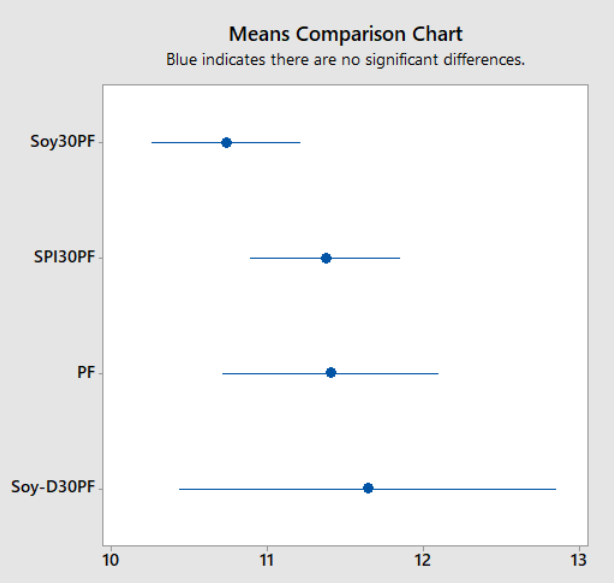

Figure 64: Comparison of normalized time of cure for the first curing reaction of neat PF (PF), 70/30 PF/SPI (SPI30PF), 70/30 PF/soy-D (Soy-D30PF), and 70/30 PF/SF (Soy30PF)

There was not a significant difference between the time of cures for all the mixes (p=0.075), although the PF/SF displayed the lowest time of cure. The lesser amount of mass loss needed to achieve full cure (8.4% for PF/soy flour versus 10.5% for neat PF) was believed to reflect the times of cure. This was further evidence to refute the primary hypothesis showing soy products do not significantly affect the curing kinetics of PF during the curing reaction.

PF – FT-IR Analysis

FT-IR spectral analysis involved observation of each transition spectra identified earlier between the dynamic DTGA temperature peaks of PF and the 70/30 PF/soy product mixtures. This involved the uncured sample and the first, second, third, and fourth transitions of the sample. It was believed that the second transition represented the end of the first curing reaction (formation of methylene linkage), and the third transition represented the end of the second curing reaction (formation of ether linkage). Absorbance was measured in arbitrary units and offset equally for all transitions for each spectrum for comparison purposes.

Figure 65 shows the deformation bands associated with unsubstituted hydrogen bonds in the benzene ring. The band at 777 cm^{-1} represented the deformation vibrations of the C-H bond in benzene rings of three or four adjacent unsubstituted C-H bonds. This indicated substitution at positions 1,2 and 1,2,3 on the benzene ring. This band was assigned to substitution at positions 1,2 and 1,2,6 on the benzene ring which represented substitution at the ortho sites on the phenol group [116]. This band was diminishing as the cure progressed due to para substitution on the phenols during the polymerization reaction. The band at 755 cm^{-1} became more pronounced as the band at 777 cm^{-1} diminished.

The bands at 841 and 852 cm^{-1} represented two adjacent unsubstituted C-H bonds and were assigned to substitutions at positions 1,4 and 1,2,4 on the benzene ring indicating para as well as para and ortho substitution on the phenol group [116]. The band at 880 cm^{-1} representing a single, isolated C-H bond was also assigned to the 1,2,4 positions [116]. The bands at 841 and 852 cm^{-1} could be seen strengthening from no cure to the second transition at full cure meaning more substitution on the phenol suggesting polymerization. The band at 880 started to diminish

as compared to the 841 and 852 cm^{-1} bands in the third and fourth transitions signifying a breakdown of the polymer due to degradation.

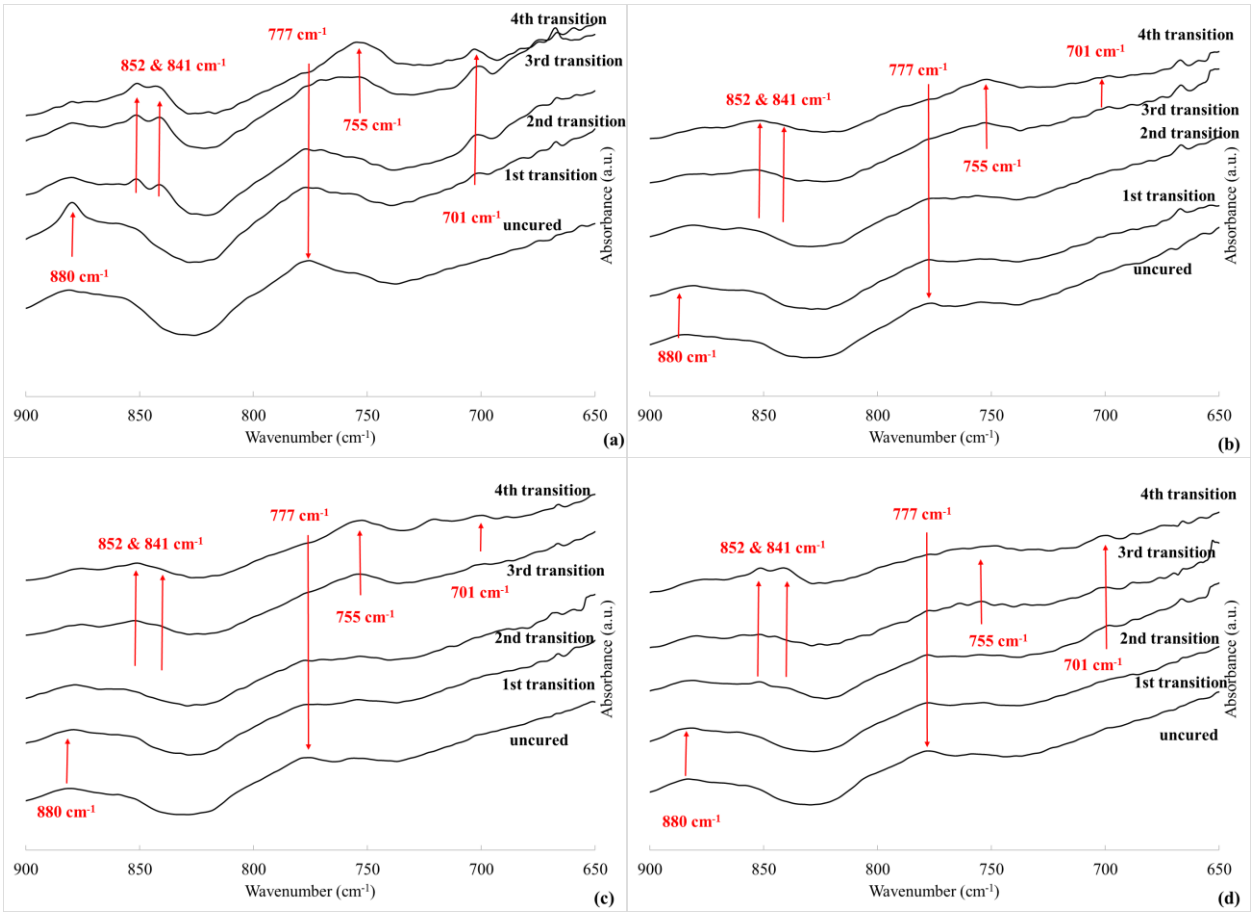

Figure 65: FT-IR spectra for wavenumbers 900-650 cm^{-1} comparison of non-cured and transitional TGA thermally treated samples of PF (a), 70/30 PF/SF (b), 70/30 PF/SPI (c), and 70/30 PF/soy-D (d)

The bands in neat PF (Figure 65 a) were more pronounced than the PF/soy product mixture bands at 880, 852, and 841 cm^{-1}. This was likely due to a lesser amount of PF in the mixture attenuating the signal. The PF/soy-D (Figure 65 d) showed more signal in the wavenumber bands of 852 and 841 cm^{-1} in the fourth transition which compared to the neat PF. This fourth transition could be the point at which the ether bridges were cleaved [111]. This would explain why it was more pronounced after observing the 880 cm^{-1} band signifying more benzene positions filled in the first transition of the neat PF. It could show that the PF/soy-D

mixture showed better resistance to cleavage along with neat PF compared to the other PF/soy product mixtures. It was likely that the other signals were attenuated because of the substituted SF or SPI.

As far as degradation, a band at 701 cm^{-1} could be seen in the degradation transitions representing five adjacent unsubstituted C-H bonds on the benzene ring [117], [118] suggesting a phenol with detached methylol groups as well as methylene and ether bridges. This band becomes more prevalent after curing and was seen increasing in the fourth transition. Neat PF (Figure 65a) displays more activity in this band likely because of the presence of more phenol.

The band at 1005 and 1031 cm^{-1} (Figure 66) represented either the C-O stretching in the C-OH group of the hydroxymethyl group attached to the phenol or the C-O-C stretching in the dimethylene ether bridges in the polymer matrix. Ebewele et. al. have explained that there was considerable variation in the assignment of absorption bands in the literature [118]. The C-OC stretch of the ether bridge had been reported as 1100 cm^{-1}, [119], 1064 cm^{-1}, [118], and 1050 cm^{-1}, [118], and the C-O stretch of the methylol group had been reported as 1045 cm^{-1}, [119], 1040 cm^{-1}, [120], 1010 cm^{-1}, [121], [122], 1000 cm^{-1}, [118], 1050 cm^{-1}, [123], and 1058 cm^{-1}, [112]. The formation of ether and methylene bridges was enhanced as the polymerization reaction progressed and used free methylol groups in the process. Therefore, the increase in the band at 1031 cm^{-1} coincides with the ether bridge formation while the slight decrease in intensity of the band at 1005 cm^{-1} accounted for the hydroxymethyl groups forming ether and methylene bridges during the polymerization reaction up to the second transition.

It was expected to observe a larger signal in the 1031 cm^{-1} band in the third transition, but it was either the same or slightly attenuated compared to the second transition. This was evidence that the second curing reaction could be occurring at a lower temperature, and the volatile gas

given off seen at the higher temperature in the DSC experiment could be formaldehyde given off from ether bridges becoming degraded into methylene bridges.

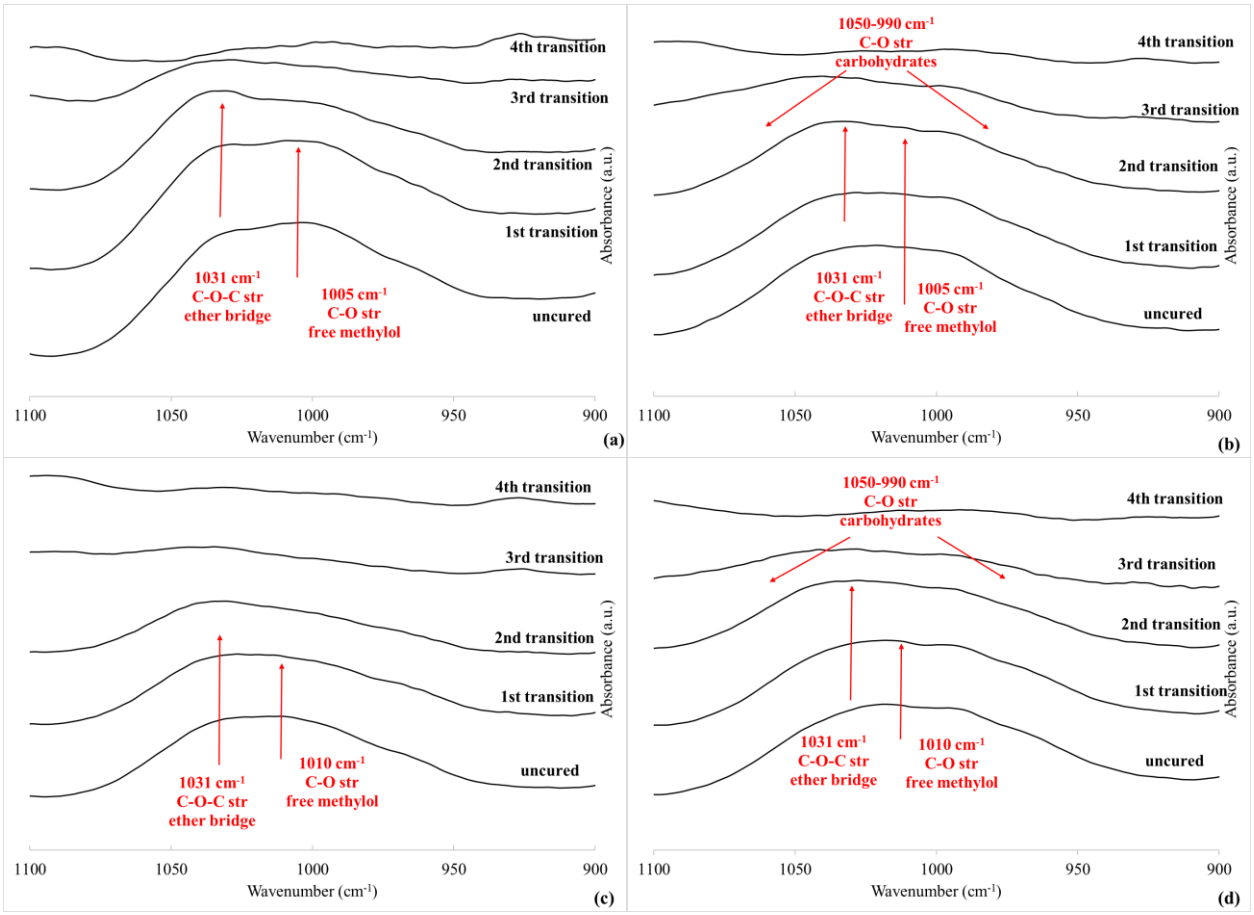

Figure 66: FT-IR spectra for wavenumbers 1100-900 cm^{-1} comparison of non-cured and transitional TGA thermally treated samples of PF (a), 70/30 PF/SF (b), 70/30 PF/SPI (c), and 70/30 PF/soy-D (d)

In the PF/SF and PF/soy-D mixture spectra (Figure 66 b & d), there was a combination of in the wavenumber band region of about 1050-990 cm^{-1}. There was a combination of the hydroxymethyl group and ether bridge formation described previously in the PF at 1010 and 1031 cm^{-1} and the C-O stretching from soy flour indicating sugar molecules [124] shown at a band of 1049 cm^{-1} in Kim and Netravali's work [125]. Similarities were seen between this peak and the PF peak at 1025 and 1031 cm^{-1} described above although the overlaying of SF and soy-D

carbohydrates attenuates some of the signal. The PF/SPI mixture spectra (Figure 66 c) does not include the carbohydrate band due to the high protein content.

The peaks at wavenumbers 1441,1458, and 1472 cm^{-1} (Figure 67) represented the C-H bend of the methylene bridge [82]. Roczniak et. al. reported methylene bridges at para-para' at 1450 cm^{-1}, ortho-ortho' at 1460 cm^{-1}, and ortho-para at 1480 cm^{-1}, [116]. The band at 1458 cm^{-1} was likely the band representing methylene bridges between ortho-ortho' sites. As the polymerization reaction progresses, the band at 1472 cm^{-1} strengthens as compared to the one at 1458 cm^{-1} signifying more ortho-para' methylene bridges forming. Para-para' was represented by the band at 1441 cm^{-1}. The PF/soy-D mixture spectra (Figure 67 d) was observed as favoring ortho-ortho' methylene bridges rather than ortho-para methylene bridges. Ortho-ortho bridges were prevalent in the crosslinking network because of steric hindrance of the methylated phenol groups. It was likely that the ortho-para bridge content was less prevalent in the PF/soy-D mixture as compared to the neat PF, and the neat PF's band at 1472 cm^{-1} overlaid the 1458 cm^{-1} peak.

There was an extra peak (1390-1400 cm^{-1}) that appeared in all PF/soy product mixture spectra (Figure 67 b-d) not seen in the neat PF. This peak represented the CH_3 bending vibration that was seen in soy flour [126].

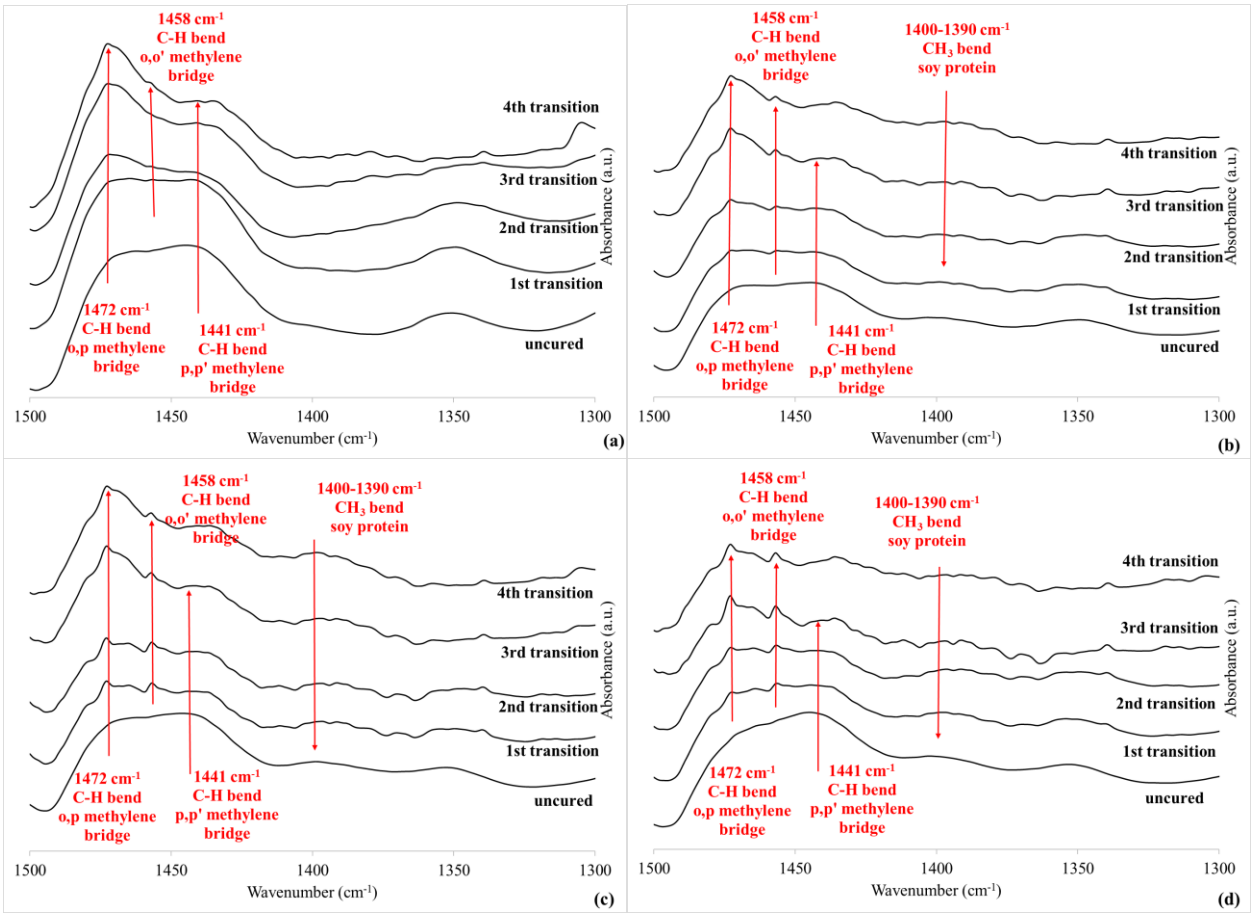

Figure 67: FT-IR spectra for wavenumbers 1500-1300 cm^{-1} comparison of non-cured and transitional TGA thermally treated samples of PF (a), 70/30 PF/SF (b), 70/30 PF/SPI (c), and 70/30 PF/soy-D (d)

Overall, there was no unambiguous evidence of new chemical modification present due to the interaction of soy products and PF before or during the curing process. There were some differences between the FT-IR spectra of soy product substitution in PF and neat PF including bands from the soy protein itself, but other differences were mainly attenuation of the PF/soy product FT-IR spectra indicative of less PF content. There were no clear indications of the curing reaction being affected. There were no new peaks observed in the mixture that were not seen in the neat components with curing. This was also evidence that there was very little or no cross-linking occurring between the PF and soy product mixture during curing.

The FT-IR spectra were also analyzed to compare the SF spectra with subtraction spectra. The subtraction spectra consisted of the PF spectra subtracted out of the PF/SF mixture spectra. This was performed to identify any major differences in the mixture spectra from the neat components that were not identified with observation of the spectra by themselves. If there was no crosslinking between the SF and PF, then the PF/SF mixture spectra would just be a combination of the neat components of PF and SF. The Dewiggle algorithm [127] from Thermo Fisher was used for the spectral subtraction.

The neat PF, neat SF, and 70/30 PF/SF mixture samples were heated in a mechanical convection oven to cure the samples for 30 minutes at 130 °C. The samples were then taken out of the oven and scanned with the FT-IR spectrometer.

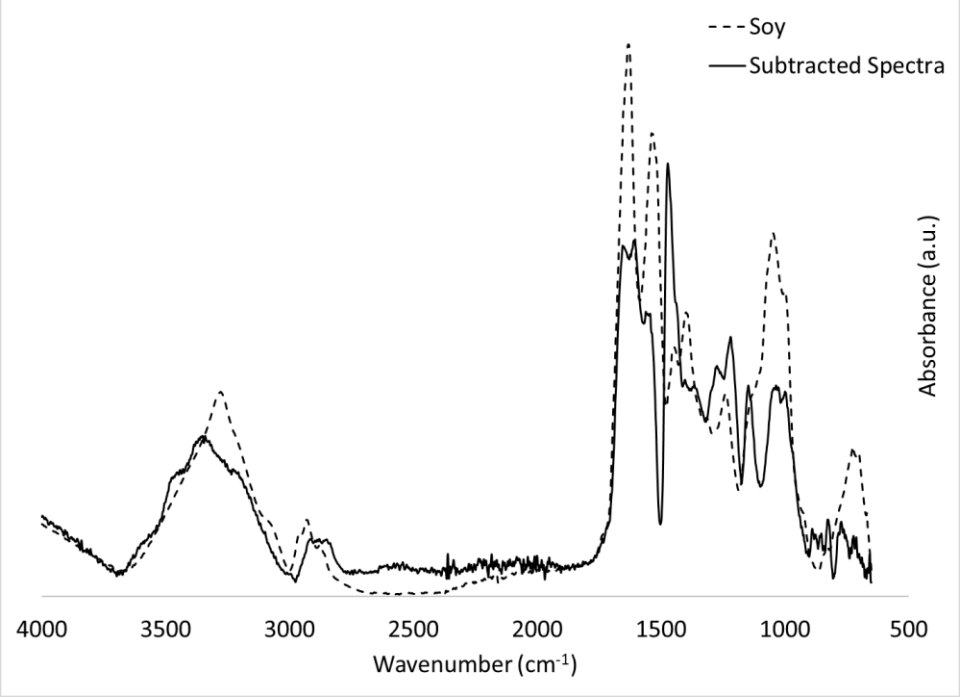

Figure 68: Spectra of cured soy flour and of a subtraction spectrum of a cured mixture of 70/30 PF/SF with the cured PF component stripped out

The spectra in Figure 68 were similar but not indistinguishable. Spectral subtraction was difficult and could lead to ghost peaks as pointed out by Myers et. al. [104]. An example of this

was observed with the bands at the wavenumber range of 1050-990 cm^{-1} which included the ether linkage and free methylol groups from the PF and the carbohydrates from the SF. This combination showed the largest ghost peak observed in this range as a result. The Dewiggle algorithm eliminated any bias, but some differences remained. All FT-IR analyses were considered supportive of the absence of significant chemical interaction between PF and soy products during curing performed in the process described.

The FT-IR work showed the accuracy of the data analysis through extensive identification of functional groups throughout the cure and degradation of PF, SF, and PF/soy product mixtures. The cured samples showed evidence that refuted the hypothesis confirming results of the activation energy of the curing zone in that if there was a change in reaction kinetics with soy product substitution in PF it was not as significant as its interaction with the wood/resin interface shown in the screening experiments.

Conclusions

The TGA work revealed that overall the soy product substitution in PF exhibited mass loss events due to thermal treatments comparative to a combination of the soy product and PF components. This was especially true in the curing region (about 100-175 °C for 5 °C/min ramp). Residue analysis showed little difference between the actual and expected residues of all PF/soy product mixtures with TGA thermal treatment after the curing event (~200 °C). Powder PF was shown to reflect the effects of SF substitution in liquid PF in TGA/DTGA data and therefore shown to have similar chemical crosslinking characteristics as defined by TGA experimentation since liquid and powder PF were essentially the same species according to evidence of TGA. This experiment showed that the primary mechanism of adhesion changed for liquid PF with the addition of soy products can be assumed for powder PF.

DSC work was performed to identify the curing reactions. The first reaction was defined as the formation of methylene bridges, and the second curing reaction was identified as the formation of ether bridges – although there was a possibility that the event identified could possibly be the degradation of the ether bridge into a methylene bridge.

The DSC data for the first curing reaction was then compared with the DTGA temperature peaks to corroborate the TGA data as well as the activation energy calculation that employed the DTGA temperature peaks in the method. No significant differences were observed between activation energies of neat PF and PF/soy product mixtures in either the first or second curing reaction.

The evidence from the TGA study and the activation energy analysis corroborated each other in suggesting that if there was a change in the crosslinking mechanism due to the interaction of soy products with PF, it did not play as significant of a role as its interaction with the wood/resin interface. The work from the screening sections was therefore corroborated to more of a degree in refuting the hypothesis for SF and PF.

Isothermal TGA was used to corroborate transition temperatures between reaction events through identification of inflection point temperatures of dynamic DTGA data. The temperature of the transition from the first curing reaction to the next was verified with DSC data and DTGA inflection point temperatures. The time of cure was comparable between the neat PF and PF/soy products indicating corroboration that soy product substitution did not enhance the cohesiveness of PF found with the TGA work.

FT-IR spectral analysis determined wavenumber band peaks relevant to the polymerization of PF. Functional groups were identified throughout the cure and degradation of PF, SF, and PF/soy product mixtures. The cured samples showed evidence that refuted the

hypothesis again confirming results of the activation energy of the curing zone in that if there was a change in reaction kinetics with soy product substitution in PF, it was not as significant as its interaction with the wood/resin interface shown in the screening experiments.

Additional formaldehyde would be required to match the crosslinking demonstrated by prior published work since formaldehyde was shown to methylate soy protein. This explained why the denatured soy (soy-D) did not show a significant difference in activation energy of the curing reactions as compared with the other resin formulations. It was also possible that the soy products were physically crosslinked in the PF polymer matrix and did not benefit the crosslinking bulk due to a chemical reaction between the PF and soy products. Crosslinking demonstrated through prior publications was not possible with the process in this work because the phenol and formaldehyde had already reacted together to a certain degree therefore leaving minimal formaldehyde to methylate the soy products.

Chapter 7: Methylene Diphenyl Diisocyanate and Soy Product Curing Kinetics

Introduction

The work in this chapter focused on understanding the interaction between soy products and the wood adhesive, polymeric methylene diphenyl diisocyanate (pMDI). Understanding the interaction aided in determining whether soy products affected the overall resin to a higher degree in adhesive failure or cohesive failure. The curing kinetics were studied in neat pMDI and mixtures of various soy products with pMDI to understand how the overall adhesive was affected. These soy products included defatted soy flour (SF), soy protein isolate (SPI), and denatured, defatted soy flour (Soy-D).

Thermogravimetric analysis (TGA) was used to characterize the curing reaction of each of the resins. TGA was also performed to characterize degradation pathways to understand the products produced from the pMDI/soy product mixtures as well as compare them with the neat pMDI resin. The experimental activation energies of the curing reactions of the pMDI/SF mixtures and the neat pMDI were also calculated using data obtained from thermal treatment of the resins. Data obtained from Fourier Transform-Infrared (FT-IR) spectroscopy of the cured and non-cured pMDI/SF mixtures and the neat pMDI were analyzed through spectral interpretation. Identified wavenumber bands of importance through examination of prior published work or identification of appearing or disappearing bands were analyzed.

Materials and Experimental Method

Soy protein isolate (SPI), ProCote 4200, was donated by Solae, LLC. Defatted soy flour (7B) was provided by Archer Daniels Midland, of which about half of the mass of soy flour was constituted of soy protein [29]. The pMDI resin used was MONDUR 541 manufactured by Bayer Material Science LLC and donated by J. M. Huber Corporation. pMDI and MDI were used interchangeably throughout this section. The denatured, defatted soy flour (Soy-D) was prepared according to the Wescott/Frihart method [34].

Thermogravimetric Analysis (TGA)

Thermogravimetric Analysis (TGA) was applied on data from resin samples thermally treated using the TA Instruments Q5000 IR thermal analyzer. This thermal weight-change instrument was operated in conjunction with the TA Instruments Universal Analysis 2000 program version 4.5A.

Thermal treatment was administered to various samples containing pMDI and/or soy products during constant temperature increases (dynamic TGA or ramp) treatments while measuring mass loss and time. Ramp thermal treatments were administered to characterize volatile evaporation, curing reactions, and degradation reactions.

Weight and temperature calibration was performed on the thermal analyzer at least every two days of testing. The chamber was purged with 90/90 mL/mL of N_2/N_2 in the balance/sample for 30 minutes if there was a period of non-testing. Longer intervals of inactivity on the thermal analyzer required 200/200 mL/mL of N_2/N_2 in the balance/sample for 12 hours.

TGA Sample Preparation

Prior to thermal treatment, samples were prepared of uncured neat pMDI and mixtures of pMDI and soy products. The following resin ratios were prepared: 70/30 (dry weight /dry weight) pMDI/SF, 70/30 pMDI/SPI, and 70/30 pMDI/Soy-D. The neat SF, SPI, and Soy-D TGA and DTGA data were the same data as the PF TGA experiment. The liquid MDI mixtures were mechanically mixed with the soy product in a sample tray with a metal spatula until sample was visually uniform. The SF and SPI were in powder form and assumed dry when mixed with pMDI. The Soy-D samples were not dry and prepared as described in the Wescott/Frihart procedure [34] with the same water content when mixed with pMDI.

Approximately 15 mg of the sample (neat pMDI or pMDI/soy product mixture) was weighed out into a tared platinum-HT pan. The pan was then loaded into the TA Instruments Q5000 IR thermal analyzer. A purge rate of 10/90 mL/mL of N_2/N_2 in the balance/sample was used.

The thermal analyzer was programmed to increase the temperature at a constant rate (i.e. ramp) to a certain final temperature (500 °C in most cases). The temperature ramp consisted of constant rates of 2.5, 5.0, 10.0, 15.0, or 20.0 °C/min from room temperature to the desired temperature.

There was a minimum of five replications per temperature ramp per sample. These five replications were required to produce data that contained no noise in the TGA/DTGA data. The DTGA temperature peaks were also required to have no outliers when compared with each other. Grubbs and Dixon's ratio outlier tests were used with the Minitab® 18.1 software to eliminate any outliers.

Activation Energy Calculation

The DTGA data was employed to identify temperatures at which the maximum amount of mass loss occurred during each of these characterization events, referred throughout this work as temperature peaks. These temperature peaks were identified for each event at various ramp rates, and a temperature range was identified containing these temperature peaks for each event, referred throughout this work as zones. The temperature peaks were used to calculate activation energy for each of those events.

The following shows a plot of typical TGA and DTGA data for a 70/30 MDI/SPI sample.

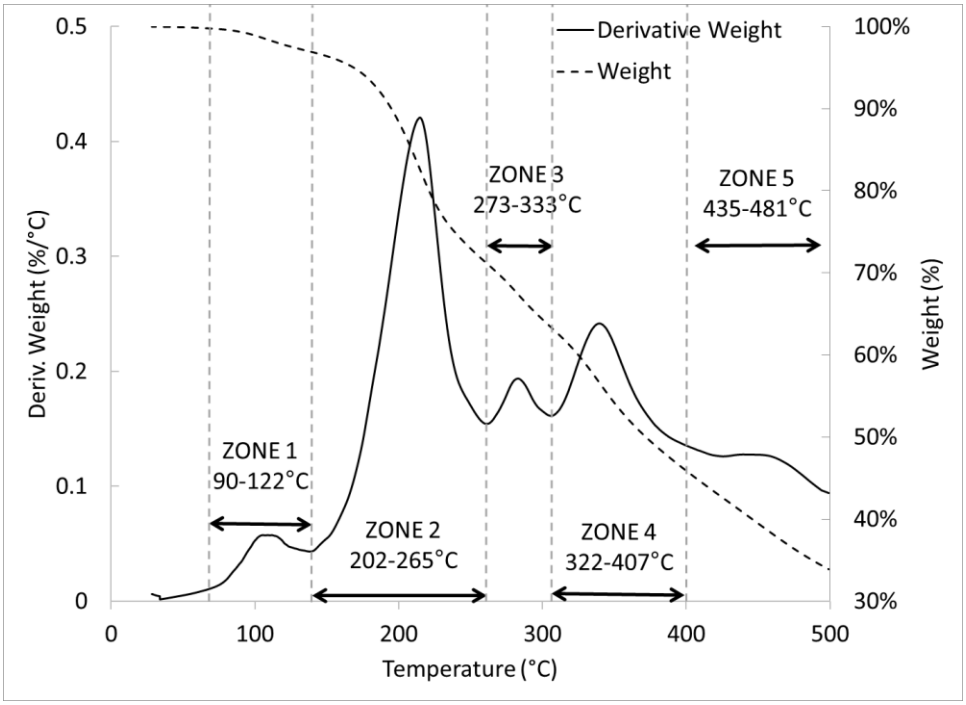

Figure 69: TGA and DTGA data showing five temperature ranges (or zones) of reaction events that were analyzed

Figure 69 was shown as a visual aid to help identify temperature ranges (or zones) of the DTGA temperature peaks found for all ramp rates for each. It should be noted that the neat MDI only has DTGA peaks in zones 2 and 3.

There was a wide temperature distribution for each of the events because of the range of ramp rates (2.5, 5.0, 10.0, 15.0, and 20.0 °C/min). These events were identified for neat pMDI and all pMDI/soy product resin mixtures. The temperature ranges were calculated for the pMDI and the pMDI/soy product mixtures for each event.

Each of the DTGA temperature peaks in the curing reaction temperature range (or zone) for a particular sample with their respective ramp rates were used to calculate the activation energy for the curing reaction. This was performed using the Kissinger method by plotting $-ln\left(\frac{\beta}{T_p^2}\right)$ versus $1/T_p$, where T_p was the DTGA temperature peak and β was the ramp rate. The data had a linear relationship, and the slope and y-intercept of the plotted line was used to solve for the activation energy in the same fashion as was performed in the PF activation energy method.

Fourier Transform-Infrared (FT-IR) Analysis

Spectral analysis was performed on pMDI and pMDI/SF samples using Fourier transform-infrared (FT-IR) spectroscopy. Chemical structures were identified and compared for the samples through spectral analysis to determine the characteristics of cure. An experiment was designed to acquire spectrum data from samples heated in the TGA at varying temperatures and compare the data with each other. The data was used in conjunction with the TGA data to determine whether chemical crosslinking occurred due to this heat treatment process and to what degree that the curing reaction was affected with SF substitution.

Samples were prepared of cured and non-cured resins. The resins were either neat pMDI or 70/30 pMDI/SF mixture. The components of the 70/30 pMDI/SF mixture were mechanically mixed in a glass beaker with a metal spatula until visually homogeneous. Both neat pMDI and 70/30 pMDI/SF were scanned on the FT-IR spectrometer before heat treatment was applied to represent the no-cure samples. Both pMDI and 70/30 pMDI/SF samples were then placed in a

mechanical convection oven set at 180 °C. The pMDI took 20 hours to fully cure. The pMDI/SF mixture foamed out of the aluminum pan holding it after five minutes but was fully cured after 60 minutes. Another sample of pMDI/SF was heated at a lower temperature of 105 °C for 17 hours, 130 °C for 30 minutes, and 140 °C for 45 minutes. More details were given in the results and discussion section. All samples were scanned on the FT-IR spectrometer to represent full cure samples.

The FT-IR data was collected by the PerkinElmer software. FT-IR spectra were collected using a PerkinElmer Spectrum 400 Imaging System spectrometer. Two scans were performed for each sample.

The FT-IR spectra were all normalized to the neat pMDI spectra using the area under the curve of the wavenumber band containing the band intensity peak located at the approximate wavenumber of 754 cm^{-1} based on the prior published work of Garrett, et. al [128]. Normalization was attempted with other wavenumber bands containing peaks at 2980 [129], 2960 [130], 1600 [130], 1595 [131], 1591 [132], and 1412 [128] cm^{-1}. These normalizations did not produce comparable data primarily because of overlap from other wavenumber bands.

Results and Discussion

Carbodiimide Formation

Curing and degradation reaction kinetics were examined to compare characteristics of weight loss due to thermal treatment with and without the substitution of soy products in pMDI. TGA and DTGA data for the thermal treatment of neat pMDI, neat SF, 70/30 pMDI/SF, neat SPI, 70/30 pMDI/SPI, neat Soy-D, and 70/30 pMDI/Soy-D at a heating rate of 5 °C/min under nitrogen were shown in the following figures.

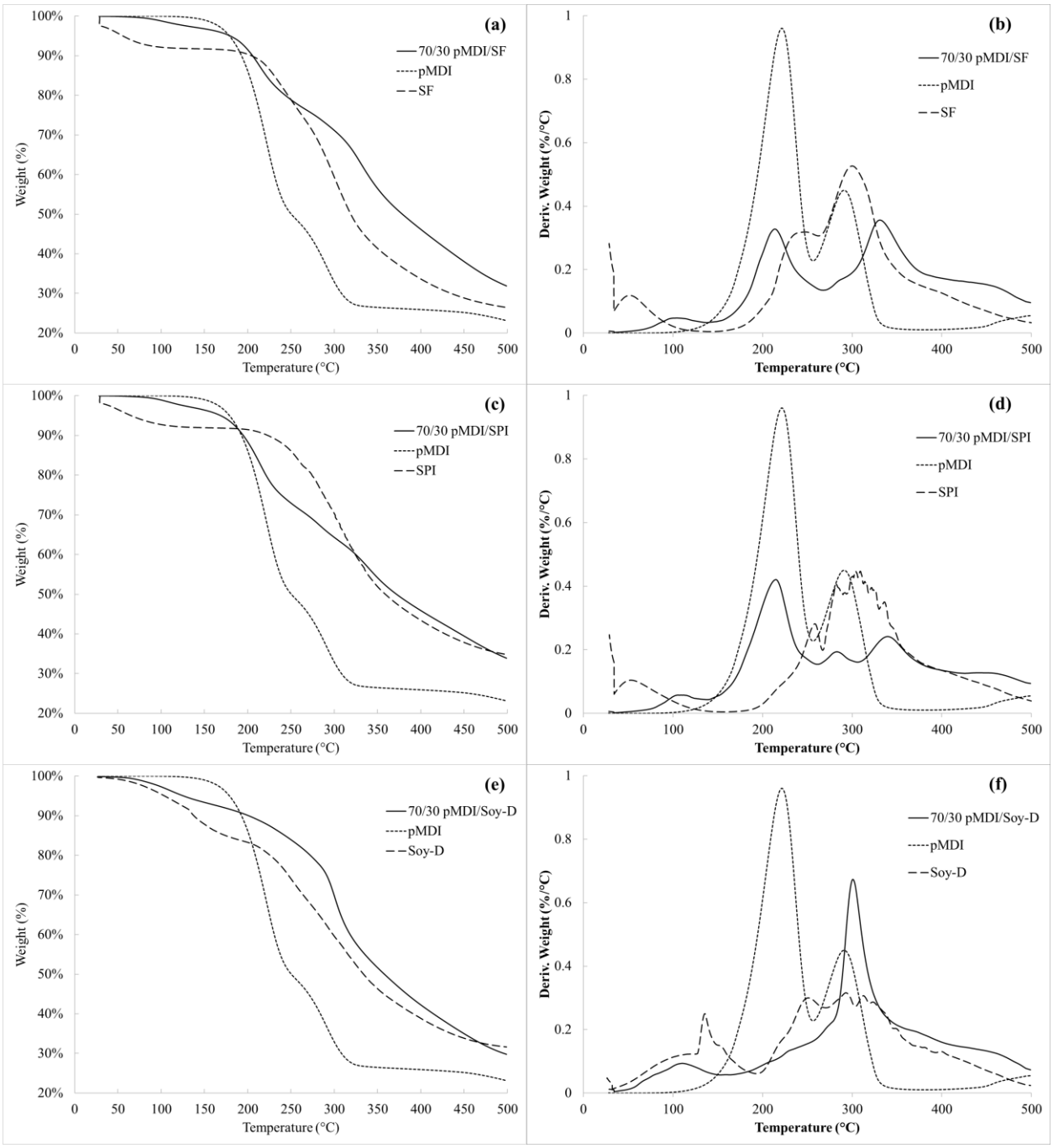

Figure 70: Dynamic TGA (left) and DTGA (right) data for neat pMDI, neat SF, and 70/30 pMDI/SF (a&b); neat pMDI, neat SPI, and 70/30 pMDI/SPI (c&d); neat pMDI, neat Soy-D, and 70/30 pMDI/Soy-D (e&f)

The main thermal degradation for defatted soy flour (Figure 70 a & b) began at the onset temperature of about 210 °C where the cleavage of glucoside units occurred [105]. The DTGA data displayed two peaks associated with the degradation in this temperature range (peaks at 248

°C and 300 °C). Guettler's work with soluble sugar extract from SF suggested that the lower temperature degradation peak (most thermally sensitive fraction of SF) was the soluble sugar fraction whereas the peak at the higher temperature was the insoluble soy [106].

The SPI (Figure 70 c & d) indicated a similar range of degradation temperatures as the SF in the TGA and DTGA data. A smaller amount of mass was lost at the lower temperature degradation peak in the SPI as compared to the SF, but there was a higher onset temperature of 232 °C and higher DTGA peak of 258 °C indicating that this was not part of the soluble sugar fraction as in SF. This was expected with the isolate as the soluble sugars have been extracted [106]. The degradation in the temperature range of 200-400 °C was a degradation of the soy protein [107]. This involved the breaking of hydrogen bonds (intramolecular and intermolecular), electrostatic bonds, and cleavage of the peptide bonds of amino acids in the protein structure [108].

The soy-D (Figure 70 e & f) also displayed a similar range of degradation temperatures as the other soy products in the TGA and DTGA data. An onset temperature (224 °C) and DTGA peak (251 °C) for the soy-D degradation region laid between the SF and SPI onset temperatures and DTGA peaks suggesting there were still soluble sugars present, but the denaturation process has eliminated a partial amount of these soluble sugars. Qi and Sun performed TGA on a modified soy flour and showed protein degradation between 208 and 400 °C [107]. This followed closely with the soy-D thermal degradation in the same temperature range. The higher amount of mass lost as compared to the other soy products between room temperature and 190 °C was attributed to the large water content of the soy-D.

There were two clear mass loss events due to thermal treatment in neat pMDI (Figure 70 a & b). The neat pMDI began to show a relevant loss of mass at an onset temperature of 188 °C.

This loss occurred lower in temperature than polyurethanes formed from pMDI shown in prior work. Aguirresarobe, et. al. described the possibility of a polymerization reaction occurring in this temperature range [26]. Upon spectral interpretation of the FT-IR spectra obtained from cured samples of neat pMDI, the polymerization that was believed to occur was the formation of carbodiimide formed by the dimerization of isocyanate groups. The release of carbon dioxide gas in carbodiimide production was evidence of such to explain the weight loss seen in the temperature range.

The following figure shows the FT-IR spectra used to confirm evidence of carbodiimide formation.

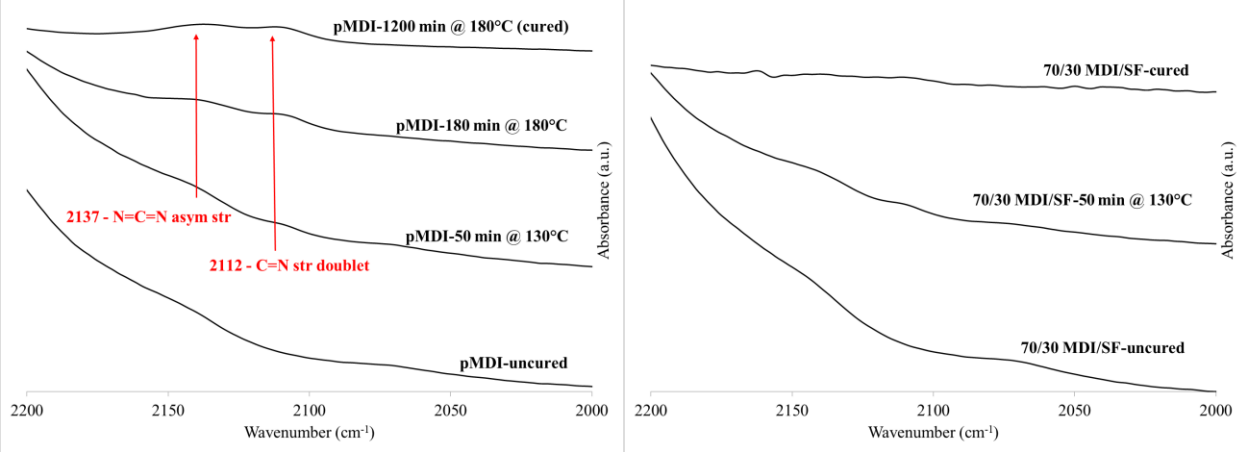

Figure 71: FT-IR spectra showing peaks for carbodiimide in the neat pMDI offset to show the progression of the cure (left) compared to minimal carbodiimide peaks in the 70/30 pMDI/SF mixture

Sonnenschein described in his text the formation of carbodiimide and its characteristic absorption of the asymmetric N=C=N stretch absorption at 2140 cm^{-1} [21]. A small peak could be seen forming after three hours heating at 180 °C at 2147 cm^{-1} and a clearer peak after 20 hours of heating at 2137 cm^{-1} signifying an aryl carbodiimide which was what was expected due to the aromatic structure of pMDI (Figure 71 – left). The C=N stretch doublet due to the Fermi

resonance band was observed at 2114 cm^{-1} for the three-hour heated sample and 2112 cm^{-1} for the cured sample [133].

When preparing samples for FT-IR scanning, the curing reaction of neat pMDI was observed proceeding at a longer duration than the pMDI/SF mixture. The pMDI was cured in a mechanical convection oven for approximately 20 hours at 180 °C for a full cure whereas the pMDI/SF mixture was fully cured after one hour in the oven at 180 °C. The pMDI showed no visual evidence of crystallization during the first few hours and remained at relatively the same volume. The pMDI/SF mixture created a foam-like structure after five minutes of heat and had a porous structure in contrast. Another curing attempt was made with the pMDI/SF mixture at a lower initial temperature of 105 °C for a longer duration of time of 17 hours which reduced the foaming of the mixture considerably. That sample was then placed in an oven at 130 °C for 30 minutes then 140 °C for 45 minutes to finalize the cure. FT-IR spectral analysis of the foamed and reduced foam structure showed no considerable differences when compared. The pMDI cured at a slower rate in part because there were no reactive groups with a fast rate of reaction with isocyanate groups, like amine or hydroxyl groups. The carbodiimide reaction proceeded at a slow rate as compared to the pMDI/SF mixture.

Carbodiimide was also part of the urethane degradation pathway when heated to about 240-270 °C [25], [26]. The spectral analysis of the FT-IR data for the pMDI/SF mixture showed little to no evidence of carbodiimide (Figure 71 – right). This evidence suggested that the carbodiimide was formed more preferentially from the dimerization of isocyanate groups in neat pMDI rather than urethane degradation.

It was believed that the carbodiimide was formed in the pMDI as the primary curing reaction due to the longer duration and higher temperature required to cure the specimen. The

lower temperature range identified as the formation of carbodiimide in the neat pMDI matched correspondingly to the pMDI/SF mixture's TGA/DTGA data (Figure 70 a & b). The onset temperatures were closely matched at 188 °C for pMDI and 189 °C for pMDI/SF. Carbodiimide was not as prevalent in the pMDI/SF mixture FT-IR spectral analysis (Figure 71 – right) because of the lower temperature heating required for the curing reaction of the pMDI/SF mixture. Therefore, it was believed that the curing reaction for the pMDI/SF mixture did not involve the formation of carbodiimide but did involve urethane formation. The carbodiimide TGA/DTGA curve in the pMDI/SF mixture was likely the thermal degradation of urethane to carbodiimide described above.

TGA/DTGA work was also performed on mixtures of pMDI and other soy products. SPI and soy-D were mixed with pMDI at the same ratios as the pMDI/SF mixture and studied under TGA/DTGA. The TGA/DTGA data for the pMDI/SPI mixture (Figure 70 c & d) showed an onset temperature of 186 °C for the thermal treatment region described as the carbodiimide formation region above. The TGA/DTGA data for the pMDI/soy-D mixture (Figure 70 e & f) showed an onset temperature of 189 °C for the same thermal treatment region. These onset temperatures matched closely to the onset temperatures of neat pMDI and the pMDI/SF mixture in the same thermal treatment region. Therefore, it was assumed that these regions described carbodiimide formation for pMDI/SPI and pMDI/soy-D mixtures as well. It was also assumed that carbodiimide formation was a result of the thermal degradation of urethane in these mixtures because of the similar TGA/DTGA thermal regions of degradation of proteins in SPI and soy-D to SF.

Residue analysis was performed on the TGA data to confirm a difference of the carbodiimide formation between neat pMDI and pMDI/SF mixture (Figure 70 a & b). The

residue was determined for neat pMDI, SF, and pMDI/SF at the temperature identified as the end of the carbodiimide formation event. The expected residue of the pMDI/SF due to the combination of the neat pMDI and SF was calculated by using the following equation:

$$m_{mix} = 70\% m_{pMDI} + 30\% m_{SF} \quad (10),$$

where m_{mix} was the calculated mass percentage of the residue left that would be expected in the mixture if the components lost the same amount of mass, m_{pMDI} was the mass percentage of the residue left of the pMDI at that temperature, and m_{SF} was the mass percentage of the residue left of the SF at that temperature. The results of the residue analysis can be seen in Table 7. The actual residue left of the pMDI/SF mixture was 29% higher than the calculated residue of the pMDI/SF mixture. This evidence suggested that the substitution of SF did not promote the formation of carbodiimide to as high of a degree as the neat pMDI while heated in this temperature range.

Table 7: Actual versus calculated residues left after the formation of carbodiimide in pMDI/soy product mixtures

Resin Mixture	m_{mix} *actual (%)*	m_{mix} *calculated (%)*	*percentage difference (%)*	*Temperature @ end of event (°C)*
70/30 pMDI/SF	76%	54%	29%	268
70/30 pMDI/SPI	71%	58%	18%	261
70/30 pMDI/soy-D	83%	55%	33%	257

Residue analysis was also performed on the pMDI/SPI and the pMDI/soy-D mixtures that can be seen in Table 7. The pMDI/soy-D mixture showed a similar percentage difference in the actual and calculated resin residues as the pMDI/SF, although the temperature at the end of the carbodiimide formation event was over 10 °C lower for the pMDI/soy-D. This lower temperature could be an indication of the soy-D favoring a separate reaction pathway with pMDI than the

other soy products. The DTGA curve for pMDI/SF during this event (Figure 70 f) was lower in magnitude than the other pMDI/soy product mixtures indicating less change in mass. The possibility could be either the soy-D does not react with pMDI to as high of a degree as the other soy products do, or the soy-D reacts with the pMDI in a different reaction pathway that does not promote the formation of carbodiimide. The higher difference between the calculated and actual residues left could be influenced by the water content of soy-D. The mass loss in the lower temperature range (room temperature to 205 °C) of the pMDI/soy-D was higher than the other pMDI/soy product mixtures (Figure 70). This was believed to be the extra water content of the soy-D, but it should not be mistaken as an evaporation of water in this mass loss event. It was likely that the water was reacting with pMDI forming carbamic acid which decomposed to form an amine and carbon dioxide. This liberated carbon dioxide would display as a mass loss during this event, although evaporation of water cannot be ruled out. It was likely that this reaction between water and pMDI released a majority of the carbon dioxide at room temperature before the TGA experiment occurred. This would explain the increased difference between the actual and calculated residues.

The residue analysis performed on the pMDI/SPI showed a reduced difference between the actual and calculated residue left after the carbodiimide formation event when compared to the other pMDI/soy product mixtures (Table 7). It was believed that the higher amount of protein due to the higher protein content in the SPI reacted with pMDI to form more urethane than the pMDI/SF mixture. This urethane degrades to carbodiimide. More carbodiimide formation would explain less residue left after the carbodiimide event seen in the pMDI/SPI mixture as compared to the pMDI/SF. There was about an 80% increase in protein (~90% in SPI and ~50% in SF).

This matches closely to the 71% increase seen in the differences of actual and calculated residues of pMDI/SPI mixture when compared to pMDI/SF.

The activation energy could be utilized to characterize the curing reaction of the neat pMDI and the degradation of urethanes to carbodiimide in pMDI/soy product mixtures. The activation energy was calculated for the formation of carbodiimide (Figure 72) using DTGA temperature peak ranges of 202-265 °C and their corresponding temperature ramp rates of 2.5, 5.0, 10.0 15.0, and 20.0 °C/min taken from TGA/DTGA data for neat pMDI and mixtures of pMDI/soy products.

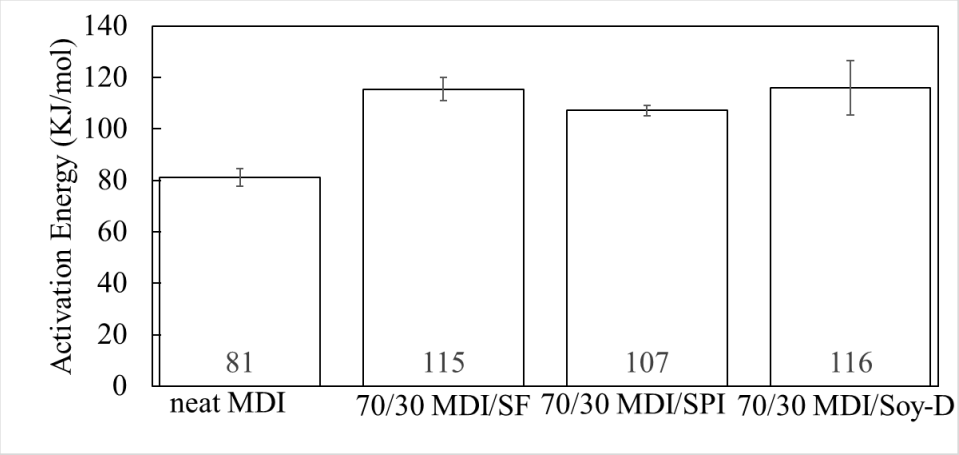

Figure 72: Calculated activation energies for the formation of carbodiimide (202-265 °C)

The activation energies for the carbodiimide formation of soy product substituted resins were larger than the neat pMDI. If this temperature range was a characterization of the formation of carbodiimide, as evidence suggested, the reaction kinetics were affected when soy products were substituted into pMDI, not only with SF.

No published comparisons for activation energy differences between carbodiimide formation and degradation of urethanes to carbodiimide were discovered. If one considered the reaction steps involved between the two reactions, there was an extra reaction step in the

degradation of urethane. Chain scission must occur during the depolymerization of urethane linkage leaving an isocyanate group. This isocyanate then reacts with other isocyanates to dimerize into carbodiimide [22], [25], [134]–[136]. This was the same reaction mechanism for the formation of carbodiimide in neat pMDI. This depolymerization reaction step combined with the carbodiimide formation can therefore be assumed to consume additional energy to proceed. This was relevant unless there was a negative activation energy, which was highly unlikely since heat energy was being added to the TGA sample during this degradation reaction. Therefore, it was assumed that the higher activation energies for the pMDI/soy product mixtures as compared to the neat pMDI was a result of degradation of urethanes into carbodiimide. This also supported the preferential formation of carbodiimide in pMDI as the curing reaction over pMDI/SF mixtures due to the higher amount of energy required for the reaction to proceed in the pMDI/SF mixtures.

The small decrease in activation energy for carbodiimide formation in the pMDI/SPI as compared to the other pMDI/soy product mixtures could be attributed to a different reaction pathway due to the protein content difference. Urea formation compared to urethane formation could be different with the pMDI/SPI mixture. Urea has been shown to degrade to isocyanate which could react with more isocyanate to form carbodiimide [137]. The scission reaction in the degradation of urethane and urea could be slightly different resulting in a slight difference in the activation energies for the formation of carbodiimide.

The isocyanate peaks were observed through spectral interpretation of the FT-IR data obtained from neat pMDI and the 70/30 pMDI/SF mixture at the wavenumbers of 2241-2256 cm^{-1} (Figure 73). Numerous references defined this isocyanate band at 2300-2250 cm^{-1} [133], [138]–[142]. Kurimoto et. al. showed the decrease and eventual elimination of this band while

forming polyurethane films [143]. This characteristic band for MDI was shown losing intensity as polymerization proceeded signifying the consumption of the isocyanate groups.

The ratios of the band intensity areas of the fully cured resin to the non-cured resin were calculated for the isocyanate wavenumber band for each of the resins. This was performed to determine the relative amount of the isocyanate consumed in the polymerization process for neat pMDI and the pMDI/SF mixture. The ratio of cured to non-cured isocyanate for pMDI was 0.11 and 0.12 for the pMDI/SF mixture. Approximately the same amount of isocyanate was consumed in each of the resins during the curing reaction.

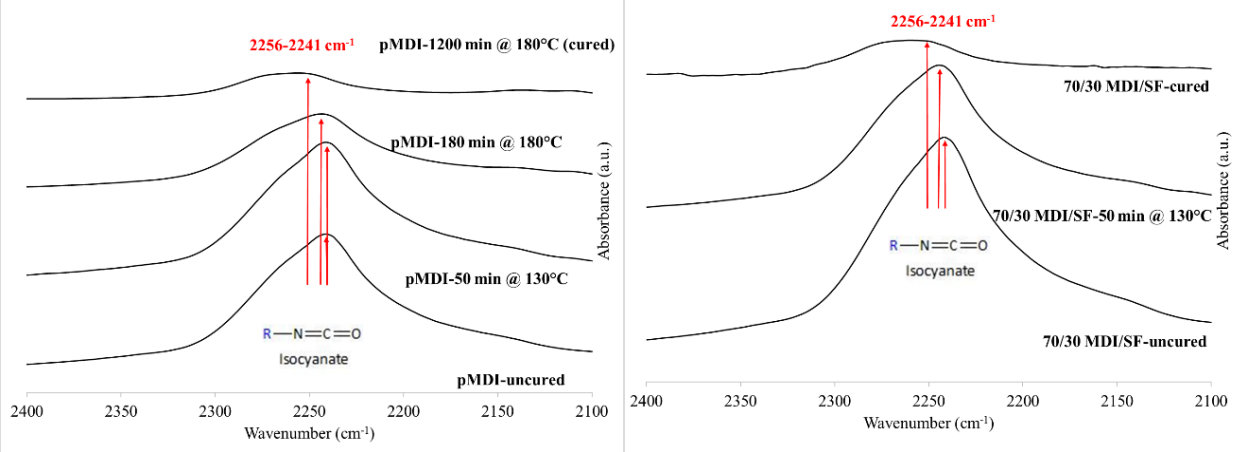

Figure 73: FT-IR spectra showing peaks for isocyanate in the neat pMDI offset to show the progression of the cure (left) compared to isocyanate peaks in the 70/30 pMDI/SF mixture

If similar amounts of isocyanate were consumed during the curing reaction for both resins, the isocyanate must have a different reaction mechanism for the pMDI/SF mixture than the neat pMDI because of the lack of carbodiimide present in the cured pMDI/SF FT-IR spectra. Therefore, the preferred curing reaction of pMDI/SF mixture will be studied since it was believed that urethane linkage was occurring due to carbodiimide formation from the urethane degradation.

Urethane and Urea Formation

The TGA weight loss in the higher temperature region observed in the neat pMDI (Figure 70 a & b) around 290 °C represented the urethane degradation of the hard segments of the polymer. As explained in Petrovic, et. al. there were two stages of degradation for polyurethane. The first of these occurred with urethane degradation of the hard segments starting at about 250 °C. The second stage involved the dissociation of the soft segment [144]. Grassie et. al. proposed a detailed thermal degradation mechanism for mainly hard segments of polyurethane [134]. There was an expected soft segment degradation at higher temperatures but was not seen since there was no soft segment production included in neat pMDI due to formation of carbodiimide over urethane and urea linkage.

The 70/30 pMDI/SF mixture showed a TGA weight loss in the same region as the higher temperature TGA weight loss for neat pMDI reflected by a peak in the DTGA cure around 285 °C. This corresponded to the decomposition of the hard segment of the cured resin mixture. The DTGA curve for the mixture was attenuated when compared to the neat pMDI peak in the same region. There were several possible reasons for this attenuation. There was a region identified at a higher temperature range reflected by the DTGA peak at about 330 °C for the mixture believed to represent the degradation of the soft segments of the polymer mixture not found in the pMDI. This soft segment degradation curve was overlapping the hard segment degradation curve causing some of the attenuation. There was also the possibility that another curve from the neat SF (DTGA peak at about 300 °C) could be influencing the hard segment curve of the mixture. The onset peak of the mixture (279 °C) fell between the neat SF (281 °C) and neat pMDI (274 °C). The ratio of the derivative weight (%/°C) at the hard segment DTGA peak and the carbodiimide formation DTGA peak was also calculated and found to be comparable for the

mixture (0.47) and the neat pMDI (0.50). It was determined that the DTGA peak for the mixture favored the hard segment peak due to the ratio calculation and of the DTGA peak temperature of the mixture (285 °C) being closer to the neat pMDI (290 °C) than the neat SF (300 °C).

The TGA weight loss region reflected by the DTGA peak of 330 °C in the pMDI/SF mixture was a separate peak from the components, neat pMDI and SF. This region signified the degradation of the soft segments identified in prior published work with polyurethane degradation [134], [144]. The SF and pMDI were clearly reacting with each other to form more urethane and urea linkage. FT-IR spectral analysis confirmed this.

Urethane linkage in the neat pMDI polymerization reaction was observed in the spectra (Figure 74). The carbonyl stretching vibration (amide I band) representative of associated (hydrogen bonded) aryl urethanes has a characteristic peak at 1735-1705 cm^{-1} and unassociated aryl urethanes at 1760-1730 cm^{-1} [145]–[151]. The hydrogen bonding occurred between the carbonyl and N-H groups of the urethane linkages, and the unassigned designation represented a "free" carbonyl group [131], [132], [152], [153]. A peak at 1732 cm^{-1} was observed in the uncured pMDI which became more pronounced after 50 minutes of heat. This peak was attributed to the unassociated urethane signal. It started to weaken and become overlapped by another peak with more heat treatment signifying the "free" carbonyl groups were hydrogen bonding to other urethane groups. Another peak appeared in the sample heated for three hours that strengthened in the fully cured sample at 1716 cm^{-1}. This was attributed to the associated urethane signal. This followed closely with the Ning, et. al. work with pMDI (1735 cm^{-1} for unassociated and 1709 cm^{-1} for associated) [129].

Urethane linkage in the 70/30 pMDI/SF was also observed in the spectra (Figure 75). Unassociated urethanes at 1733 cm^{-1} showed similarities to the neat pMDI, but the cured mixture

had a higher band intensity signifying that either the added soy promoted more unassociated urethane linkage, or a smaller amount of urethane exhibited hydrogen bonding in the mixture. The wavenumber band associated with hydrogen bonded urethane linkage showing at 1715 cm^{-1} for the mixture shows comparatively more hydrogen bonded urethane linkage than what was found in the neat pMDI. This suggested comparatively more urethane linkage occurring in the pMDI/SF mixture than the neat pMDI during the curing reaction.

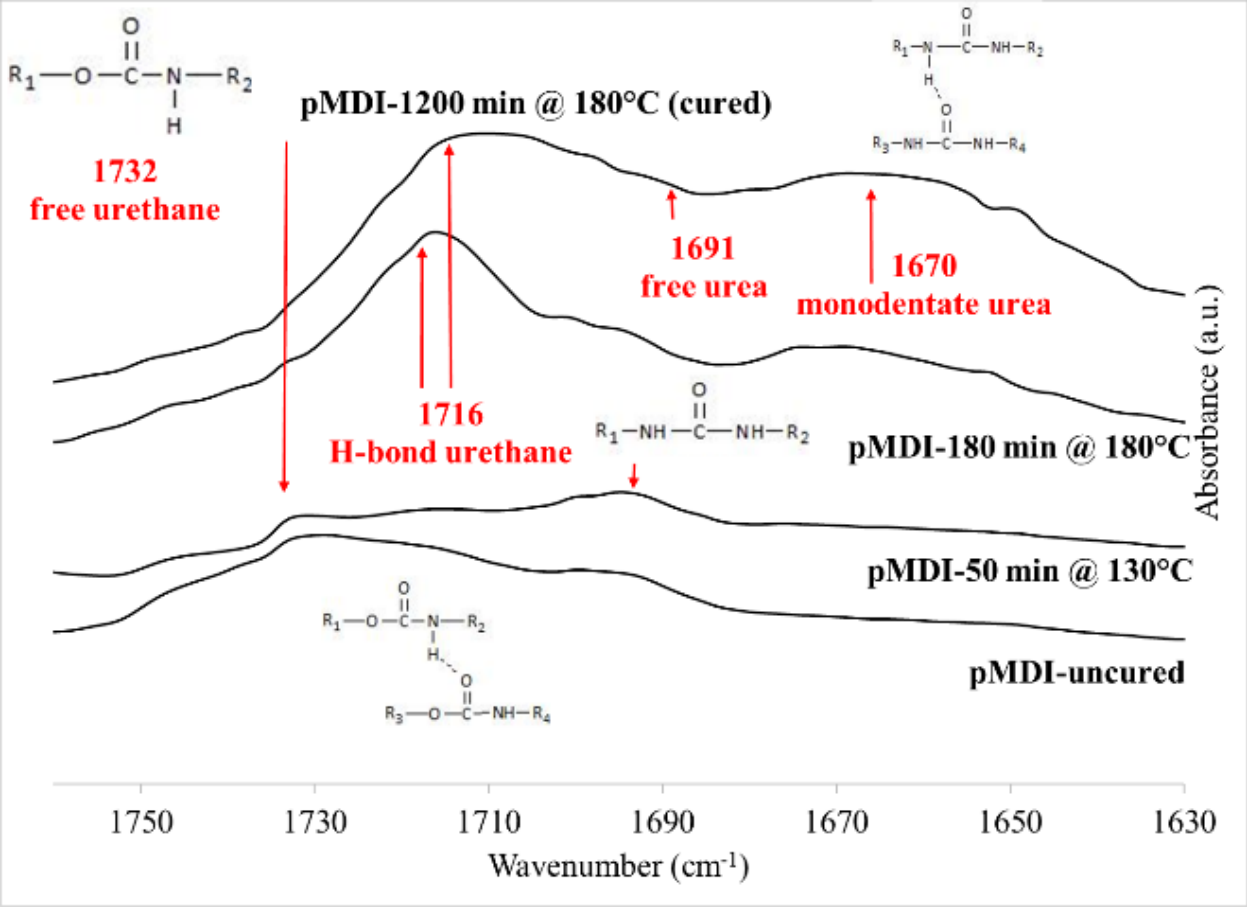

Figure 74: FT-IR spectra showing the Amide I band region with carbonyl stretching vibrations in the neat pMDI offset to show the progression of the cure (left) compared to the Amide I band region in the 70/30 pMDI/SF mixture (right)

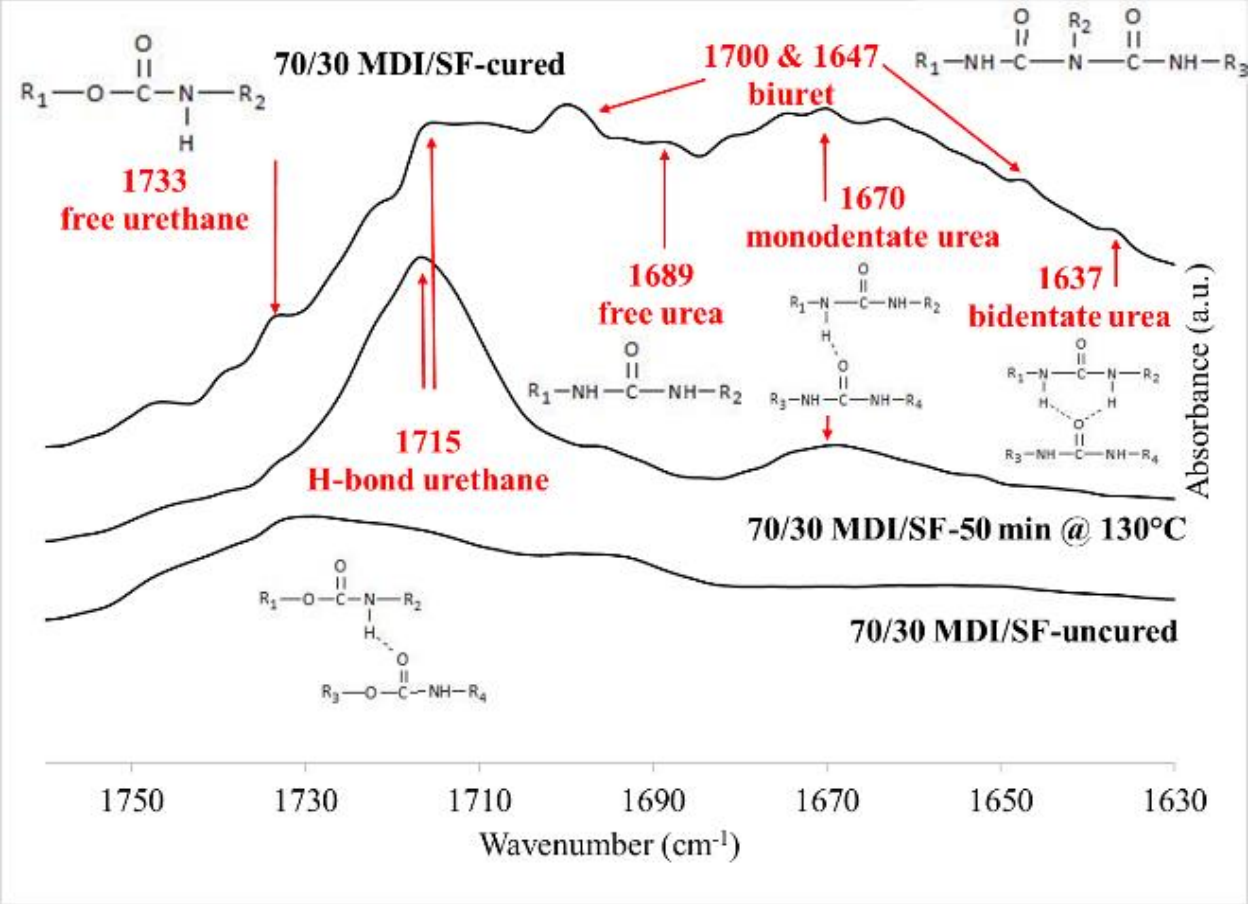

Figure 75: FT-IR spectra showing the Amide I band region with carbonyl stretching vibrations in the neat pMDI offset to show the progression of the cure (left) compared to the Amide I band region in the 70/30 pMDI/SF mixture (right)

Urea linkage in the neat pMDI polymerization reaction was observed in the spectra (Figure 74). The peak that appeared at 1694 cm^{-1} in the uncured sample represented the carbonyl stretching vibration in urea linkage (amide I band) [154]–[156]. The Socrates text described an expected peak at 1705-1660 cm^{-1} in a liquid phase [133]. This followed with the unassociated urea linkage that increased in intensity in the sample heated for 50 minutes but was overlapped by other peaks in the samples with a higher degree of cure. The Ning, et. al. work confirmed this (1691 cm^{-1}) [129]. The region in the range 1678-1659 cm^{-1} represented monodentate urea linkages which represented a single hydrogen bonded amine from a urea group to a carbonyl from another urea group and was observed at 1669 cm^{-1}. The bidentate (1643-1632 cm^{-1}) urea

linkage representing hydrogen bonding of both amine groups from urea to the carbonyl of another urea was observed slightly at 1638 cm^{-1} in the fully cured sample but was overlapped by other peaks [128]–[130], [157], [158]. This followed the Sung, et. al. work closely [159].

Urea linkage in the 70/30 pMDI/SF was also observed in the spectra (Figure 75). The signal for unassociated urea was observed for the mix at 1689 cm^{-1}. The fully cured mixture showed a higher intensity for unassociated urea than cured neat pMDI indicating that either more free urea linkage occurred, or a smaller amount of urea exhibited hydrogen bonding in the mixture. An observation of the 1670 cm^{-1} band peak displayed a higher intensity than the neat pMDI suggesting there were a higher amount of monodentate urea linkages present in the mixture. The band peak at 1637 cm^{-1} for bidentate urea linkage was more pronounced and higher in intensity for the mixture than the neat pMDI. It was suggested that the amino groups from the SF were influencing the urea reactions for both unassociated and hydrogen bonded urea linkage. The 1637 cm^{-1} peak signified that there were a higher amount of double hydrogen bonded urea linkages indicating a stronger adhesive.

Biuret linkage was expected in the presence of isocyanate groups and urea linkage. Hummel, et. al. reported two peaks for carbonyl stretching at the range of 1725-1695 cm^{-1} and 1645 cm^{-1} [153]. The neat pMDI (Figure 74) did not show a well-defined peak, but a slight peak was observed at 1706 cm^{-1} at 1650 cm^{-1} in the cured sample spectra likely overlapped by other peaks.

Biuret linkage was observed in the FT-IR spectra of the fully cured sample of the pMDI/SF mixture (Figure 75) at the wavenumber band of 1700 cm^{-1} and was much more prevalent than in the neat pMDI. This was also observed in the peak at 1647 cm^{-1} for the

carbonyl stretch. The pMDI/SF mixture showed more biuret linkage than the neat pMDI in both peaks.

Urethane N-H stretching vibrations for associated secondary urethanes (-HN-CO-O-) were defined in the region of 3340-3250 cm^{-1} and unassociated secondary urethanes in the region of 3410-3390 cm^{-1} according to the Socrates text [133]. The unassociated band was observed in all samples of neat pMDI (Figure 76 – left) but increasing as the cure progressed at a peak of 3402 cm^{-1}. The associated band was observed only slightly in the fully cured sample at 3293 cm^{-1} likely overlapped by other bands. The unassociated secondary urethane band for the pMDI/SF mixture (Figure 76 – right) was observed at the peak of 3406 cm^{-1}. The associated band was observed at 3285 cm^{-1} but only slightly as there was overlap from other bands.

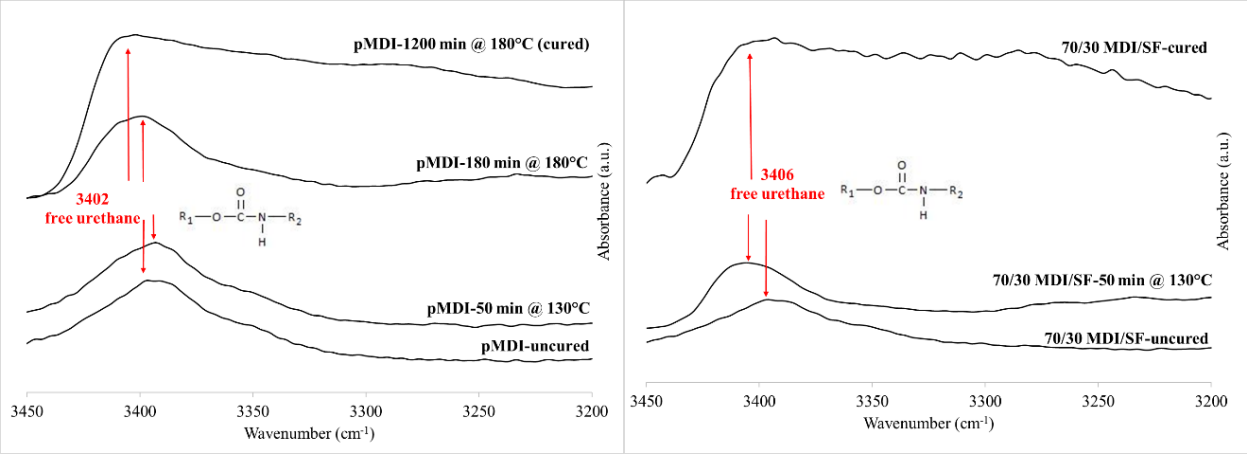

Figure 76: FT-IR spectra showing the N-H stretching vibrations in the neat pMDI offset to show the progression of the cure (left) compared to the N-H stretching vibrations region in the 70/30 pMDI/SF mixture

The N-H stretch was expected in the region of 3360-3320 cm^{-1} for secondary urea linkage according to the Socrates text [133]. The neat pMDI (Figure 76 – left) spectra did not show evidence of a peak in this range due to the signal being either too weak or overlapped by other

signals. Although slight, the secondary urea band for pMDI/SF mixture (Figure 76 – right) was observed at the peak of 3336 cm^{-1} also overlapped by other signals.

The absorption due to the CHN group was described in the range of 1600-1500 cm^{-1} for associated secondary urethanes (amide II band) in the Socrates text [133]. The band was observed in the fully cured neat pMDI sample (Figure 77 – left) at 1506 cm^{-1}. The band was observed in the fully cured pMDI/SF mixture (Figure 77 – right) at 1504 cm^{-1}. Both neat pMDI and the pMDI/SF mixture bands showed a shift to lower wavenumbers as the cure progressed.

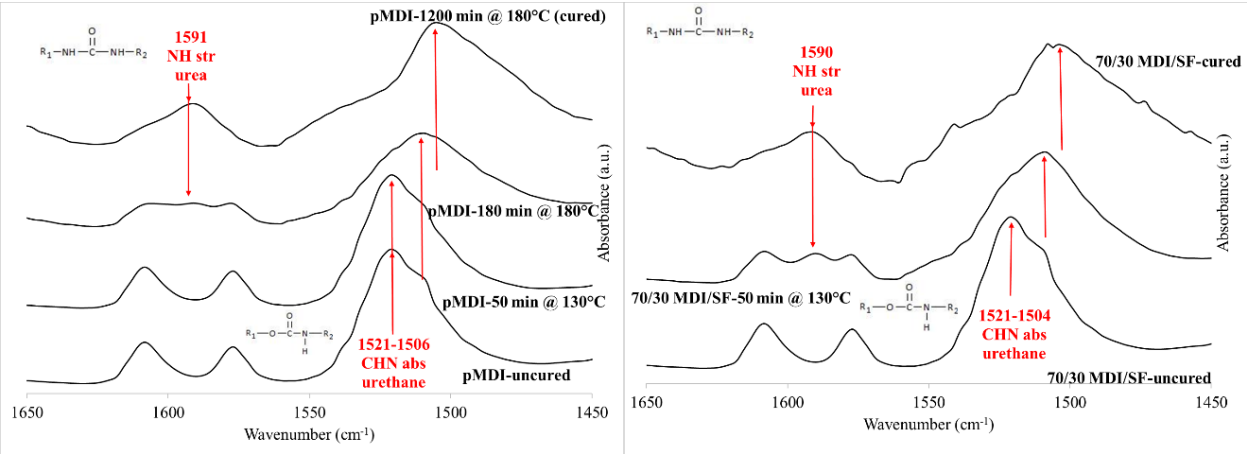

Figure 77: FT-IR spectra showing the Amide II band region in the neat pMDI offset to show the progression of the cure (left) compared to the Amide II band region in the 70/30 pMDI/SF mixture

The N-H deformation vibration was described in the Socrates text in the range of 1585-1515 cm^{-1} for secondary urea linkage [133]. This band was observed at 1591 cm^{-1} in the neat pMDI sample (Figure 77 – left) starting in the 3-hour heated sample and increasing in intensity for the fully cured sample. It was also observed at a peak of 1590 cm^{-1} in the pMDI/SF mixture (Figure 77 – right) starting in the partially cured (50 minute heated) sample and increasing in intensity for the fully cured sample.

The absorption due to coupled C-N and C-O stretching vibrations (amide IV band) for urethanes was described in the Socrates text [133] in the range of 1265-1200 cm^{-1}. The band was

observed in the neat pMDI sample (Figure 78 – left) at a peak of 1230 cm^{-1} starting in the 3-hour heated sample and increasing in magnitude in the fully cured sample. This followed the Kurimoto work with pMDI (1216 cm^{-1}) [143]. The band was also observed for the pMDI/SF mixture (Figure 78 – right) at 1230 cm^{-1} starting in the partially cured sample and increasing in intensity in the fully cured sample.

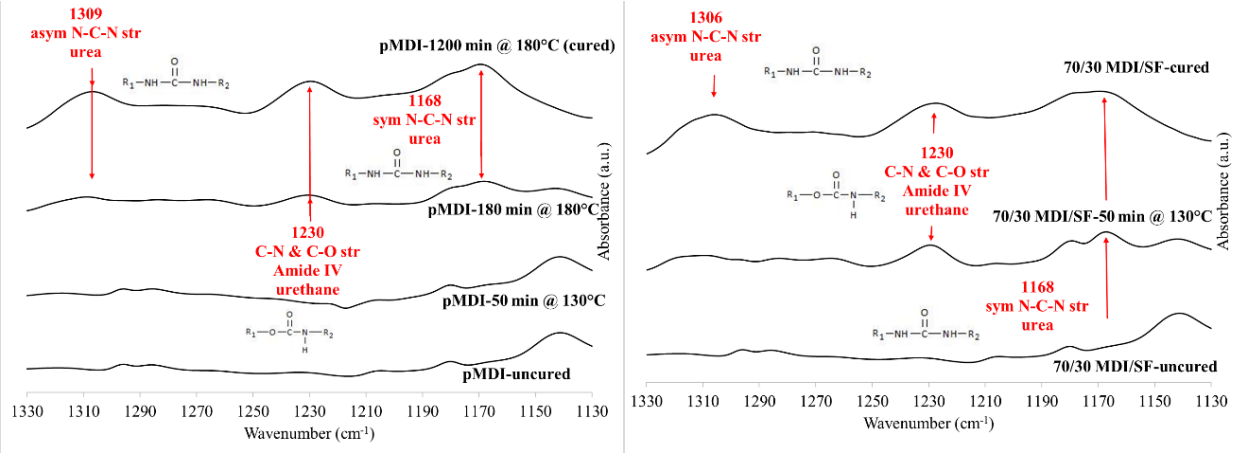

Figure 78: FT-IR spectra showing the Amide IV band region and N-C-N stretching vibrations in the neat pMDI offset to show the progression of the cure (left) compared to the Amide I band region in the 70/30 pMDI/SF mixture

For urea, the asymmetric N-C-N stretch was described in the 1360-1300 cm^{-1} region and the symmetric N-C-N stretch in the 1190-1140 cm^{-1} region in the Socrates text [133]. The asymmetric N-C-N stretch was observed at 1309 cm^{-1} and symmetric stretch at 1168 cm^{-1} in the fully cured sample of pMDI (Figure 78 – left). The asymmetric N-C-N stretch was observed at 1306 cm^{-1} and symmetric stretch at 1168 cm^{-1} in the fully cured sample of the pMDI/SF mixture (Figure 78 – right).

Although normalization techniques were performed on the FT-IR spectra, there were no calculations performed on the intensities of the bands and no deconvolution of individual curves due to the complexity of the fingerprint region of the wavenumber region. Observations were

instead employed for spectral data in the fingerprint region as a means to compare neat pMDI with the pMDI/SF mixture spectra.

The spectral interpretation of the FT-IR data indicated urethane and urea linkage with both neat pMDI and pMDI/SF mixtures. The Amide I band region was observed as the best indicator for urethane and urea linkage as a comparison between neat pMDI and the pMDI/SF mixture. Biuret linkage and hydrogen bonding was also better identified in the Amide I band region. The spectral analysis in the other band regions were utilized as verification of the urethane and urea linkages in both resins.

While more urethane linkage (associated and unassociated) was observed in the pMDI/SF spectra than the neat pMDI spectra, urea linkage was even more prevalent than urethane linkage for the pMDI/SF spectra which was expected with the substituted SF. The monodentate and bidentate urea linkage activity was higher in the pMDI/SF spectra as well signifying a stronger adhesive. Biuret linkage was also more clearly identified in the pMDI/SF spectra indicating there was a sufficient amount of urea to promote this reaction.

Conclusions

FT-IR spectral interpretation confirmed the findings of the TGA study of the formation of carbodiimide due either to the polymerization of neat pMDI or the degradation of urethane in pMDI/SF mixtures. The degradation of hard segments in neat pMDI and the degradation of hard and soft segments in the pMDI/SF mixture was also confirmed with TGA and FT-IR spectral interpretation. The following findings supported the hypothesis that substitution of soy products in pMDI affected the overall adhesive to a higher degree in cohesive failure.

TGA was used to characterize the weight loss region identified as the formation of carbodiimide in neat pMDI and pMDI/soy product mixtures. FT-IR spectral analysis identified

the formation of carbodiimide in the cured sample of neat pMDI which was not observed in the cured pMDI/SF mixture confirming that the formation of carbodiimide was a degradation of the polymer formed in the pMDI/SF mixture rather than the polymerization of virgin isocyanate groups as in the pMDI curing. Polymerization degradation forming carbodiimide in the pMDI/SF mixture was further confirmed through the following: a shorter duration of curing for the pMDI/SF mixture, residue analysis identifying carbodiimide formation as a more favorable reaction for neat pMDI, a higher activation energy for the reaction for the pMDI/soy product mixtures suggesting an extra chain scission reaction to degrade the polymer before carbodiimide formation, and FT-IR spectral analysis showing similar isocyanate consumption for both neat pMDI and the pMDI/SF mixture during the curing reaction.

TGA/DTGA described the similarities in protein content of the soy products, SF, SPI, and soy-D. Soluble sugars were also identified in SF as well as their reduction in SPI and soy-D. The similarities of the TGA work with the pMDI/soy product mixtures were assumed because of the protein similarities. The influence of larger protein content of SPI was explained in the residue analysis due to more carbodiimide formation in the pMDI/SPI mixture as compared to the pMDI/SF mixture. The water content of the soy-D was explained as a probable reason for less carbodiimide formation in the pMDI/soy-D mixtures as compared to the other pMDI/soy product mixtures.

Hard and soft segment polymerization was identified in the TGA data for pMDI/soy product mixtures. The lack of soft segment polymerization in neat pMDI was confirmed through comparison of the TGA/DTGA data of the pMDI/soy product mixtures and prior published work. The hard and soft segment polymerization was reflected through indication of more urethane and urea linkage through FT-IR spectral analysis in the pMDI/SF mixture as compared

to the neat pMDI. Hydrogen bonding between urethanes and urea also increased in the pMDI/SF mixture likely due to the hydrogen bonding between soft segments. More biuret linkage in the pMDI/SF mixture was also confirmed through FT-IR spectral analysis indicating a higher amount of urea available to react with isocyanate groups.

The formation of carbodiimide due to degradation of the polymer in the pMDI/soy product mixtures and the formation of soft segment polymers through urethane, urea, and biuret linkage in the pMDI/SF mixture supported the hypothesis that the primary mechanism affected by the substitution of soy products into pMDI was a chemical crosslinking one.

Chapter 8: Conclusions and Future Work

The overall objective of this work was to advance the understanding of resultant properties from mixing between soy products used as wood adhesives (e.g. defatted soy flour, soy protein isolate, and denatured soy flour) and synthetic wood adhesives (e.g. phenol formaldehyde and methylene diphenyl diisocyanate) and the physical characteristics of the wood composites created with those wood adhesives. Although research has been performed on soy products and their substitution into phenol formaldehyde (PF) as a wood adhesive, limited published work existed involving defatted soy flour (SF) without expensive chemical pre-modifications substituted into PF in the production of oriented strand board (OSB). Limited published work existed of soy product substitution in methylene diphenyl diisocyanate (MDI) at all. When well understood, the OSB manufacturing process and the SF/synthetic resin itself could be leveraged to meet the technological and engineering challenges associated with the incorporation of this bio-adhesive in the composite wood industry. Because the production process of both PF and MDI involved non-renewable resources, there was a need for an alternative bio-adhesive. The incorporation of this bio-adhesive in composite wood manufacture also needs to be cost-effective and meet strength requirements in today's advanced composite wood industry if it was to compete with current synthetic resins. An in-situ substitution of SF during the OSB manufacturing process will also minimize the extra cost of equipment needed to apply a new adhesive in the process. Research on the effects of SF substitution in current

synthetic resins was desired because of the following: cost benefits of SF over synthetic resins, need for the understanding of the mechanism of adhesion to modify the manufacturing process in a cost-effective way, and partial elimination of adhesives made with non-renewable resources through substitution of a bio-adhesive.

The objective of this research was to determine whether SF hydrolyzes in the board manufacturing process to chemically crosslink with the synthetic resin to which the soy was substituted affecting the cohesive bulk. The alternative being the SF interacts with the resin by altering the wood/resin interface. Previous studies have indicated the crosslinking of soy products with PF based on research involving soy protein reacting with formaldehyde – not the primary reactive monomer found in PF, methylated phenol. This crosslinking must be performed in the production process of PF before it was received by the OSB manufacturer, eliminating the possibility of an in-situ SF substitution during the OSB manufacturing process. Modifying the SF before the OSB manufacturing process decreases the pot life of the resin which can decrease its effectiveness to bond. The limited amount of published work that has been conducted with soy products and polymeric MDI (pMDI) involved either modified soy protein isolates (glyoxylated or denatured) or very small amounts of pMDI. This work was distinct from other prior published work in that the modification of soy products during the OSB manufacturing process was considered.

In order to achieve the prior stated objective, this research focused on two separate goals. The aim of the first goal was to determine whether SF hydrolyzed in the board manufacturing process. was the substitution of SF in synthetic resins used in board production possible without loss of properties of the finished product? If possible, what degree of substitution can be achieved without loss of properties of the finished product? Experiments were designed to form

lab-made strand boards under conditions similar to the OSB manufacturing process. Resins were formulated by substituting SF in synthetic resins at different substitution rates to be used in the formation of the strand boards whose properties were tested and compared to strand boards formed with a control synthetic resin.

The aim of the second goal was to determine whether soy flour affects the overall adhesive to a higher degree in adhesive failure or cohesive failure. This goal involved identifying the primary mechanism of adhesion that the SF influenced with the substitution in each of the synthetic resins (PF or pMDI). This primary mechanism of adhesion affects the failure mode of the wood composite made by the adhesive. Three possible failure points exist in a wood composite: the adhesive itself (cohesive failure), the wood itself, or the wood/resin interface (adhesive failure). Does the SF chemically crosslink with synthetic resin in the mixture affecting the cohesive failure to a higher degree than SF affects adhesive failure?

Experiments were designed to calculate activation energy of the curing reactions of the SF/synthetic resin mixtures and the synthetic resins. Data obtained from Fourier transform-infrared (FT-IR) spectroscopy of the cured and non-cured SF/synthetic resin mixtures and the synthetic resins was analyzed through spectral interpretation. Identified wavenumber bands of importance through examination of prior work or identification of appearing or disappearing bands were identified that were related to the curing reaction in the synthetic resins and SF to ascertain what was occurring chemically. These band intensities were compared to band intensities found in the SF/synthetic resin mixtures. The band intensity differences from non-cured to cured resins were also analyzed and compared for SF/synthetic resin mixtures and the synthetic resins.

A lap shear test with 10% soy protein isolate (~90% protein) substitution in PF (dry wt./dry wt.) displayed about an 80% improvement in shear stress when compared with a PF control. The lap shear test results warranted additional experimentation into strand board formation. An experiment was designed to determine the heat transferred to the center of a mat of wood strands during the pressing process into strand boards by measuring temperature with a temperature probe inserted into the center of the mat. The density of the mat was varied to determine the effect of mat density on heat energy transfer to the center of the mat during pressing. The boiling point of water was reached after 80 seconds of pressing in the center of the mat for all mat densities, but full vaporization of all bound water in the center of higher density mats required additional time compared to lower density mats. Taken together these observations warranted a pressing time of four minutes for forming strand boards based on the vaporization results.

Resin spread was studied by measuring the contact angle of resin droplets on a glass slide using the sessile drop method. Contact angles for droplets of 10% soy protein isolate substituted in PF measured to a higher degree than droplets of neat PF resin. It was believed that a higher viscosity in the soy protein isolate substituted PF than the neat PF was the cause of the higher contact angle. The higher viscosity was confirmed in Wescott and Frihart's research. This higher viscosity in the resin mixture will reduce resin spread when resin droplets were applied to the strands during blending. At higher board densities, soy substituted PF will spread at a lesser extent thereby resulting in a lower relative bonded area when compared to lower density boards.

An experiment was designed to confirm an expected reduction in strand board properties due to higher viscosity resins resulting in reduced resin spread in higher density strand boards. Modulus of rupture (MOR) and modulus of elasticity (MOE) were measured and compared for

strand boards formed at different densities using the following resins: a control PF and 5% SF substituted into PF. When the density of the strand board increased, the MOR and MOE for the control PF strand boards improved at a faster rate than the SF substituted strand boards. This confirmed the assumption that higher viscosity resins were better utilized at lower density board formations.

The prior experiments were essential to define the control parameters of the pressing process during formation of strand boards. These included time, temperature of the platens, press pressure, density of the mat, and total adhesive loading. Experiments were then designed to test and compare the properties of strand boards formed with and without SF substituted into synthetic resins. Up to 10-14% SF substitution in liquid PF was possible without the loss of strand board properties. Up to 21-30% SF substitution in powder PF was possible without loss of strand board properties. Up to 20-30% SF substitution in pMDI was possible without loss of strand board properties. Wet properties of the strand boards were the limiting factor in all SF substitutions in the synthetic resins due to SF solubility in water. Higher viscosity reducing resin spread and resin penetration in strands for liquid PF and SF mixtures was believed to be the reason for the lower strand board properties resulting in a lower substitution rate for that particular resin in strand boards.

Analysis of curing kinetics was performed to confirm or refute the existence of chemical crosslinking between the synthetic resin and SF. Data from thermogravimetric analysis (TGA) and differential scanning calorimetry (DSC) of both PF and pMDI as controls and SF substituted at 30% into both synthetic resins (PF/SF or MDI/SF) were analyzed.

Derivative TGA (DTGA) data was analyzed to identify the temperature at which the highest rate of mass loss occurred indicating the release of volatiles from the curing reaction and

referred to as peak temperature. This was corroborated using DSC data. Activation energy was calculated through the Kissinger method by utilizing these peak temperatures determined at different heating rates (2.5, 5.0, 10.0, 15.0, and 20.0 °C/min).

The curing reaction activation energies for PF and PF/SF did not show a significant difference when compared with each other. This evidence refuted the existence of new chemical crosslinking between SF and PF being the primary adhesive mechanism. TGA/DTGA work corroborated these findings through identification and comparison of mass loss events.

Analysis of the intensity of the identified bands of functional groups that were related to the curing reaction in the cured PF and PF/SF FT-IR spectra showed no significant difference. Spectral subtraction confirmed this by comparing the FT-IR spectra of SF with subtracted spectra of PF from the spectra of PF/SF. Differences in intensity of the identified bands of functional groups that were related to the curing reaction of non-cured and cured resins were analyzed and compared separately for PF and PF/SF. The non-cured to cured band intensity differences did not show a significant difference when comparing those for PF with PF/SF.

The hypothesis that chemical crosslinking of PF and SF modified the primary adhesive mechanism to a higher degree than the wood/resin interface was disproved due to evidence discovered in the activation energy analysis and FT-IR spectral interpretation. Therefore, the primary adhesive mechanism modified was the wood/resin interface. The discussion of a reduction in resin spread and resin penetration due to higher viscosity during board formation confirms this. It is recommended to investigate rheological properties of PF and SF adhesives further to characterize their behavior at the wood/resin interface.

The curing reaction activation energies for pMDI and pMDI/SF did show a significant difference when compared with each other. This evidence supported the existence of new

chemical crosslinking between SF and MDI. TGA/DTGA work showed the formation of soft segment polymerization with the substitution of SF in pMDI which led to better thermal degradation properties.

Analysis of the intensity of the identified bands of functional groups that were related to the curing reaction in the cured pMDI and pMDI/SF FT-IR spectra showed a significant difference. The band intensity for unassociated urethane was slightly higher in the pMDI/SF FT-IR spectra, but hydrogen bonded urethane band intensity was much higher than the pMDI FT-IR spectra. The band intensity for unassociated urea as well as the monodentate (single hydrogen bond) and bidentate (double hydrogen bond) urea was higher in the pMDI/SF FT-IR spectra. A band for biuret linkage was confirmed in the pMDI/SF FT-IR spectra which was not identified in the pMDI spectra signifying evidence of more urea linkage present to react with isocyanate to form biuret linkage. A band for carbodiimide was confirmed in the neat pMDI FT-IR spectra which was not identified in the pMDI/SF spectra signifying evidence of more dimerization of isocyanate groups to form carbodiimide in the neat pMDI and more isocyanate reacting with something other than other isocyanate groups in the pMDI/SF.

There was evidence to support the hypothesis that chemical crosslinking occurred between pMDI and SF in the mixture and that it modified the primary adhesion mechanism to a higher degree than the wood/resin interface. There was evidence to refute the hypothesis in the discussion of higher viscosity which reduced resin spread and resin penetration. However, evidence discovered in the activation energy analysis and FT-IR spectral interpretation confirmed chemical crosslinking between the pMDI and SF. It is recommended to also investigate rheological properties of pMDI and SF adhesives further to characterize their

behavior at the wood/resin interface. It is also recommended that the MDI/SF bond should be investigated and characterized using nuclear magnetic resonance analysis.

References

[1] "Phenol Formaldehyde Resin Price / Phenolic Resin Hardener In Bulk Stock - Buy Phenolic Resin,Phenolic Resin Hardener,Phenol Formaldehyde Resin Product on Alibaba.com." [Online]. Available: https://www.alibaba.com/product-detail/Phenol-formaldehyde-resin-price-phenolic-resin_60625941293.html?s=p. [Accessed: 16-Mar-2018].

[2] "Polymeric Mdi Isocyanate/methylene Diphenyl Diisocyanate For Polyurethane Foam - Buy Methylene Diphenyl Diisocyanate,Polymeric Mdi,Mdi Isocyanate Product on Alibaba.com." [Online]. Available: https://www.alibaba.com/product-detail/Polymeric-MDI-Isocyanate-Methylene-Diphenyl-Diisocyanate_1954267966.html. [Accessed: 16-Mar-2018].

[3] "Soybean Meal Price: Latest Price & Chart for Soybean Meal - NASDAQ.com." [Online]. Available: https://www.nasdaq.com/markets/soybean-meal.aspx. [Accessed: 08-Apr-2018].

[4] International Agency for Research on Cancer, "International Agency for Research on Cancer classifies formaldehyde as carcinogenic to humans." 2004.

[5] B.-D. Park, B. Riedl, E. W. Hsu, and J. Shields, "Application of cure-accelerated phenol-formaldehyde (PF) adhesives for three-layer medium density fiberboard (MDF) manufacture," *Wood Sci. Technol.*, vol. 35, no. 4, pp. 311–323, 2001.

[6] P. S. Mehta, A. S. Mehta, S. J. Mehta, and A. B. Makhijani, "Bhopal tragedy's health effects: a review of methyl isocyanate toxicity," *J. Am. Med. Assoc.*, vol. 264, no. 21, pp. 2781–2787, 1990.

[7] T. Ghosh Dastidar and A. N. Netravali, "A soy flour based thermoset resin without the use of any external crosslinker," *Green Chem.*, vol. 15, no. 11, pp. 3243–3251, 2013.

[8] G. A. Amaral-Labat, A. Pizzi, A. R. Goncalves, A. Celzard, S. Rigolet, and G. J. M. Rocha, "Environment-friendly soy flour-based resins without formaldehyde," *J. Appl. Polym. Sci.*, vol. 108, no. 1, pp. 624–632, 2008.

[9] Office of Standards Services and National Institute of Standards and Technology, "PS 2-10 Performance Standard for Wood-Based Structural-Use Panels." p. 66, 2011.

[10] ASTM:D1037, “Standard Test Methods for Evaluating Properties of Wood-Base Fiber and Particle Panel Materials,” *Current*, pp. 1–8, 2012.

[11] C. R. Frihart, M. J. Birkeland, A. J. Allen, and J. M. Wescott, “Soy Adhesives that Can Form Durable Bonds for Plywood , Laminated Wood Flooring , and Particleboard,” *Proc. Int. Conv. Soc. Wood Sci. Technol. United Nations Econ. Comm. Eur. – Timber Comm. Oct. 11-14, 2010, Geneva, Switz.*, no. August, pp. 1–13, 2010.

[12] E. Atta-obeng, B. K. Via, O. Fasina, M. L. Auad, W. Jiang, and F. Products, “Cellulose Reinforcement of Phenol Formaldehyde : Characterization and Chemometric Elucidation,” *Int. J. Compos. Mater.*, vol. 3, no. 3, pp. 61–68, 2013.

[13] A. Pizzi, *Advanced wood adhesives technology*. CRC Press, 1994.

[14] H.-J. Deppe and K. Ernst, “Isocyanate als Spanplattenbindemittel,” *Eur. J. Wood Wood Prod.*, vol. 29, no. 2, pp. 45–50, 1971.

[15] C. E. Frazier, “Isocyanate Wood Binders In: Handbook of Adhesive Technology, Revised and Expanded, A. Pizzi and KL Mittal, eds. 2003.” New York: Taylor & Francis (Marcel Dekker Inc.), 2003.

[16] R. N. Hawke, B. C. H. Sun, and M. R. Gale, “Effect of fiber mat moisture content on physical properties of polyisocyanate-bonded hardboard,” *For. Prod. J.*, vol. 43, no. 1, p. 15, 1993.

[17] S. L. Wendler and C. E. Frazier, “Effect of moisture content on the isocyanate/wood adhesive bondline by 15N CP/MAS NMR,” *J. Appl. Polym. Sci.*, vol. 61, no. 5, pp. 775–782, 1996.

[18] H. J. Twitchett, “Chemistry of the production of organic isocyanates,” *Chem. Soc. Rev.*, vol. 3, no. 2, pp. 209–230, 1974.

[19] W. F. Gum and W. Riese, *Reaction polymers: polyurethanes, epoxies, unsaturated polyesters, phenolics, special monomers, and additives: chemistry, technology, applications, markets*. Hanser Publishers, 1992.

[20] S. S. Chadwick, “Ullmann’s encyclopedia of industrial chemistry,” *Ref. Serv. Rev.*, vol. 16, no. 4, pp. 31–34, 1988.

[21] M. F. Sonnenschein, *Polyurethanes: science, technology, markets, and trends*, vol. 11. John Wiley & Sons, 2014.

[22] F. Wang, “Polydimethylsiloxane Modification of Segmented Thermoplastic Polyurethanes and Polyureas Polydimethylsiloxane Modification of Segmented Thermoplastic Polyurethanes and Polyureas,” 1998.

[23] W. Darwish, E. Seikel, R. Käsmarker, K. Harms, and J. Sundermeyer, “Synthesis and X-ray crystal structures of imido and ureato derivatives of titanium(iv) phthalocyanine and their application in the catalytic formation of carbodiimides by metathesis from isocyanates,” *Dalt. Trans.*, vol. 40, no. 8, p. 1787, 2011.

[24] J. C. Anderson and R. Bou-Moreno, “The efficient synthesis of carbodiimides using a titanium imido complex,” *Tetrahedron*, vol. 66, no. 47, pp. 9182–9186, 2010.

[25] D. Joel and A. Hauser, “Thermal dissociation of urethanes studied by FTIR spectroscopy,” *Macromol. Mater. Eng.*, vol. 217, no. 1, pp. 191–199, 1994.

[26] R. H. Aguirresarobe, L. Irusta, and M. J. Fernandez-Berridi, “Application of TGA/FTIR to the study of the thermal degradation mechanism of silanized poly(ether-urethanes),” *Polym. Degrad. Stab.*, vol. 97, no. 9, pp. 1671–1679, 2012.

[27] M. Kuo, D. J. Myers, H. Heemstra, D. Curry, D. O. Adams, and D. D. Stokke, “Soybean-based adhesive resins and composite products utilizing such adhesives,” 2001.

[28] C. Howe *et al.*, “Soy Adhesive TAP Meeting March 16-17, 2011 Hilton St. Louis Airport Hotel,” 2011.

[29] A. Malhotra and J. N. Coupland, “The effect of surfactants on the solubility, zeta potential, and viscosity of soy protein isolates,” *Food Hydrocoll.*, vol. 18, no. 1, pp. 101–108, 2004.

[30] A. Pizzi and K. L. Mittal, *Handbook of adhesive technology, revised and expanded*. CRC press, 2003.

[31] H. F. Rippey, C. N. Cone, D. Glenn, I. F. Laucks, and H. P. Banks, “Process of making a water resistant, animal protein adhesive, and the product thereof,” 1,814,768, 1931.

[32] G. Davidson, “Process of preparing substances composed in part of protein-containing cells for the manufacture of adhesives,” 1,724,695, 1929.

[33] T. Satow, “Waterproof Glue Product and Method of making the same,” 1,994,050, 1935.

[34] J. M. Wescott, C. R. Frihart, and A. E. Traska, “High-soy-containing water-durable adhesives,” vol. 20, no. 8, pp. 859–873, 2006.

[35] X. Huang and A. Netravali, “Biodegradable green composites made using bamboo micro/nano-fibrils and chemically modified soy protein resin,” *Compos. Sci. Technol.*, vol. 69, no. 7–8, pp. 1009–1015, 2009.

[36] D. Tome and N. Naulet, “Carbon 13 Nuclear Magnetic Resonance Studies on Formaldehyde Reactions with Polyfunctional Amino Acids,” *Chem. Biol. Drug Des.*, vol. 17, no. 4, pp. 501–507, 1981.

[37] D. P. Kelly, M. K. Dewar, R. B. Johns, S. Wei-Let, and J. F. Yates, “Cross-linking of amino acids by formaldehyde. Preparation and 13C NMR spectra of model compounds,” in *Protein Crosslinking*, Springer, 1977, pp. 641–647.

[38] J. Bjorksten, “Cross linkages in protein chemistry,” *Adv. Protein Chem.*, vol. 6, pp. 343–381, 1951.

[39] A. A. Marra, *Technology of wood bonding*. Van Nostrand Reinhold, 1992.

[40] ASTM, “Standard Terminology of Adhesives.” pp. 1–13, 2015.

[41] S. S. Voyutskii, “Adhesion and Autohesion of High Polymers,” *Interscience, New York*, 1963.

[42] S. S. Voyutskii, “Adhesion and autohesion of polymers,” *Adhes. Age*, vol. 5, no. 4, p. 30, 1962.

[43] S. S. Voyutskii, “S., Markin, Yu I., Gorchakova, v. M. and Gul, VE,” *Adhes. Age*, vol. 8, pp. 11–24, 1965.

[44] C. R. Frihart, “Adhesive interaction with wood,” *Fundam. Compos. Process. Proc. a Work.*, pp. 29–54, 2004.

[45] J. N. Anand and H. J. Karam, “Surface deformation of thin coatings caused by evaporative convection: III. Theoretical and experimental observations,” *J. Colloid Interface Sci.*, vol. 31, no. 2, pp. 208–215, 1969.

[46] J. N. Anand and R. Z. Balwinski, “Interfacial Contact and Bonding in Autohesion II-Intermolecular Forces,” *J. Adhes.*, vol. 1, no. 1, pp. 24–30, 1969.

[47] J. N. Anand, “Interfacial Contact and Bonding in Autohesion: III-Parallel Plate Attraction,” *J. Adhes.*, vol. 1, no. 1, pp. 31–37, 1969.

[48] J. N. Anand and L. Dipzinski, “Interfacial Contact and Bonding in Autohesion IV Experimental Verification of Theory,” *J. Adhes.*, vol. 2, no. 1, pp. 16–22, 1970.

[49] J. N. Anand, “Interfacial Contact and Bonding in Autohesion V Bonding of Flat Surfaces,” *J. Adhes.*, vol. 2, no. 1, pp. 23–28, 1970.

[50] J. N. Anand, “Re: Contact Theory of Adhesion,” *J. Adhes.*, vol. 5, no. 3, pp. 265–267, 1973.

[51] B. V Deryaguin, “The definition and magnitude of disjoining pressure and its role in the statics and dynamics of thin fluid films,” *Kolloid Zh*, vol. 17, pp. 207–214, 1955.

[52] B. V Deryaguin, N. A. Krotova, V. V Karassev, Y. M. Kirillova, and I. N. Aleinikova, "Electrical Phenomena Accompanying the Formation of New Surfaces, and Their Role in Adhesion and Cohesion," in *Proc. 2nd Int. Congress of Surface Activity*, 1957, vol. 3, p. 417.

[53] B. V Deryaguin and V. P. Smilga, "Adhesion: fundamentals and practice," *London: McLaren*, 1969.

[54] C. Weaver, "Adhesion, Fundamentals and Practice," *McLaren, London*, 1969.

[55] C. Weaver, "Adhesion of metals to polymers," *Faraday Spec. Discuss. Chem. Soc.*, vol. 2, pp. 18–25, 1972.

[56] D. J. Alner, *Aspects of Adhesion, vol. 5*. University of London Press, 1969.

[57] A. D. Roberts, "Surface charge contribution in rubber adhesion and friction," *J. Phys. D. Appl. Phys.*, vol. 10, no. 13, p. 1801, 1977.

[58] F. L. Browne and D. Brouse, "Nature of Adhesion between Glue and Wood1: A Criticism of the Hypothesis that the Strength of Glued Wood Joints Is Due Chiefly to Mechanical Adhesion," *Ind. Eng. Chem.*, vol. 21, no. 1, pp. 80–84, 1929.

[59] A. Pizzi and N. J. Eaton, "A conformational analysis approach to phenol-formaldehyde resins adhesion to wood cellulose," *J. Adhes. Sci. Technol.*, vol. 1, no. 1, pp. 191–200, 1987.

[60] A. Pizzi, "A molecular mechanics approach to the adhesion of urea-formaldehyde resins to cellulose. Part 2. Amorphous vs. crystalline Cellulose I," *J. Adhes. Sci. Technol.*, vol. 4, no. 1, pp. 589–595, 1990.

[61] A. Pizzi, "An assessment of the future industrial prospects for panel adhesives from renewable natural materials," *Holzforsch. Holzverwertung*, vol. 43, pp. 83–87, 1991.

[62] D. Levendis, A. Pizzi, and E. Ferg, "The correlation of strength and formaldehyde emission with the crystalline/amorphous structure of UF resins," *Holzforschung-International J. Biol. Chem. Phys. Technol. Wood*, vol. 46, no. 3, pp. 263–269, 1992.

[63] W. E. Johns, *The chemical bonding of wood. Wood Adhesive Chemistry and Technology, Vol. 2*. Marcel Dekker, New York, NY, 1989.

[64] A. Pizzi, E. P. Von Leyser, J. Valenzuela, and J. G. Clark, "The chemistry and development of pine tannin adhesives for exterior particleboard," *Holzforschung-International J. Biol. Chem. Phys. Technol. Wood*, vol. 47, no. 2, pp. 168–174, 1993.

[65] K. C. Frisch, L. P. Rumao, and A. Pizzi, "Diisocyanates as wood adhesives," *Wood Adhes. Chem. Technol. Ed. Pizzi, A. Marcel Dekker, Inc. New York*, pp. 289–317, 1983.

[66] J. W. McBain and D. G. Hopkins, “On adhesives and adhesive action,” *J. Phys. Chem.*, vol. 29, no. 2, pp. 188–204, 1925.

[67] A. V Pocius, *Adhesion and Adhesives Technology*. *Hanser*. 1997.

[68] M. G. Sturgeon and N. M. Lau, “Continuous pressing medium density fibreboard at Nelson Pine Industries New Zealand,” in *Proceedings of the Washington State University International Particleboard/Composite Materials Series Symposium (USA)*, 1989.

[69] A. J. Bolton and P. E. Humphrey, “The Hot Pressing of Dry-formed Wood-based Composites-Part I. A Review of the Literatlire, Identifying the Primary Physical Processes and the Nature of their Interaction,” *Holzforschung-International J. Biol. Chem. Phys. Technol. Wood*, vol. 42, no. 6, pp. 403–406, 1988.

[70] T. Hata, S. Kawai, and H. Sasaki, “Computer simulation of temperature behavior in particle mat during hotpressing and steam injection pressing,” *Wood Sci Technol*, vol. 24, p. 65, 1990.

[71] F. A. Kamke and M. P. Wolcott, “Fundamentals of flakeboard manufacture: wood-moisture relationships,” *Wood Sci. Technol.*, vol. 25, no. 1, pp. 57–71, 1991.

[72] S. Suo and J. L. Bowyer, “Simulation modeling of particleboard density profile,” *Wood fiber Sci.*, vol. 26, no. 3, pp. 397–411, 2007.

[73] B. G. Zombori, F. A. Kamke, and L. T. Watson, “Simulation of the Mat Formation Process,” *Wood Fiber Sci.*, vol. 33, pp. 564–579, 2001.

[74] A. W. Coats and J. P. Redfern, “Thermogravimetric analysis. A review,” *Analyst*, vol. 88, no. 1053, pp. 906–924, 1963.

[75] “TGA Q5000 IR Thermogravimetric Analyzer,” vol. Revision E. TA Instruments-Waters LLC, New Castle, DE, Sep-2011.

[76] M. Nič, J. Jirát, B. Košata, A. Jenkins, and A. McNaught, Eds., *IUPAC Compendium of Chemical Terminology*. Research Triagle Park, NC: IUPAC, 2009.

[77] “theories of non-isothermal kinetics and DSC curve solutions.” [Online]. Available: http://www.caotechnology.com.au/nonisothermal.htm. [Accessed: 09-Aug-2017].

[78] H. E. Kissinger, “Reaction Kinetics in Differential Thermal Analysis,” *Anal. Chem.*, vol. 11, no. 5, pp. 1702–1706, 1957.

[79] H. E. Kissinger, “Variation of peak temperature with heating rate in differential thermal analysis,” *J. Res. Natl. Bur. Stand. (1934).*, vol. 57, no. 4, p. 217, 1956.

[80] Y. Chen, D. Fan, T. Qin, and F. Chu, “Thermal degradation and stability of accelerated-curing phenol-formaldehyde resin,” *BioResources*, vol. 9, no. 3, pp. 4063–4075, 2014.

[81] “Differential Scanning Calorimeter.” New Castle, DE, pp. 1–76, 2011.

[82] I. Poljanšek and M. Krajnc, “Characterization of phenol-formaldehyde prepolymer resins by in line FT-IR spectroscopy,” *Acta Chim. Slov.*, vol. 52, no. 3, pp. 238–244, 2005.

[83] C. Y. Hse, F. Fu, and B. S. Bryant, “Development of formaldehyde-based wood adhesives with co-reacted phenol/soybean flour,” *Wood Adhes. 2000 Conf. For. Prod. Soc.*, no. November, pp. 13–19, 2001.

[84] J. M. Wescott and C. R. Frihart, “Competitive Soybean Flour/Phenol-Formaldehyde Adhesives for Oriented Strandboard,” *38th Int. Wood Compos. Symp.*, no. Lambuth 2003, pp. 199–206, 2004.

[85] L. Lorenz, C. R. Frihart, and J. M. Wescott, “Analysis of Soy Flour/Phenol-Formaldehyde Adhesives for Bonding Wood,” *Wood Adhes. 2005*, pp. 501–505, 2005.

[86] Z. Wu, X. Xi, and H. Lei, “Soy-based adhesive cross-linked by phenol-formaldehyde-glutaraldehyde,” *Polymers (Basel).*, vol. 9, no. 5, 2017.

[87] L. Lorenz, C. R. Frihart, and J. M. Wescott, “Chromatographic analysis of the reaction of soy flour with formaldehyde and phenol for wood adhesives,” *J. Am. Oil Chem. Soc.*, vol. 84, no. 8, pp. 769–776, 2007.

[88] C. P. Dai and C. M. Yu, “Heat and mass transfer in wood composite panels during hot-pressing: Part I. A physical-mathematical model,” *Wood Fiber Sci.*, vol. 36, no. 4, pp. 585–597, 2004.

[89] C. Pereira, L. Carvalho, and C. Costa, “Modeling the continuous hot-pressing of MDF,” *Wood Sci. Technol.*, vol. 40, no. 4, pp. 308–326, 2006.

[90] Y. Zhang, W. Zhu, Y. Lu, Z. Gao, and J. Gu, “Nano-scale blocking mechanism of MMT and its effects on the properties of polyisocyanate-modified soybean protein adhesive,” *Ind. Crops Prod.*, vol. 57, pp. 35–42, 2014.

[91] Y. Zhang, W. Zhu, Y. Lu, Z. Gao, and J. Gu, “Water-resistant soybean adhesive for wood binder employing combinations of caustic degradation, nano-modification, and chemical crosslinking,” *BioResources*, vol. 8, no. 1, pp. 1283–1291, 2013.

[92] Z. Zhong and X. S. Sun, “Properties of soy protein isolate / polycaprolactone blends compatibilized by methylene diphenyl diisocyanate,” *Glass*, vol. 42, 2001.

[93] Georgia-Pacific Chemicals LLC, “Material Safety Data Sheet: GP(R) 240C11 RResi-stran (R) Oriented Strand Board Resin.” p. 7, 2014.

[94] E. Lange, “GMO Status of ADM Soy Protein Products,” 2005.

[95] European Committee for Standardization, “Wood adhesives for non-structural applications: Determination of tensile shear strength of lap joints,” no. DIN EN 205. 2003.

[96] K. Shaheed, Y. H. Chui, M. H. Schneider, and A. O. Barry, “Wettability of treated flakes of selected species with commercial adhesive resins,” *J. Inst. Wood Sci.*, vol. 16, no. 5; ISSU 95, pp. 258–265, 2004.

[97] Z. Qin, Q. Gao, S. Zhang, and J. Li, “Surface free energy and dynamic wettability of differently machined poplar woods,” *BioResources*, vol. 9, no. 2, pp. 3088–3103, 2014.

[98] Monarch Industries, “3.5 Cu. Ft. Durable Multi-use Portable Mixer.” Winnipeg, MB, Canada, p. 12, 2006.

[99] R. H. Myers and D. C. Montgomery, “Response Surface Methodology: Process and Product in Optimization Using Designed Experiments,” 1995.

[100] C. W. B. Lee, H. M. Budman, and M. D. Pritzker, “Simulation and optimization of the continuous oriented strand board pressing process,” *Ind. Eng. Chem. Res.*, vol. 45, no. 6, pp. 1974–1988, 2006.

[101] W. Hand, G. Cheng, B. Via, and S. Banerjee, “Soy-substituted liquid phenol formaldehyde binders for flakeboard,” *Eur. J. Wood Wood Prod.*, vol. 75, no. 1, pp. 135–138, 2017.

[102] O. G. Udvardy, P. E. Titus, and M. Navratil, “Powdered phenol-formaldehyde resin,” 4,424,300, 1984.

[103] S. E. Johnson and F. A. Kamke, “Quantitative analysis of gross adhesive penetration in wood using fluorescence microscopy,” *J. Adhes.*, vol. 40, no. 1, pp. 47–61, 1992.

[104] G. E. Myers, A. W. Christiansen, R. L. Geimer, R. A. Follensbee, and J. A. Koutsky, “Phenol–formaldehyde resin curing and bonding in steam-injection pressing. I. Resin synthesis, characterization, and cure behavior,” *J. Appl. Polym. Sci.*, vol. 43, no. 2, pp. 237–250, 1991.

[105] R. R. N. Sailaja, B. G. Girija, G. Madras, and N. Balasubramanian, “Effect of compatibilization on mechanical and thermal properties of polypropylene-soy flour composites,” *J. Mater. Sci.*, vol. 43, no. 1, pp. 64–74, 2008.

[106] B. E. Guettler, “Effect of Thermal and Chemical Treatment of Soy Flour on Soy-Polypropylene Composite Properties,” University of Waterloo, 2012.

[107] G. Qi and X. S. Sun, “Soy protein adhesive blends with synthetic latex on wood veneer,” *J. Am. Oil Chem. Soc.*, vol. 88, no. 2, pp. 271–281, 2011.

[108] S. N. Das, M. Routray, and P. L. Nayak, “Spectral, thermal, and mechanical properties of furfural and formaldehyde cross-linked soy protein concentrate: A comparative study,” *Polym. Plast. Technol. Eng.*, vol. 47, no. 6, pp. 576–582, 2008.

[109] M. V. Alonso, M. Oliet, J. C. Domínguez, E. Rojo, and F. Rodríguez, “Thermal degradation of lignin-phenol-formaldehyde and phenol-formaldehyde resol resins : Structural changes, thermal stability, and kinetics,” *J. Therm. Anal. Calorim.*, vol. 105, no. 1, pp. 349–356, 2011.

[110] M. a. Khan and S. M. Ashraf, “Studies on thermal characterization of lignin,” *J. Therm. Anal. Calorim.*, vol. 89, no. 3, pp. 993–1000, 2007.

[111] Z. Katovic and K. Kombinat, “Curing of Resole-Type Phenol-Formaldehyde Resin,” vol. 11, pp. 85–93, 1967.

[112] W. M. Jackson and R. T. Conley, “High temperature oxidative degradation of phenol–formaldehyde polycondensates,” *J. Appl. Polym. Sci.*, vol. 8, no. 5, pp. 2163–2193, 1964.

[113] R. Burns and E. W. Orrell, “A thermal analytical study of phenol formaldehyde resins,” *J. Mater. Sci.*, vol. 2, no. 1, pp. 72–77, 1967.

[114] P. W. King, R. H. Mitchell, and A. R. Westwood, “Structural analysis of phenolic resole resins,” *J. Appl. Polym. Sci.*, vol. 18, no. 4, pp. 1117–1130, 1974.

[115] J. M. Kenny, G. Pisaniello, F. Farina, and S. Puzziello, “Calorimetric analysis of the polymerization reaction of a phenolic resin,” *Thermochim. Acta*, vol. 269–270, no. C, pp. 201–211, 1995.

[116] K. Roczniak, T. Biernacka, and M. Skarzynski, “Some properties and chemical structure of phenolic resins and their derivatives,” *J. Appl. Polym. Sci.*, vol. 28, no. 2, pp. 531–542, 1983.

[117] T. Holopainen *et al.*, “IR spectroscopy as a quantitative and predictive analysis method of phenol-formaldehyde resol resins,” *J. Appl. Polym. Sci.*, vol. 69, no. 11, pp. 2175–2185, 1998.

[118] R. O. Ebewele, B. H. River, and J. A. Koutsky, “Relationship between phenolic adhesive chemistry and,” *J. Appl. Polym. Sci.*, vol. 31, no. 7, pp. 2275–2302, 1986.

[119] L. J. Bellamy, *The Infrared Spectrum of Complex Molecules*, 2nd ed. New York: Wiley, 1958.

[120] S. Chow, “A curing study of phenol-resorcinol-formaldehyde resins using infrared spectrometer and thermal analysis,” *Holzforschung-International J. Biol. Chem. Phys. Technol. Wood*, vol. 31, no. 6, pp. 200–205, 1977.

[121] S. Chow and P. R. Steiner, “Comparisons of the cure of phenol–formaldehyde novolac and resol systems by differential scanning calorimetry,” *J. Appl. Polym. Sci.*, vol. 23, no. 7, pp. 1973–1985, 1979.

[122] M. Yamao, Y. Tanaka, S. Tanaka, S. Nukui, and A. Kubota, “Analysis of resorcinol-formaldehyde resins by infrared spectroscopy,” *Japan Anal.*, vol. 21, no. 4, p. 491, 1972.

[123] O. D. Shreve, *Synthetic Organic Coating Resins, Organic Analysis*, Vol. 3. New York: Wiley-Interscience, 1956.

[124] M. Kačuráková and M. Mathlouthi, “FTIR and laser-Raman spectra of oligosaccharides in water: Characterization of the glycosidic bond,” *Carbohydr. Res.*, vol. 284, no. 2, pp. 145–157, 1996.

[125] J. T. Kim and A. N. Netravali, “Mechanical, thermal, and interfacial properties of green composites with ramie fiber and soy resins,” *J. Agric. Food Chem.*, vol. 58, no. 9, pp. 5400–5407, 2010.

[126] X. Chen, Y. Ru, F. Chen, X. Wang, X. Zhao, and Q. Ao, “FTIR spectroscopic characterization of soy proteins obtained through AOT reverse micelles,” *Food Hydrocoll.*, vol. 31, no. 2, pp. 435–437, 2013.

[127] S. Banerjee and D. Li, “Interpreting Multicomponent Infrared Spectra by Derivative Minimization,” *Appl. Spectrosc.*, vol. 45, no. 6, pp. 1047–1049, 1991.

[128] J. T. Garrett, R. Xu, J. Cho, and J. Runt, “Phase separation of diamine chain-extended poly(urethane) copolymers: FTIR spectroscopy and phase transitions,” *Polymer.*, vol. 44, no. 9, pp. 2711–2719, 2003.

[129] L. Ning, W. De-Ning, and Y. Sheng-Kang, “Crystallinity and hydrogen bonding of hard segments in segmented poly(urethane urea) copolymers,” *Polymer.*, vol. 37, no. 16, pp. 3577–3583, 1996.

[130] M. J. Elwell, A. J. Ryan, H. J. M. Grunbauer, and H. C. VanLieshout, “An FT IR study of reaction kinetics and structure development in model flexible polyurethane foam systems,” *Polymer.*, vol. 37, no. 8, pp. 1353–1361, 1996.

[131] G. Spathis, M. Niaounakis, E. Kontou, L. Apekis, P. Pissis, and C. Christodoulides, “Morphological changes in segmented polyurethane elastomers by varying the NCO/OH ratio,” *J. Appl. Polym. Sci.*, vol. 54, no. 7, pp. 831–842, 1994.

[132] Y. Wu, C. Sellitti, J. M. Anderson, A. Hiltner, G. A. Lodoen, and C. R. Payet, “An FTIR–ATR investigation of in vivo poly(ether urethane) degradation,” *J. Appl. Polym. Sci.*, vol. 46, no. 2, pp. 201–211, 1992.

[133] G. Socrates, *Infrared and Raman characteristic group frequencies: tables and charts*. John Wiley & Sons, 2001.

[134] N. Grassie and M. Zulfiqar, "Thermal degradation of the polyurethane from 1, 4-butanediol and methylene bis (4-phenyl isocyanate)," *J. Polym. Sci. Part A Polym. Chem.*, vol. 16, no. 7, pp. 1563–1574, 1978.

[135] N. Grassie, M. Zulfiqar, and M. I. Guy, "Thermal degradation of a series of polyester polyurethanes," *J. Polym. Sci. Part A Polym. Chem.*, vol. 18, no. 1, pp. 265–274, 1980.

[136] K. Herzog, "Degradation behaviour of polyurethane studied by linear temperature programmed pyrolysis FTIR spectroscopy," in *Macromolecular Symposia*, 1991, vol. 52, no. 1, pp. 307–312.

[137] W. H. Awad and C. A. Wilkie, "Investigation of the thermal degradation of polyurea: The effect of ammonium polyphosphate and expandable graphite," *Polymer.*, vol. 51, no. 11, pp. 2277–2285, 2010.

[138] G. W. Chantry, E. A. Nicol, D. J. Harrison, A. Bouchy, and G. Roussy, "Vibrational spectrum, assignment and molecular symmetry of phenyl isocyanate in the liquid phase," *Spectrochim. Acta*, vol. 30, no. 9, pp. 1717–1722, 1974.

[139] G. L. Caldow and H. W. Thompson, "Vibrational bands of isothiocyanates, thiocyanates and isocyanates," *Spectrochim. Acta*, vol. 13, no. 3, pp. 212–216, 1958.

[140] R. P. Hirschmann, R. N. Kniseley, and V. a. Fassel, "The infrared spectra of alkyl isocyanates," *Spectrochim. Acta*, vol. 21, no. 12, pp. 2125–2133, 1965.

[141] R. A. Nyquist and G. L. Jewett, "IR and NMR correlations for alkyl isocyanates," *Appl. Spectrosc.*, vol. 46, no. 5, pp. 841–842, 1992.

[142] R. A. Nyquist, D. A. Luoma, and C. L. Putzig, "Vibrational study of alkyl isocyanates in solution," *Appl. Spectrosc.*, vol. 46, no. 6, pp. 972–980, 1992.

[143] Y. Kurimoto, M. Takeda, A. Koizumi, S. Yamauchi, S. Doi, and Y. Tamura, "Mechanical properties of polyurethane films prepared from liquefied wood with polymeric MDI," *Bioresour. Technol.*, vol. 74, pp. 151–157, 2000.

[144] Z. S. Petrovic, Z. Zavargo, J. H. Flynn, and W. J. Macknight, "Thermal-Degradation of Segmented Polyurethanes," *J. Appl. Polym. Sci.*, vol. 51, no. 6, pp. 1087–1095, 1994.

[145] S. Pinchas and D. Ben-Ishai, "The Carbonyl Absorption of Carbamates and 2-Oxazolidones in the Infrared Region," *J. Am. Chem. Soc.*, vol. 79, no. 15, pp. 4099–4104, 1957.

[146] M. Sato, “Studies on l-Alkenyl Isocyanates and Their Derivatives1,” *J. Org. Chem.*, vol. 26, no. 3, pp. 770–779, 1961.

[147] A. R. Katritzky and R. A. Jones, “Infrared Absorption of Substituents in Heteroaromatic Systems. Part IV. Ethyl N-Arylurethanes.,” pp. 676–679, 1960.

[148] J. C. Carter and J. E. Devia, “Vibrational analysis of methylcarbamate and N,N-dichloromethylcarbamate,” *Spectrochim. Acta Part A Mol. Spectrosc.*, vol. 29, no. 4, pp. 623–632, 1973.

[149] H. S. Randhawa, G. K. Rao, and C. N. R. Rao, “Vibrational spectra and normal vibrations of methyl N-methyl- carbamate and N-methylcarbamoyl halides,” vol. 30A, pp. 1915–1922, 1974.

[150] R. A. Nyquist, “Infrared Spectra-Structure Correlations of Carbamic Acid-Aryl Esters, Alkyl Esters,” *Spectrochim. Acta Part A-Molecular Biomol. Spectrosc.*, no. 8, pp. 1635–1641, 1973.

[151] P. L. Lang and J. E. Katon, “The vibrational spectra, structure, and conformational behavior of dimethyl dicarbonate,” *J. Mol. Struct.*, vol. 172, no. C, pp. 113–128, 1988.

[152] H. Ishihara, I. Kimura, K. Saito, and H. Ono, “Infrared studies on segmented polyurethane-urea elastomers,” *J. Macromol. Sci. Part B Phys.*, vol. 10, no. 4, pp. 591–618, 1974.

[153] D. O. Hummel, G. Ellinghorst, A. Khatchatryan, and H.-D. Stenzenberger, “Segmented copolyethers with urethane and urea or semicarbazide links for blood circulation systems II. Infrared-spectroscopic investigations,” *Macromol. Mater. Eng.*, vol. 82, no. 1, pp. 129–148, 1979.

[154] H. K. Hall and R. Zbinden, “Infrared Spectra and Strain in Cyclic Carbonyl Compounds,” *J. Am. Chem. Soc.*, vol. 80, no. 23, pp. 6428–6432, 1958.

[155] E. Spinner, “The vibration spectra and structures of the hydrochlorides of urea, thiourea and acetamide. The basic properties of amides and thioamides,” *Spectrochim. Acta*, vol. 15, pp. 95–109, 1959.

[156] Y. Mido, “of Various Dialkyhreas in Solution,” *Spectrochim. Acta Part A*, vol. 29A, no. 1969, pp. 431–438, 1973.

[157] A. M. Heintz *et al.*, “A spectroscopic analysis of the phase evolution in polyurethane foams,” *Macromolecules*, vol. 38, no. 22, pp. 9192–9199, 2005.

[158] W. Li, A. J. Ryan, and I. K. Meier, “Effect of chain extenders on the morphology development in flexible polyurethane foam,” *Macromolecules*, vol. 35, no. 16, pp. 6306–6312, 2002.

[159] G. Sung, S. K. Kim, J. W. Kim, and J. H. Kim, “Effect of isocyanate molecular structures in fabricating flexible polyurethane foams on sound absorption behavior,” *Polym. Test.*, vol. 53, pp. 156–164, 2016.